Reviewer #1

(Responses in blue)

General Comments:

The authors present results of topographic analysis and catchment-scale denudation rates determined using cosmogenic nuclides in the Olympic Mountains of Washington, USA. The goal of the analyses is to assess controls on the spatial patterns of denudation. The authors find that denudation rates scale with multiple metrics of topographic steepness and previously recognized spatial patterns of exhumation. Present day precipitation patterns and the extent of prior glaciation do not explain patterns denudation measured by cosmogenic nuclides.

The finding that denudation rates are not spatially correlated with precipitation, but instead are correlated with tectonic forcing is consistent with findings from a number of recent studies in other mountain ranges. Hence the work contributes to an emerging view on the role of climate in influencing erosion rates in tectonically-active landscapes and is hence appropriate for publication in Earth Surface Dynamics. However, I have a number of comments that should be addressed in a revised manuscript below.

More generally, the manuscript begins (in the abstract) by indicating the role of topographic adjustment by glaciers in setting post-glacial erosion rates is unknown and that there are intense spatial variations in the glacial modification of topography. These statements are both correct, and in the Olympic Mountains there is evidence for spatial variation in topographic modification (e.g., Montgomery, 2002; Prasicek et al., 2014).

However, the manuscript does not exploit the spatial variability in glacial modification to ask whether the degree of topographic modification and Holocene erosion rates scale with glacier size or whether Holocene erosion rates scale with the degree of glacial topographic modification. The manuscript stands on its own without addressing these questions, however, addressing these questions would increase the impact of the manuscript and help determine whether rock uplift alone drives the observed patterns in erosion or whether there is also an additional signature caused by glacier-induced increases in relief.

We agree that this is an important and interesting topic; however, it goes beyond the scope of this manuscript. Such an endeavor would require a new study that focused on quantifying ice volumes and or ELA histories throughout the range. As it stands, evidence of non-eroded moraines is limited to the western side of the range, and estimates of glacier size can only be deduced using the elevations of cirque basins and impeding ice sheet lobes on the eastside of the range, all estimates and observations that we have utilized in this manuscript, and expanded upon in further suggestions below.

Comments:

Line 21-24: It could easily be argued that buildup of topography, high relief, high erosion rates, etc., has also occurred after the onset of Cenozoic cooling and glaciation. Willett (1999) presents results of a modeling exercise, which does not directly support the claims regarding controls on topography and erosion prior to the Cenozoic. Hence it is not clear that these introductory sentences properly motivate the story that follows.

We agree with the reviewer on this topic. However, the point we are making first is that there must have been Cenozoic mountain ranges present in order to form large areas of generally cold landscapes were snow/ice could accumulate to form alpine glaciers. Without this precondition, alpine glaciers would not have formed. After these sentences, we then discuss the idea that glaciers changed topography and erosion thereafter. To communicate this point better we have modified the opening of the Introduction (4th sentence) to read – “This increase

in cooler, higher elevation landscapes created the necessary conditions for alpine glaciers to form in the Late Cenozoic."

Line 24: 'between these characteristics' – please be explicit and write out what is meant by 'these'

Corrected: This sentence now reads – "Because of the covariation between climate, topography and rock uplift, erosion rates in fluvially dominated orogens have been shown to correlate with climatic and topographic metrics such as precipitation rate, relief, hillslope angle, and channel steepness via linear, non-linear and threshold relationships…"

Line 27: It would be useful to include a citation to a study or studies that document glacier fluctuations on response to climate change.

We have decided to remove this superfluous sentence to make the Introduction more to the point.

Line 47: It is not clear what is meant by 'efficiency' and also not clear what data/prior study support that statement.

Corrected: We have changed this sentence to read – "Here we address this uncertainty and test whether Plio-Pleistocene glaciers have masked long-lived patterns of rock uplift as recorded by millennial-scale erosion rate estimates and modern topography."

Line 158: The description of why effective latitude and altitude values calculated for each catchment do not incorporate temporal variation in production rates needs to be re-visited or further explained. The time-variation in production is caused by temporal variation in earth's magnetic field. Given the size and elevation range of the catchments sampled, it is not clear (without a calculation to demonstrate it) that using effective altitude and latitude inputs would substantially distort predictions from a time varying production model. Alternatively, simply state the reported values are based on a constant production rate model.

Corrected: This sentence now reads – "We report erosion rates from the CRONUS calculator from the constant production rates determined by the constant production rate models of Lal (1991) and Stone (2000). To enable comparison between new and previous measurements, we recalculated erosion rates from 7 sand samples within the Olympic Mountains previously reported by Belmont et al. (2007)."

Line 194-196: The text explaining why statistics were not performed on subsets of the data is cumbersome, primarily because there first is not a justification for why the data would or could be divided into subsets.

Corrected: We agree these statements are not necessary. These two sentences have been removed.

Line 197: If the regressions account for uncertainty in both variables, then the regression technique should be reported; York or RMA or ?

Corrected: The first two sentences of this section now read – "We performed non-linear, least-square regressions on our new and existing erosion rate data. To provide a better sense of the distribution of topographic metrics within a basin, we provide box-and-whisker plots within our bivariate plots, though our regressions discussed in the following sections are based on

mean statistics. We included the uncertainties in both variables by using a Mote Carlo sampling protocol."

Line 199: Given the MSWD statistic is little used in the geosciences outside of isochron geochronology, it would be useful to also report the correlation coefficient (R-squared) values.

We agree that the MSWD is not often used in the geosciences, and find this unfortunate. However, standard R^2 values are not appropriate for these regressions as they are not linear, and therefore, R^2 values can exceed 1, thus making it a poor indicator of goodness of fit. As the MSWD is a standard data analysis tool that is well documented in text books, and appropriate for the data sets with the properties such as ours we have chosen to use it.

Equations 3 and 4: It should be noted what values were used for K, Sc, and Rc.

There are no set values for K, Sc, and Rc. These values are found through the regression techniques and reported in the following sections.

Line 245: Here (and elsewhere, e.g., line 376) reference is made to the size of glaciers, but the manuscript does not report quantitative measures of glacier size, but instead refers to contours of ELA. Although they may be related, ELA is not the same as 'size'.

Corrected: We have clarified this topic by adding the following text to the background section – "Alpine glaciers were likely active in every valley of the Olympics (Porter, 1964); however, the size of the glaciers was highly variable, as the east flowing glaciers would have been limited to the rugged core of the range by the Cordilleran Ice Sheet (see glacial deposits Fig. 1B). This suggests that the west flowing glaciers may have been nearly twice as long as those flowing east."

Line 271: A citation reporting the expected 26Al/10Be ratio is needed.

Corrected: A citation to Balco et al 2008 added.

Line 343: An alternative explanation is that normalized channel steepness does not linearly track erosion.

We agree with this observation, and discuss it in a previous section (3.4) when describing our non-linear regression technique.

Line 414: 'this study'; it is not clear if the phrase relates to the study cited in the previous sentence or to the present manuscript.

Corrected: "this study" changed to "these numerical models" for clarification that the reference was to the previous study.

Line 406: The sentence is asking a question ('whether' appears twice), but then needs to end with a phrase that starts: 'depends on. . ."

Corrected: We have restructured this sentence to be much clearer – "The balance between post-glacial erosion and longer-lived rock uplift depends on whether post-glacial climate conditions (e.g. increase or decrease in precipitation), or topographic perturbations (e.g. hillslope steeping or channel shallowing) have changed the activity of extant surface processes."

Line 419-423: It is not clear that landscapes where glaciers are efficient agents of erosion are necessarily areas where glaciation reduces relief. It seems quite plausible that the excavation of glacial valleys/troughs could increase relief; indeed Montgomery (2002) reports that glacial valleys in the Olympic Mountains have 500 m more relief than fluvial valleys. Hence the text here needs reflect what is known empirically.

Indeed, glacial incision can increase or decrease relief. Whether an increase or decrease is detected is a matter of scale of observation. There are a few studies which have shown this to occur. We have added references to a well-known study (Whipple et al., 2009) and our recent paper in the Olympic Mountains (Adams and Ehlers, 2017) to provide context.

Further, the following conclusion text (through line 423) is rather unsatisfactory, as these conclusions are not at all drawn from the findings presented in the manuscript. Such material could appear in the Discussion, albeit with less generalization, and a more robust discussion.

Corrected: We have moved most of this material to the Discussion section and reshaped the Conclusion.

Line 424-425: References to mismatches between Holocene erosion and rock uplift seem better brought up in the Discussion; i.e., it is sufficient here to indicate there is a general agreement between erosion and rock uplift rates and to make conclusions based on that statement.

Corrected: We have moved most of this material to the Discussion section and reshaped the Conclusion.

Tables: The topographic shielding factor should appear in one of the tables so that all data needed to re-produce the denudation rates are reported in the manuscript (see Frankel et al., 2010, EOS).

We have opted to include these data in the supplement for the sake of space in the main manuscript.

Editorial comments:
Line 68: there is a missing word ‘pattern accreted materials’

Corrected: This now reads – “pattern of accreted materials”

Line 108-109 (and elsewhere): Several sentences begin with ‘This’. Replacing ‘This’ with ‘Equation 1. . .’ or ‘The value of 0.45. . .’ would be clearer to the reader.

Corrected: Sentences now read – “Eq. 1 normalizes slope values, for the concavity of the channel. For our calculations, we use $\theta = 0.45$. A θ value of 0.45 has been shown to describe the concavity of fluvial systems in the Olympic Mountains (Adams and Ehlers, 2017).”
Some other instances throughout the text have also bee changed.

Line 144: lowercase ‘v’ in von.

Corrected.

Line 168: there is an extra word at the end of the sentence.

Corrected. The extra “the” has been removed.

Line 220: it would be clearer to indicate that C and p are ‘coefficients’

Corrected.

Line 311-312: this sentence is missing an ending

Corrected. Sentence now reads – “Recent studies suggest that our samples should have natural $^{26}Al/^{10}Be$ ratios of ~6.75 (Balco et al., 2008), a value that is very close to most of our measured ratios (Figure 4).”

Line 410: there is extra text here; initials, first names

Corrected.

Figure 2e. The scale bar for erosion rates isn’t very useful, as it is difficult to determine the rates for the catchments with yellow-green color.

Corrected. Scale now runs only from red to blue.

Figure 3. The legend (east-, west-side basins) should appear in the top panel, because the text pointing out the rain shadow effect does not make sense without this information.

Corrected.

Reviewer #2 (George Hilley)
(Responses in blue)
Summary:
This contribution presents 14 new cosmogenically derived erosion rate measurements from the Olympic Mountains, Washington State, USA. These rates are compared to various climate measures, morphometrics, and exhumation / incision proxies to provide insight into the following questions: 1) Is there a discernible imprint of climate gradient on erosion rates measured by these cosmogenic inventories? 2) Is there a signal of disequilibrium conditions recorded by a discrepancy between erosion and exhumation measures over various time-scales?, 3) Do landscape morphometrics scale with erosion rates?, and 4) What is the relationship between measured erosion rates and inferred long-term rock uplift rates? The authors generally find that variations in modern climate measures do not scale with measured erosion rates, but, at least at low erosion rates, measures such as local relief and mean channel steepness scale in some way with erosion rates. The authors find that there is a general correspondence between river incision rates, exhumation gauged by low-temperature thermochronology, and modern-day cosmogenically derived erosion rates. As such, even modern (millennial time-scale) erosion rates appear to track long-term exhumation (and perhaps rock-uplift) rates in the Olympics, and that glacial processes do not appear to disrupt landscape equilibrium to an extent that would produce a divergence between modern and long-term measures of erosion of the range.

Recommendation:
This paper presents interesting new data and analyses of an active, glaciated mountain belt, where large precipitation gradients and temporal changes in surface processes may be

expected to leave some imprint on the erosion of the range. The authors finding that, despite these spatial and temporal variations, erosion rates measured over various time-scales are approximately constant, should be of interest to the readership of Earth Surface Dynamics. The study appears thoughtfully conceived and executed, and is written in a clear and concise manner that requires few grammatical changes. Thus, with consideration of the comments below, I would feel comfortable recommending acceptance pending MINOR to MODERATE REVISIONS. Below, I make some general suggestions, as well as some specific comments geared to individual lines in the text.

General Comments:

1) The authors have carried out a detrital 10-Be study that supposes that erosion rates in the catchments are everywhere equal. This is somewhat addressed in the text under the 5.1 section, last paragraph, where the authors discuss the impact of the introduction of dosed and shielded material into their samples. Yet, this does not address the fact that the authors' approach assumes that each point in the basin is equally represented in the sample, as well as the fact that the calculated mean production rate could be biased by increased contributions from different elevation ranges because of the non-linear increase of production rate with elevation. I am not uncomfortable with the authors' assumptions (in addition to the fact that quartz is uniformly distributed in the sourced lithologies). But, given that some of these catchments have a good amount of local relief and lithologic variability leading to heterogeneous quartz "fertility", some discussion of this effect, and its potential impact might be appropriate to include in section 5.1.

Corrected. We have added the following discussion in section 5.1 – "Like a previous study (Belmont et al, 2007) we have assumed that there is no risk to erosion rate calculations due to quartz infertility or proportional quartz sourcing from all parts of our basins in the Olympic Mountains. While there are some quartz-free lithologies in the range, these rocks are a minor occurrence the in Olympic Subduction Complex, and we have avoided sampling the Coast Range Terrane completely. In locations where nested catchments are found, erosion rates are with error of each other, suggesting a proportional scouring of quartz from all parts of even the largest sampled basin (compare WA1526, DEN101, and DEN106)."

2) I found the correspondence between river incision, exhumation, model-derived erosion rates, and 10-Be denudation rates compelling. One way in which these relationships could be made more effective and illustrative would be to actually plot the quantities versus one another, rather than distance (Figure 7). I think I understand why the authors plotted these rates in the particular space they did, in that some of the primary studies were carried out within areas that do not overlap with the cosmogenic samples directly, but lie within similar tectonic positions when these data are projected onto a cross section. My reading of the primary literature is that 1) the Clearwater (which I think are the black dots) is located outside of the sampled area shown in Figure 2E, and so must be projected into the sampled basins to be used in this study.

The river incision data (black dots) are within the sampled basins (most the CRN data from the previous study. As such there is substantial overlap between the datasets.

2) The AFT ages are from throughout the range, and so there is probably a good path forward for interpolating these across the sampled basins to calculate point-by-point estimates of exhumation rate, and to use these to quantify basin-averaged exhumation rates within each sampled watershed.

Indeed, we have considered a method very similar to what is being described here. However, we found the method of interpolating/extrapolating to be unsatisfactory as a means of direct comparison with our data for the following reasons. 1) The integrating spatial scales of erosion are not clear for AFT data. What portion of the landscape surrounding a bedrock sample could be exhuming at the rate recorded using AFT data? 2) An interpolating/extrapolating method will create a smooth function between AFT points while the erosion field from CRN data will be discontinuous. 3) The density of AFT data throughout the range is variable, and only 4 of our new samples in the core of the range with acceptable erosion rates contain an AFT sample. Taken together, it would be difficult to constrain the uncertainty introduced into the regression by using interpolated/extrapolated data.

3) Drew Stolar's modeling study is a profile model, which is fine. But, it is tuned to a specific mean erosion rate that I think was chosen with the AFT exhumation rates in mind. Thus, it is not particularly surprising that the magnitudes match up with what is observed, since the AFT exhumation rates roughly align with the 10-Be rates.

This is a fair point. We have opted to remove these modeling results to make the means of comparison more straightforward.

This is all to say that the most robust and comparable of these datasets appear to be the AFT- and 10-Be-derived rates. To use the other measures, it seems like some sort of projection has to be made, which introduces its own set of assumptions. Please correct me if I am wrong about this. This being the case, it might be interesting to carry out a direct comparison of the most comparable of the datasets, meaning the (interpolated) AFT-derived exhumation rates for each watershed that was sampled for 10-Be. One would then have a direct comparison that could be used to carry out a formal analysis to reveal the strength of correspondence (through regression analysis), the presence / absence of systematic discrepancies between datasets that could reveal more insight into where correspondences are best versus where they might break down to some degree. I feel that a map of the difference between exhumation and erosion rates in the spirit of Figure 2E might be revealing.

Please see comments above for more on this topic. It is true that compressing the data from the Olympic Mountains to a single profile requires some assumptions; however, we believe that this technique introduces less bias, and is less likely to over interpret the data available, than a direct 1:1 comparison of AFT and CRN rates.

Specific Comments:

Lines 115-120: For documentation, it would probably be good to have some description of how you calculated ks. There are a few different solution methods available, and a few different software packages to do this. Quick mention of these would be good for completeness of documentation.

Corrected: We have added a new sentence in this section that reads: "We used the Profiler tool (Wobus et al., 2006) to extract and analyze our river channels, and calculated steepness values over 0.5 km reaches."

Lines 290-300: The relationship with channel steepness looks good between $0 \leq e \leq 600$ m/Myr. At higher erosion rates, it does not do so well, even for the samples with reasonable 26Al/10Be.

This appears to be more of an observation (which we completely agree with) than a concern that needs addressing. We have made the same observation and discuss how this pattern may be important in glaciated landscape where topographic relief has been limited by glaciers.

Also, you might consider adjusting your concavity to 0.4, so that you can use the multiplier of the power law to calculate K and compare this to the range for your lithologies via Stock and Montgomery (1999). This will help provide some additional validation.

This is an interesting idea; however, the data and analysis presented here does not allow for the precise vetting of a specific incision law. The power law in Eq 5 may not be recording the stream power law in Stock and Montgomery because our new data may not be in topographic steady-state. To compare the power law coefficient from our data with that of Stock and Montgomery would be an over interpretation.

Lines 310-315: As per general comment 1 above, I don't think that spatial variations in erosion rates are covered here, meaning that one could have a 6.75 ratio (i.e., no complex exposure history) but your sample might not be representative of all sediment in the basin. Also, I assume that the "deep" landslide mechanism would be one in which dosed material was buried for a long time (a fraction of the 1/2 life of 26-Al) and then reworked into transported sediment. But, I think a "deep" bedrock landslide should still have the 6.75 ratio, since it did not get dosed and re-buried.

This topic is covered in detail above after General Comment 1. In addition, we have removed "deep landslide" reference from this sentence as it was incorrectly added there.

Tectonic controls of Holocene erosion in a glaciated orogen

Byron A. Adams[1,2], Todd A. Ehlers[1]

[1]Department of Geosciences, Univsität Tübingen, D-72074, Germany
[2]Now at the School of Earth Sciences, University of Bristol, Bristol, BS8 1RJ, UK

Correspondence to: Byron A. Adams (byron.adams@bristol.ac.uk)

Abstract. Recent work has highlighted a strong, worldwide, alpine glacial impact on orogen erosion rates over the last 2 Ma. While it may be assumed that glaciers increased erosion rates when active, the degree to which past glaciations influence Holocene erosion rates through the adjustment of topography is not known. In this study, we investigate the influence of long-term tectonic and post-glacial topographic controls on erosion in a glaciated orogen, the Olympic Mountains, USA. We present 14 new ^{10}Be and ^{26}Al analyses which constrain Holocene erosion rates across the Olympic Mountains. Basin-averaged erosion rates scale with basin-averaged values of 5-km local relief, channel steepness, and hillslope angle throughout the range, similar to observations from non-glaciated orogens. These erosion rates are not related to mean annual precipitation or the marked change in Pleistocene alpine glacier size across the range, implying that glacier modification of topography and modern precipitation parameters do not exert strong controls on these rates. Rather, we find that despite spatial variations in glacial modification of topography, patterns of recent erosion are similar to those from estimates of long-term tectonic rock uplift. This is consistent with a tectonic model where erosion and rock uplift patterns are controlled by the deformation of the Cascadia subduction zone.

1 Introduction

Before the onset of Late Cenozoic cooling and glaciation, the topographic expression of mountain belts resulted from tectonic processes, and the fluvial and hillslope processes which acted as the primary agents of erosion. High rock uplift rates in many of these ranges led to the buildup of topography and in some cases high relief, steep river channels and hillslopes, and commensurate high erosion rates (Willett, 1999). Because of the covariation between climate, topography and rock uplift, erosion rates in fluvially dominated orogens have been shown to correlate with climatic and topographic metrics such as precipitation rate, relief, hillslope angle, and channel steepness via linear, non-linear and threshold relationships (Ahnert, 1970, Montgomery and Brandon, 2002, Ouimet et al., 2009, DiBiase et al., 2010). The development of rugged mountain belts led to an increase in cooler, higher elevation landscapes, which created the necessary conditions for alpine glaciers to form in the Late Cenozoic. These glaciers possessed variable capacity to erode at the same rate as the rivers that existed before them, and regional rock uplift rates. In many mountain ranges, glaciers appear to have accelerated erosion (Hallet et al., 1996, Shuster et al., 2005, Ehlers et al., 2006, Valla et al., 2011, Herman et al., 2013, Christeleit et al., 2017, Michel et al., 2018), while in other areas, glaciers may have done little to change erosion rates over the past few million years (Koppes and Montgomery, 2009, Thomson et al., 2010, Willenbring and von Blanckenburg, 2010).

As a result of Cenozoic climate change, the relationships between topographic metrics and observed Holocene (last ~12 kyr) erosion rates in glaciated mountain ranges are more complex than in purely fluvial settings (Moon et al., 2011, Godard et al., 2012, Glotzbach et al., 2013). These poorly understood relationships are likely caused for two reasons. (1) Glaciers reorganized previously fluvial channel networks and relief to create a landscape with their preferred geometry,

Deleted: f

Deleted: intense

Deleted: these characteristics

Deleted: In

Deleted: , alpine glaciers formed, and then advanced and receded many times due to climate oscillations.

radically changing the orogen topography (Whipple et al., 1999, MacGregor et al., 2000, Brocklehurst and Whipple, 2002, Brocklehurst and Whipple, 2004, Brocklehurst and Whipple, 2006, Anderson et al., 2006, Adams and Ehlers, 2017). (2) Holocene erosion rates may be dominated by transient signals as surface process remove the topographic disequilibrium imposed by glacial erosion (Moon et al., 2011).

In light of the previous studies, what remains uncertain is how much (if any) signal of tectonic processes can be discerned from a heavily glaciated orogen, and the degree to which common relationships between erosion and topographic metrics hold in post-glacial landscapes. Here we address this uncertainty and test whether Plio-Pleistocene glaciers have masked long-lived patterns of rock uplift as recorded by millennial-scale erosion rate estimates and modern topography. To do so, we have conducted a systematic study of basin-averaged erosion rates from ^{26}Al and ^{10}Be concentrations in modern river sediments from the Olympic Mountains, USA (Fig. 1). The Olympic Mountains are well suited for this study because the efficiency of Plio-Pleistocene glaciers was controlled by spatially variable glacial mass balance, and the orogen has been shown to contain a wide range of rock uplift rates. We use our new data, in addition to ^{10}Be concentrations from a previous study (Belmont et al., 2007), to investigate the spatial variations in erosion rates with respect to characteristics of the modern topography including local relief, hillslope angle, and channel steepness, as well as precipitation. Further, we utilize ^{26}Al/^{10}Be ratios, and new modelling efforts to investigate the degree to which cosmogenic nuclide inventories can accurately constrain erosion rates in glaciated mountain ranges.

Deleted: the efficiency of

Deleted: to mask

2 Background

The Olympic Mountains are part of a chain of mountain ranges that define the forearc high of the Cascadia subduction zone (Fig. 1A). This forearc high marks the topographic and structural apex of an accretionary wedge which formed between the North American plate and the subducting Juan de Fuca plate (Tabor and Cady, 1978). The core of the range is comprised of an essentially unmetamorphosed, homogenous assemblage of medium- to fine-grained, greywacke interbedded with minor siltstone, mudstone, conglomerate, and basalt lenses. This group of rocks is referred to as the Olympic Subduction Complex, and is located in the footwall of the Hurricane Ridge Fault (Fig. 1). Pillow basalts, breccias, volcaniclastic rocks and diabase make up the hanging wall of the fault, referred to as the Coast Range Terrane. Sedimentological and bedrock cooling histories suggest accelerated rock uplift and unroofing of the range began around 17-12 Ma (Tabor and Cady, 1978, Brandon et al., 1998). Rock uplift rates have been interpreted across the range from Neogene thermochronometric exhumation rates (apatite fission track) and Quaternary river incision rates (Pazzaglia and Brandon, 2001). These rates vary from ~300 m/Myr at the fringes of the range to ~800 m/Myr in regions close to the geographic center of the range, forming a concentric pattern. Previous interpretations of these erosion rates suggest that they are governed by rock uplift rates (Brandon et al., 1998, Pazzaglia and Brandon, 2001, Batt et al., 2001). In most orogenic wedges, the rock velocity field is governed by the subducting plate geometry and convergence rate, as well as the pattern of accreted materials from the subducting plate (Willett, 1999). The Olympic Mountains are thought to be no different (Batt et al., 2001); however, the subduction zone dynamics are complicated by the significant arch in the subducting Juan de Fuca plate and the dome of accreted sedimentary units that make up the east-plunging Olympic Anticline (Brandon and Calderwood, 1990). Indeed, it is likely that these nuanced characteristics of the subduction zone may be responsible for the observed concentric pattern in erosion/rock uplift rates (Brandon et al., 1998, Pazzaglia and Brandon, 2001, Batt et al., 2001, Bendick and Ehlers, 2014).

The Olympic Mountains have a general dome shape where the major drainages exhibit a radial pattern. The dome is asymmetric where the locus of highest topography lies to the northeast of the range divide (Fig. 1B). Plio-Pleistocene alpine

glaciers carved large valleys in the core of the range (Porter, 1964, Montgomery and Greenberg, 2000, Montgomery, 2002, Adams and Ehlers, 2017). The largest glaciers which occupied the Hoh, Queets and Quinault valleys all extended to the Pacific Ocean (Fig. 1B) (Thackray, 2001). Alpine glaciers were likely active in every valley of the Olympics (Porter, 1964); however, the size of the glaciers was highly variable, as the east flowing glaciers would have been limited to the rugged core of the range by the Cordilleran Ice Sheet (see glacial deposits Fig. 1B). This suggests that the west flowing glaciers may have been nearly twice as long as those flowing east. Due to the W-SW prevailing wind direction and the effects of topography on precipitation patterns, mean annual precipitation values decrease from ~6000 mm/yr in the southwest to less than 500 mm/yr in the northeast (Fig. 2A). This same precipitation gradient greatly influenced the Pleistocene equilibrium line altitude (ELA; the position where the ice flux in a glacier is at a maximum), and created an opposing pattern where the ELA increases at a rate of ~ 25 m/km toward the northeast (Porter, 1964) (Fig. 1B), thus controlling the size and efficiency of alpine glaciers (Adams and Ehlers, 2017). The range was bordered to the north and east by the Cordilleran Ice Sheet (Fig. 1B) (Porter, 1964), which also likely restricted the size of alpine glaciers. This dichotomy in glacier size and erosional capacity is likely to have influenced the pattern in erosion rates during glacial times. A recent study by Michel et al. (2018) shows that bedrock cooling histories record a near doubling of exhumation rates around the time of the onset of glaciation (2 Ma). This affect is most pronounced on the west side of the range, where valley glaciers were larger. While the impact of Plio-Pleistocene glaciation on more recent erosion has not been previously quantified, the suggestion of significant glacial erosion would imply that Holocene erosion rates may not simply be a function of rock velocities as suggested by older erosion histories discussed above.

3 Methods

3.1 Topographic analysis

Our topographic analysis is based on the 10 m National Elevation Dataset provided by the United States Geological Survey (www.ned.usgs.gov). Within this paper we calculate three topographic metrics which record relief at different spatial scales and controlled by different surface process – hillslope angle, local relief, and channel steepness. Each metric also has strengths and weaknesses in quickly eroding, glaciated ranges. There is good evidence that hillslope angle values can reach maximum values due to the limitations of the internal angle of friction of hillslope materials. In such high erosion areas, hillslope angle values become insensitive to changes in erosion rates (Schmidt and Montgomery, 1995). Local relief values may also be limited in glaciated ranges due to the buzzsaw effect, whereby efficiently eroding glaciers increase the area near their ELA and thus control mean elevations and restrict relief locally (Meigs and Sauber, 2000, Brozović et al., 1997).

Our local relief (R) map (Fig. 2B) was made by calculating the difference between the highest and lowest elevations within a 5 km-diameter circular window. The local relief metric is designed to encapsulate the relief of hillslopes and channels. The size of this window captures the elevation difference between peaks and valley floors of medium sized basins, but is small enough to detect changes in the relief structure of large drainage basins. The hillslope gradient (S) map (Fig. 2C) was calculated by finding the steepest angle of descent across a 3 x 3 pixel (30 x 30 m) square window.

The channel steepness map (Fig. 2C) was created by adjusting channel gradients (S) (m/m) by the non-linear change in downstream drainage area (A) (m^2) (Hack, 1957, Flint, 1974, Wobus et al., 2006):

$$S = k_s A^{-\theta} \qquad (1)$$

where k_s is the channel steepness, and θ (dimensionless) is the channel concavity. Eq. 1 normalizes slope values, for the concavity of the channel. For our calculations, we use $\theta = 0.45$. A θ value of 0.45 has been shown to describe the concavity

Deleted: This form of

Deleted: This calculation

Deleted: This

of fluvial systems in the Olympic Mountains (Adams and Ehlers, 2017). Since we utilize a single value of θ, we report normalized channel steepness values (k_{sn}) ($m^{0.9}$). We used the Profiler tool (Wobus et al., 2006) to extract and analyze our river channels, and calculated steepness values over 0.5 km reaches. To report a mean value for a basin we calculated the mean normalized channel steepness for all portions of a basin, which are governed by fluvial processes, which generally occurs at drainage areas > 1 km^2.

Normalized channel steepness index (k_{sn}) analysis, which quantifies channel relief, has been used successfully in a number of mixed fluvial and glacial landscapes as a fine scale measure of the erosion potential of glacial/fluvial processes in a landscape (Montgomery, 2001, Brardinoni and Hassan, 2006, Brardinoni and Hassan, 2007, Brocklehurst and Whipple, 2007, Robl et al., 2008, Hobley et al., 2010, Glotzbach et al., 2013, Adams and Ehlers, 2017). Many assumptions generally that are adopted in purely fluvial settings do not apply in mixed glacial-fluvial landscapes. For instance, in our study we do not require that the Olympic Mountains are in topographic steady-state (where erosion and rock uplift at a point are balanced and therefore elevations remain constant over time), nor do we imply that our slope-area analysis relates directly to the processes of glacial incision, or that rock uplift rates need to be spatially uniform. We emphasize that the normalized channel steepness index provides a robust, geometric construct for understanding the importance of spatial changes in channel relief without demanding an understanding of all parameters within a specific incision law (fluvial or glacial). Furthermore, channel relief is likely to control the relief and hypsometry of landscapes, even in glaciated ranges (e.g. Adams and Ehlers, 2017). Unlike hillslope angle calculations, channel steepness values may be able to record changes in erosion/rock uplift rates in regions where hillslopes have reached a threshold (Ouimet et al., 2009).

3.2 Processing sediment samples and calculating erosion rates

Basin-averaged erosion rates were calculated from concentrations of cosmogenic nuclides (^{10}Be and ^{26}Al) in quartz sand from modern river basins throughout the Olympic Mountains (see Fig. S1 for sample location detail). Detrital cosmogenic techniques record the average erosion/denudation rate (we note that rates presented here incorporate both physical and chemical means of mass removal) integrated across the landscape upstream of the sample location (Brown et al., 1995, Granger et al., 1996, Bierman and Steig, 1996). Basins were selected to ensure a thorough sampling across precipitation, Pleistocene ELA, rock uplift, and topographic gradients. These basins are located within the Olympic Subduction Complex, where quartz is ubiquitous throughout the landscape.

Initial attempts to separate pure aliquots of quartz sand proved difficult due to the fine-grained nature of the lithologies found throughout the range. To reduce the need for aggressive hydrofluoric acid treatment, which would prematurely dissolve the quartz, we first disaggregated the 250-1000 µm sand fraction with a Selfrag, a high-voltage pulse disaggregater, at the University of Bern, Switzerland. From this stage on, samples were processed within the facilities at the University of Tübingen. After electronic disaggregation, sediments were re-sieved to 125-1000 µm and separated using a strong magnetic field and then cleaned in concentrated, room temperature aqua regia for 24 hours. Samples were further cleaned in boiling pyrophosphoric acid and then boiling sodium hydroxide at least 3 times. The quartz was then leached 1% hydrofluoric acid while in an ultrasonic bath for 1 week. A final leach was performed on the samples with concentrated hydrofluoric acid before spiking with beryllium. Samples were not spiked with aluminum. Beryllium and aluminum were separated, oxidized and loaded into cathodes for mass spectrometer analysis using established protocols (Von Blanckenburg et al., 1996). Native Al concentrations within samples were measured with an inductively-coupled plasma optical emission

Deleted: . This

Deleted: this technique

Deleted: This technique is

Deleted: s

spectrometer at the University of Tübingen. Beryllium and aluminum ratios were measured at the University of Cologne Centre for Accelerator Mass Spectrometry.

To calculate erosion rates, we followed the approach of Portenga and Bierman (2011), which simplifies each basin to a single point where the production rate is equal to the mean production rate of the entire basin, enabling the use of the CRONUS online calculator (Balco et al., 2008). Basin-averaged production rates were based on the elevation and latitude of each pixel in a basin using the scheme of Stone (2000). The effective elevation and latitude of each basin are the elevation and latitude values corresponding to this mean scaling factor (Table S1). We calculated topographic shielding due to obstacles according to the equations of Dunne et al. (Dunne et al., 1999), and snow shielding from the equations of Gosse and Phillips (Gosse and Phillips, 2001). Pixels under extant ice are assumed to be 100% shielded. Our snow depth maps are based on satellite snow cover data that were calibrated by snow depth observations in the Olympic Mountains (see Supplement for more details). For CRONUS calculations, the following inputs were used: Elevation Flag = std, Thickness = 1 cm, Density = 2.7 g/cm^3, Be Standard = 07KNSTD, Al Standard = KNSTD. We report erosion rates from the CRONUS calculator from the constant production rates determined by the constant production rate models of Lal (1991) and Stone (2000). To enable comparison between new and previous measurements, we recalculated erosion rates from 7 sand samples within the Olympic Mountains previously reported by Belmont et al. (2007).

Deleted: . ... [1]

3.3 Isotopic equilibrium modeling

The application of detrital cosmogenic nuclide techniques as an estimator of basin-averaged erosion rates in post-glacial landscapes is not yet a common practice as there is a high potential for violation of the assumptions inherit to the calculation of erosion rates from nuclide concentrations. The assumptions that can be most problematic for a glacial terrain are: the eroding materials are in isotopic equilibrium; and modern river sediment is spatially and temporally representative of all sediment in the basin. To explore the nature of isotopic equilibrium we describe new modeling efforts in this section. The topic of sediment storage a mixing is discussed in Sections 4.2 and 5.1. Surface materials are in isotopic equilibrium when the production of cosmogenic nuclides is balanced by their removal through erosion and radioactive decay, in this state the concentration of nuclides in surface materials is steady over time. Since glacial ice intercepts, and thus shields underlying material from cosmic radiation, previously and currently glaciated basins may violate the isotopic equilibrium assumption if ice was present recently, and erosion has not been able to remove the older shielding signal (Moon et al., 2011, Portenga et al., 2014, Vance et al., 2003). Therefore, interpreting cosmogenic nuclide concentrations as direct measurements of erosion in some glaciated landscapes can lead to overestimated rates (Gosse and Phillips, 2001, Vance et al., 2003, Portenga et al., 2014).

Deleted: the

To test the hypothesis that our samples are in isotopic equilibrium we conducted a suite of numerical models to constrain the evolution of the concentration of cosmogenically produced nuclides at depth, starting at a time just after a period when ice completely shielded surface production. When the model starts, production occurs according to the equations of (Anderson et al., 1996):

$$N(z,t) = N_0 e^{-\lambda t} + \frac{P_0 e^{-\rho z/\Lambda}}{\lambda + \rho E/\Lambda}\left(1 - e^{-(\lambda + \rho E/\Lambda)t}\right) \quad (2)$$

where N is the cosmogenic nuclide concentration (atoms/g), t is time (yr), N_0 is the inherited concentration cosmogenic nuclides (atoms/g), E is the erosion rate (cm/yr), λ is the decay constant for ^{10}Be (1/yr), z is the depth below the surface (cm), P_0 is the ^{10}Be production rate at the surface (atoms/g/yr), Λ is the attenuation length for cosmogenic nuclide production (g/cm),

and ρ is the material density (g/cm^3). In our models the following values were used: λ = 4.99e-7 1/yr, P_0 = 10 atoms/g/yr (though the results of this model are not sensitive to this value), Λ = 160 g/cm, and ρ = 2.7 g/cm^3.

Using a finite difference method, the model runs forward from the time of since unshielding, and surface concentrations increase over time as production occurs, and deeply shielded materials are eroded from the top of the model. The concentration at the surface is compared to the steady-state value to assess the approach toward isotopic equilibrium. A range of erosion rates which span the observed erosion rates in this study are tested.

3.4 Relationships between erosion rates and basin parameters

We performed non-linear, least-square regressions on our new and existing erosion rate data. To provide a better sense of the distribution of topographic metrics within a basin, we provide box-and-whisker plots within our bivariate plots, though our regressions discussed in the following sections are based on mean statistics. We included the uncertainties in both variables by using a Mote Carlo sampling protocol. Goodness of fit values were determined by the mean square weighted deviation (MSWD). For well-fit data, MSWD values tend toward 1 within an uncertainty based on the degrees of freedom (based primarily on the number of samples). Elevated MSWD values, are caused by the high degree of inter-sample variability, and suggest (1) the two variables shown in the plot are not highly correlated, (2) a more complex function exists between the two variables, or (3) that uncertainties are underestimated.

Deleted: During our regression analysis, we chose to process all data together, as opposed to subsampling populations. This was decided to avoid the issue of small sample statistical bias, and because it was not obvious how to subsample our data *a priori*, without adding bias. These regressions included the influence of uncertainties on both variables.

As a means to assess the relationship between erosion and hillslope processes we use a variation of the non-linear relationship proposed by Roering et al. (2001), which captures the effects of diffusive processes and landsliding:

$$E = \frac{KS}{1-(S/S_c)^2} \quad (3)$$

where E is the basin-averaged erosion rate (m/Myr), K is a rate constant related to the diffusivity of the eroding material (m/Myr), S is the basin-averaged hillslope gradient (m/m), and S_c is a critical slope at which soil flux approaches infinity (m/m).

We used a similar equation from Montgomery and Brandon (2002) to explore the relationship between erosion rates and 5-km local relief:

$$E = \frac{KR}{1-(R/\ R_c)^2} \quad (4)$$

where K is a different rate constant (m/Myr), R is the basin-averaged local relief normalized by the diameter of the moving window (m/m), and R_c is a limit to the possible values of local relief normalized by the diameter of the moving window (m/m).

Previous studies have suggested that that channel steepness values can vary spatially according to a relationship with basin-averaged erosion rates through a stochastic threshold model of fluvial channel incision (DiBiase et al., 2010). Such a model generally produces a non-linear relationship. However, using a model based solely on fluvial incision in the Olympic Mountains would be misleading as the modern river channel likely still reflect the preferred geometry of Plio-Pleistocene glaciers (Adams and Ehlers, 2017). Instead, we implemented a least-squares power function regression to explore possible connections between erosion and channel steepness, similar to other recent studies (Scherler et al., 2013):

$$E = C k_{sn}^{\ p} \quad (5)$$

where C is the coefficient, and p is the exponent. We used the same least-squares routine to analyze the relationship between erosion and precipitation (e.g. replace k_{sn} with the mean precipitation in Eq. 5).

Deleted: pre-exponential

Deleted: k_{sn} is the mean channel steepness value of the basin,

Deleted: power

4 Results

4.1 Topographic analysis

The topography of the Olympic Mountains is a mixture of high glacial cirque basins, wide and flat-floored valleys at low elevations, and very steep landscapes in between. This juxtaposition of varied landscapes creates skewed and multi-modal distributions of topographic metrics within drainage basins throughout the range (Table 1 and 2, Fig. 2B, 2C and 2D). While it is useful to report arithmetic means of basin statistics to simplify a landscape, it can often be difficult to constrain the significance of such means in the context of their relation to erosion rates. In complex landscapes not defined by uniform and steady surface processes, like the Olympic Mountains, normally distributed topographic metrics with good central tendency are unlikely, especially for metrics which capture fine spatial scale processes like those occurring at the scale of hillslopes and channel segments. To provide a better sense of these distributions, we have included simplified histograms next to our reported statistics in Table 1 and 2. Because of this size limitation we are not able to calculate an accurate channel steepness value for one of basins from a previous study, U-WC (Belmont et al., 2007).

Basin-averaged hillslope angles are generally high, in most cases above 28°, as is the standard deviation of hillslope angles within each basin (mean $2\sigma = 21°$) (Table 2 and Fig. 2C). Basin-averaged channel steepness values range between 23 and 181 $m^{0.9}$, and also have proportionally large standard deviations (mean $2\sigma = 89$ $m^{0.9}$) (Table 2 and Fig. 2D). Basin-averaged local relief values (calculated within a 5-km diameter window) range between 350 and 1443 m (Table 2 and Fig. 2B). Relative to hillslope angle and channel steepness values, local relief values exhibit smaller variance within sampled basins (mean $2\sigma = 219$ m). The lower-elevation basins on the western flank of the range, which evaded Last Glacial Maximum (LGM) alpine glaciers (Thackray, 2001, Belmont et al., 2007), have the lowest topographic metric values of the sampled basins (8 basins: mean $R = 544$, mean $S = 23$, mean $k_{sn} = 43$). The mean values from the 8 glaciated, west side basins and the 6 glaciated, east side basins are effectively the same: mean $R = 1296$, mean $S = 31$, mean $k_{sn} = 151$; and mean $R = 1239$, mean $S = 31$, and mean $k_{sn} = 143$, respectively. Despite the rain shadow and the significant discrepancy in the size of alpine glaciers across the range divide, there is no difference in topographic metrics within the rugged core of the range across the divide.

There is a high degree of correlation between some basin-averaged precipitation values and basin-averaged elevation (Fig. 3A.), as would be expected from the PRSIM precipitation dataset which includes an orographic precipitation model to do reanalysis simulations (Daly et al., 1994). This correlation is only strong on the western flank of the mountain where the topographic and precipitation gradients are smoothest. These same sub-group of basins also exhibit a strong correlation between basin-averaged hillslope angle and basin-averaged elevation (Fig. 3B). However, there is no correlation between elevation and precipitation or hillslope angle in the core of the range. There is good correlation between basin-averaged elevation and both basin-averaged local relief and channel steepness (Fig. 3C-D), across the range.

4.2 Cosmogenic basin-averaged erosion rates

While we present both ^{10}Be and ^{26}Al data (Table 3, see Tables S1 and S2 for complete nuclide analysis), we focus our analysis on erosion rates derived from ^{10}Be in this study (Fig. 2E) to provide a means of comparison to existing data from the Olympic Mountains (Belmont et al., 2007). To a first order, basins located at elevations < 1000 m have been eroding at slow rates, all less than 240 m/Myr, whereas basins in the higher, rugged core of the range have higher erosion rates reaching over 1400 m/Myr (Table 3 and Fig. 2E). We obtained the highest apparent erosion rates (> 1500 m/Myr) from the flanks of Mount Olympus, whose drainages contain the largest extant glaciers in the Olympic Mountains (basins WA1519, WA1523, WA1524). However, the very low ^{10}Be concentrations (i.e. high apparent erosion rates) from Mount Olympus may be a

signature of isotopic disequilibrium. Samples WA1519, WA1523 and WA1524 come from basins which likely contained thick ice the longest, and still have small valley glaciers today. The ^{10}Be abundances for these three basins only range from 5-7 times the ^{10}Be blanks. These low abundances are likely caused by the shielding of rock and soil below glaciers. Such low measurements not only increase in the internal uncertainty of the concentration calculation, but also raises questions about the accuracy of the erosion rate calculation and interpretation. For this reason, we do not include these basins in our regression analysis.

Sample ^{26}Al/^{10}Be ratios from the Olympic Mountains mostly vary between 8.5 ± 3.5 (2σ) and 4.7 ± 1.6 (2σ) (Table 3 and Fig. 4). Nearly all samples have ^{26}Al/^{10}Be ratios that are statistically indistinguishable from the expected naturally occurring ratio (6.75; Balco et al., 2008) (Table 3 and Fig. 4), suggesting that the sediments in our samples record a relatively simple erosion rate history over the integration time. As such, there is no significant influence of reworking older sediments in our measurements. Furthermore, because our erosion rate calculations assume a natural production rate ratio of 6.75, and our measured ratios are mostly indistinguishable from this value, ^{10}Be and ^{26}Al derived erosion rates are statistically indistinguishable, though the ^{26}Al derived rates are much less precise (Table 3). Two samples from Mount Olympus basins, WA1519 and WA1523, have much lower ratios.

Deleted:)

Snow shielding can reduce production rates, and therefore, reduce calculated erosion rates by up to 16% in the core of the range, but only ~3% reduction is found in lower elevation basins on the western flank (Table S3). While it is difficult to assess our snow shielding estimates, we note the relative effect on erosion rates is similar to those based on snow-depth measurements within other snowy orogens (Wittmann et al., 2007, Norton et al., 2010, Scherler et al., 2013).

4.3 Isotopic equilibrium modeling

As seen in Eq. 2 the likelihood of being in isotopic equilibrium for any cosmogenic radionuclide is mostly controlled by the time since deglaciation and the local erosion rate (assuming an inheritance of zero). Figure 5 illustrates that quickly eroding terrains more quickly remove ice-shielded materials, and thus, these terrains can each a new equilibrium state faster after the ice recedes. In fact, our model output suggests that at relatively low erosion rates (~100 m/Myr), terrains can achieve isotopic equilibrium in a few thousand years. These results suggest that the cosmogenic nuclide inventories from many glaciated landscapes on Earth could record accurate erosion rates (barring other complicating factors).

4.4 Relationships between erosion rates and basin parameters

Our best-fit curve (MSWD = 17) suggests the observed relationship between hillslope gradient and erosion is controlled by a critical slope value of 37° and a rate constant of 250 m/Myr (Fig. 6B). These parameters fit our data considerably better than the previous boundary conditions suggested by Montgomery and Brandon (2002) for the Olympic Mountains (S_c = 40°, K = 500 m/Myr, MSWD = 54). Our regressions also record a limited local relief of 1820 m (K = 0.24 m/Myr, MSWD = 4.3) (Fig. 5A). These parameters are also different than those of Montgomery and Brandon (2002) based on rates from low-temperature thermochronometry (R_c = 1500, K = 0.25 m/Myr, MSWD = 13). Regressions from the least-squares technique shows a best-fit, nearly-linear model (i.e. the exponent is 0.98) for the relationship between erosion and channel steepness (Fig. 5C). The least-squares technique demonstrates that there is no strong linear or non-linear relationship between erosion and precipitation across the range (Fig. 5D).

5 Discussion

5.1 Reliability of cosmogenic erosion rates in the glaciated Olympic Mountains

While there are still a few minor extant valley/cirque glaciers, the Last Glacial Maximum occurred in the Olympics Mountains ~17 ka (Thackray, 2008). Therefore, most of our samples should largely reflect post-glacial erosion rates. Our isotopic equilibrium model results show that even the slowest eroding landscapes in the Olympic Mountains could achieve isotopic equilibrium within ~3000 yrs (Fig. 5). Furthermore, the slowest eroding basins from the western flank of the range did not contain valley glaciers during the LGM (Thackray, 2001), and thus, these samples are even less likely to violate the isotopic equilibrium assumption. The most recently deglaciated portions of the range are in the rugged core, where erosion rates are also higher, and where some landscapes can reach isotopic equilibrium in less than 1500 yrs (Fig. 5).

In landscapes where the cosmogenic nuclide inventories are a function of constant exposure or constant erosion, the ratio of ^{26}Al to ^{10}Be within sediments can be predicted based on the modeled (Lal, 1991, Balco et al., 2008) or measured (Corbett et al., 2017) ratios. Recent studies suggest that our samples should have natural ^{26}Al/^{10}Be ratios of ~6.75 (Balco et al., 2008), a value that is very close to most of our measured ratios (Figure 4). Therefore, we find it unlikely that sediment storage and reworking (e.g. from terraces or moraines) has violated our assumptions that modern sediments record a representative sample of all sediment in the basin. If anomalously low concentration quartz was introduced into our samples via incision of older deposits (glacial or fluvial), we would expect to see depressed ^{26}Al/^{10}Be ratios. Similar to previous work (Belmont et al, 2007) we have assumed that there is no risk to calculated erosion rates due to quartz infertility or proportional quartz sourcing from all parts of our basins in the Olympic Mountains. While there are some quartz-free lithologies in the range, these rocks are a minor occurrence the in Olympic Subduction Complex, and we have avoided sampling the Coast Range Terrane completely. In locations where nested catchments are found, erosion rates are with error of each other, suggesting a proportional scouring of quartz from all parts of even the largest sampled basin (compare WA1526, DEN101, and DEN106).

5.2 Interpreting relationships between erosion and basin metrics

In landscapes with high fluvial and/or glacial erosion, soil production and hillslope transport may not be able to adjust to channel incision. In such a case, hillslope angles steepen and tend toward a threshold that is controlled by the strength of the material (Schmidt and Montgomery, 1995). Once hillslopes reach such a threshold, increases in erosion can only occur with a commensurate increase in hillslope failure (Burbank et al., 1996), and the form of these hillslopes are no longer sensitive to changes in erosion. However, the gradients of channels in these very steep landscapes are generally much lower than the internal angel of friction, and as such, still have the capacity to adjust to increases in erosion rate. Therefore, it has been suggested that the morphology of channels is a more robust metric to detect erosion rate variations (Ouimet et al., 2009, DiBiase et al., 2010).

Our data show that basin-averaged hillslope gradients cease to increase in basins eroding faster than ~300 m/Myr Fig. 6B). This limit has been observed in many other landscapes around the world (DiBiase et al., 2010, Ouimet et al., 2009, Montgomery and Brandon, 2002, Binnie et al., 2007). Basin-averaged hillslope angle values tend to reach a maximum around 34°, as also shown by Montgomery (2001) using 100 km^2 grids across the Olympic range. The extent to which these threshold hillslope angles are indicative of rock uplift rates or glacial modification is not completely clear. While it is possible that the weak lithologies and fast erosion rates of the Olympic Mountains may be setting these threshold hillslopes, it has also been documented that hillslope angles have likely been increased throughout the range via glaciers widening valleys (Montgomery, 2002, Adams and Ehlers, 2017), or eroding headward and migrating ridge tops (Adams and Ehlers, 2017).

Deleted: recessional

Deleted: this

Deleted: Most

Deleted: r

Deleted: ly

Deleted: .

Deleted: Based on our measured ^{26}Al/^{10}Be ratios

Deleted: ,

Deleted: or through deep landslides,

Similarly, basin-averaged local relief values do not exceed ~1350 m despite increasing erosion rates (Fig. 6A). This apparent threshold relief may be due to the influence of the glacial buzzsaw effect, whereby efficiently eroding alpine glaciers have controlled the mean and range of elevations during the Plio-Pleistocene. If these local relief values are limited due to glacial incision, then this would be a transient topographic signal, and imply that local relief could have been higher in the past. As such, we do not suggest that the non-linear fit parameters for hillslope and local relief data presented here are related to topographic steady-state conditions; however, our fit parameters are not very different from those relating topography to long-term erosion rates (Montgomery and Brandon, 2002). Glaciers may have also reduced channel steepness values while active in the Plio-Pleistocene by incising into channel floors more deeply than rivers had previously (Adams and Ehlers, 2017). This effect may be seen in the apparent limit of channel steepness around 160 $m^{0.9}$ (Figure 6C).

What is clear from these regressions is that in as much as relationships between modern topography and erosion exist based on thermochronometric data in the Olympic Mountains (Montgomery and Brandon, 2002), so do relationships between modern topography and detrital cosmogenic erosion rates. One advantage to using detrital studies is the obvious choice for an erosion integration area (i.e. the average erosion rate is integrated across the area of the sampled basin), as opposed to selecting a given area around a specific point in the landscape for a bedrock sample. Indeed, subtle changes in the sampling area throughout the Olympic Mountains can have a large influence on the calculated topographic metric (i.e. changing the radius of a circle around a point can add topography across a drainage divide). However, there is a greater uncertainty regarding the integration timescale of cosmogenic rates in that it can often only be assumed that rates only integrate over hundreds to thousands of years. Our analyses provide good evidence for relationships between topographic metrics and basin-average erosion rates, which are likely the result of long-lived Miocene tectonics (Brandon et al., 1998), and Plio-Pleistocene climate change (e.g. hillslope gradient, local relief, channel steepness) (Porter, 1964, Montgomery and Greenberg, 2000, Montgomery, 2002, Adams and Ehlers, 2017). The key question remaining for this study area, and similarly glaciated and tectonically active orogens elsewhere is - what are the controls on post-glacial erosion rates?

5.2 Orogenic processes governing erosion rates

With our new and previously published erosion rates, we have made several important observations in the previous sections that we elaborate on below. These observations are: 1) There is no relationship between precipitation and Holocene erosion rates across the range (Fig. 6D). 2) Basins with similar topographic characteristics have equivalent erosion rates, even across the range divide where glacial size changed drastically (compare black and grey samples in Fig. 6). 3) It is apparent from our regressions there are non-linear relationships with local relief, channel steepness and hillslope angle, and Holocene erosion rates (Fig. 6). In tectonically active and previously glaciated mountain ranges there are three common orogenic processes that are most often suggested to dominate Holocene erosion rate patterns: climate gradients (Carretier et al., 2013, Olen et al., 2016), glacial modification of the landscape (Moon et al., 2011, Glotzbach et al., 2013), and patterns of tectonic rock uplift (Adams et al., 2016, Scherler et al., 2013, Godard et al., 2014). In the following we explore the relevance and applicability of these explanations to our data set.

First, we find it highly unlikely that a precipitation gradient similar to the modern has a significant control on recent erosion rates. There is no clear relationship between modern precipitation and erosion rates (Fig. 6D). Even in the neighboring, glaciated Cascade Range (~70 km to the east of the Olympic Mountains) where the modern precipitation gradient is not as large, there is a strong linear relationship suggesting erosion scales with precipitation over diverse timescales, thus making it an important condition for setting Holocene and older erosion rates (Moon et al., 2011, Reiners et al., 2003).

Second, our data do not suggest that destabilization of the landscape via glacial incision has played a primary role in setting the Holocene erosion pattern. Despite the significant gradients in the Pleistocene ELA (Fig. 2E) and the change in glacier size, and the estimated higher erosion Quaternary erosion rates (Michel et al., 2018) across the range divide (Fig. 1B), there is no statistical difference between the erosion rates across the range divide for basins of similar topographic characteristics (Fig. 2 and Fig. 5A, 5B, 5C), and there is a very weak correlation between ELA and erosion rates (Fig. S2). However, it has been observed that Plio-Pleistocene glaciers widened valleys in the Olympic Mountains (Montgomery, 2002, Adams and Ehlers, 2017), which led to the lengthening and steepening of hillslopes throughout the range. In the nearby Cascade Range, similar valley widening has led to hillslopes with higher likelihoods for failure (Moon et al., 2011). Unlike in the Olympic Mountains, findings from the Cascades suggest that the range was heavily influenced by glacial incision to an extent that the topographic form largely reflects relict glacial processes, and as a result, Holocene erosion rates are more likely to be correlated with precipitation in these landscapes further from equilibrium. Our analysis suggests that the changes in the landscape due to Plio-Pleistocene glaciation in the Olympic Mountains likely only steepened relatively small areas of hillslopes of landscapes relative to the already steep conditions imposed by high rock uplift and erosion rates. Similarly, glacial incision may have only influenced small relatively small portions of the channel network and range relief, which might appear as threshold values of channel steepness and local relief, or simply to make the distributions of these parameters within a basin more complex. Therefore, the landscapes examined the Olympics may have been only moderately perturbed by Plio-Pleistocene glacial incision, and they may still record a relatively close balance between recent erosion rates and rock uplift.

The balance between post-glacial erosion and longer-lived rock uplift depends on whether post-glacial climate conditions (e.g. increase or decrease in precipitation), or topographic perturbations (e.g. hillslope steeping or channel shallowing) have changed the activity of extant surface processes. There are many examples of ranges where there have been significant changes to topography (Brardinoni and Hassan, 2006; 2007; Brocklehurst and Whipple, 2007; Glotzbach et al., 2013; Hobley et al., 2010; Montgomery, 2001; Robl et al., 2008) and erosion during and after glaciation (Moon et al., 2011, Reiners et al., 2003, Christeleit et al., 2017), and others where such changes are not clearly observed (Thomson et al., 2010). More generally, these changes were explored in a coupled ice dynamic/landscape evolution model testing the modification of topography and erosion rates due to alpine glaciation (Yanites and Ehlers, 2012). The results of these numerical models suggest that the degree of erosion change before and after glaciation is a function of regional temperature and the rock uplift rate. These two parameters control the glaciers ability concentrate elevations at or near the ELA were ice erodes most efficiently. If too much or too little of the landscape lies above the ELA, then glacial erosion is not very efficient and little topographic perturbation occurs. In these landscapes, erosion rates may change during glacial periods, but interglacial erosion rates return to near rock uplift rates, as before. In the cases where glaciers were very effective agents of erosion, relief (on hillslopes or channels) is reduced during glaciation (Whipple et al., 1999; Adams and Ehlers, 2017), and post-glacial erosion rates can be lower than pre-glacial, and vice versa. As such, there is a sweet spot within mountain range conditions where glaciers are more efficient, and furthermore, even when glaciers are efficient it cannot be assumed how post-glacial rates might change. To put it another way, it should be assumed that landscapes will respond differently alpine glaciation depending on climate and topographic conditions before and after glaciation.

Figure 7 illustrates the similarity of the trends in other rock uplift rate proxies, and the cosmogenic erosion rates presented here in a direction parallel to the convergence across the Olympic Mountain range. When our new Holocene erosion rate pattern is compared with older patterns of estimated rock uplift rates (Fig. 7), there are a few apparent mismatches. In some locations, our rates are higher and lower than rock uplift rates (as might be expected in post-glacial landscapes), but

Deleted: across the range divide (Fig. 1B)

Moved down [3]: Our observations are in line with previous authors who have highlighted importance of subduction zone dynamics for setting the pace and pattern of erosion in the Olympic Mountains (Brandon and Vance, 1992;Pazzaglia and Brandon, 2001;Batt et al., 2001;Brandon et al., 1998;Stolar et al., 2007).

Deleted: Whether

Moved down [2]: Taken together, we suggest that the Holocene erosion rates (Fig. 2E), mean elevation, local relief (Fig. 2B), and channel steepness (Fig. 2D) observed in the Olympic Mountains most closely record a rock uplift pattern that increases from the low-relief flanks to the rugged core of the range (Fig. 7), similar to what has been shown in other datasets (Brandon et al., 1998;Batt et al., 2001;Pazzaglia and Brandon, 2001).

Moved down [1]: 6 Conclusions

Deleted: Whether

Deleted: rates balance

Deleted: rates is strongly influenced by

Deleted: changes

Deleted: as compared to before the onset of glaciation

Deleted: Simon H

Deleted: D. R.

Deleted: this study

Moved (insertion) [4]

overall the pattern of increasing rates from the flanks to the core of the range is consistent between these datasets. Adams and Ehlers (2017) and Michel et al. (2018) proposed that a spatial pattern of rock uplift similar to the one described above was consistent with the observations of the bend in the subducting Juan de Fuca plate at the Cascadia subduction zone and the dome of accreted sediments in the core of the Olympic Mountains, which form the east-plunging Olympic Anticline (Brandon and Calderwood, 1990). This pattern of focused rock uplift and erosion is also predicted for the geometry of the curved subducting Juan de Fuca plate (Crosson and Owens, 1987, Bendick and Ehlers, 2014). We suggest this long-lasting pattern is primarily controlled by tectonic forces, and while the Plio-Pleistocene alpine glaciers of the Olympic Mountains have not radically altered the topography enough to drastically change the pattern of erosion.

6 Conclusions

Taken together, we suggest that the Holocene erosion rates (Fig. 2E), mean elevation, local relief (Fig. 2B), and channel steepness (Fig. 2D) observed in the Olympic Mountains most closely record a rock uplift pattern that increases from the low-relief flanks to the rugged core of the range (Fig. 7), similar to what has been shown in other datasets (Brandon et al., 1998, Batt et al., 2001, Pazzaglia and Brandon, 2001). Our interpretations are in line with previous authors who have highlighted the importance of subduction zone dynamics for setting the pace and pattern of erosion in the Olympic Mountains (Brandon and Vance, 1992, Pazzaglia and Brandon, 2001, Batt et al., 2001, Brandon et al., 1998, Stolar et al., 2007). This result may be unexpected given the glacial impact that has been previously documented throughout the range (Porter, 1964; Montgomery and Greensburg, 2000; Montgomery, 2002; Adams and Ehlers, 2017), and further described in this manuscript. However, the Plio-Pleistocene glaciers impact on small- and range-scale may have been limited in the Olympic Mountains because large portions of the range may have already been at near-threshold conditions before glaciation (Montgomery, 2001), or a small proportion of the range was focused at the ELA during glacial periods. As such, post-glacial erosion rates exhibit the same spatial patterns and magnitudes as longer-term estimates. The alpine glaciers of the Olympic Mountains have left behind very scenic, sculpted landscapes, but these landscapes may have not been as significantly altered as once thought, at least not enough to drastically change post-glacial erosion.

Acknowledgments

We thank Lorenz Michel, Holger Sprengel, Roger Hoffman, Bill Baccus, Jerry Freilich and the Olympic National Park Rangers for assistance while in the field and logistics. We also acknowledge the help of Christine Lempe, Hella Whitmann, Mirjam Schaller, Dagmar Kost, and Jessica Starke with the processing of these stubborn samples. We are grateful to Karl Lang, Matthew Jungers, and Mirjam Schaller for fruitful discussions. Frank Pazzaglia, George Hilley, Paul Bierman, and two anonymous reviewers are thanked for their comments on an earlier version of this manuscript. This work was supported by a European Research Council (ERC) Consolidator Grant number 615703 to T. Ehlers. All data used in the manuscript are freely available in either the manuscript tables or online supplemental material. The authors declare that they have no conflict of interest.

References

Adams, B. and Ehlers, T. (2017) 'Deciphering topographic signals of glaciation and rock uplift in an active orogen: a case study from the Olympic Mountains, USA', *Earth Surface Processes and Landforms*.

Adams, B., Whipple, K., Hodges, K. and Heimsath, A. (2016) 'In situ development of high-elevation, low-relief landscapes via duplex deformation in the Eastern Himalayan hinterland, Bhutan', *Journal of Geophysical Research: Earth Surface*.

Deleted: We suggest this long-lasting pattern is primarily controlled by tectonic forces, and while the Plio-Pleistocene alpine glaciers of the Olympic Mountains have created a wonderfully sculpted landscape, they have not radically altered the topography enough to drastically change the pattern of erosion.

Deleted:

Moved up [4]: When our new Holocene erosion rate pattern is compared with older patterns of estimated rock uplift rates (Fig. 7), there are a few apparent mismatches. In some locations, our rates are higher and lower than rock uplift rates (as might be expected in post-glacial landscapes), but overall the pattern of increasing rates from the flanks to the core of the range is consistent between these datasets. We suggest this long-lasting pattern is primarily controlled by tectonic forces, and while the Plio-Pleistocene alpine glaciers of the Olympic Mountains have created a wonderfully sculpted landscape, they have not radically altered the topography enough to drastically change the pattern of erosion.

Deleted:

Moved (insertion) [1]

Moved (insertion) [2]

Field Code Changed

Moved (insertion) [3]

Deleted: observations

Field Code Changed

Deleted: is

Deleted: his

Ahnert, F. (1970) 'Functional relationships between denudation, relief, and uplift in large mid-latitude drainage basins', *American Journal of Science,* 268(3), pp. 243-&.
Anderson, R. S., Molnar, P. and Kessler, M. A. (2006) 'Features of glacial valley profiles simply explained', *Journal of Geophysical Research: Earth Surface,* 111(F1), pp. F01004.
Anderson, R. S., Repka, J. L. and Dick, G. S. (1996) 'Explicit treatment of inheritance in dating depositional surfaces using in situ 10Be and 26Al', *Geology,* 24(1), pp. 47-51.
Balco, G., Stone, J. O., Lifton, N. A. and Dunai, T. J. (2008) 'A complete and easily accessible means of calculating surface exposure ages or erosion rates from (10)Be and (26)Al measurements', *Quaternary Geochronology,* 3(3), pp. 174-195.
Batt, G. E., Brandon, M. T., Farley, K. A. and Roden-Tice, M. (2001) 'Tectonic synthesis of the Olympic Mountains segment of the Cascadia wedge, using two-dimensional thermal and kinematic modeling of thermochronological ages', *Journal of Geophysical Research: Solid Earth,* 106(B11), pp. 26731-26746.
Belmont, P., Pazzaglia, F. and Gosse, J. C. (2007) 'Cosmogenic 10 Be as a tracer for hillslope and channel sediment dynamics in the Clearwater River, western Washington State', *Earth and Planetary Science Letters,* 264(1), pp. 123-135.
Bendick, R. and Ehlers, T. A. (2014) 'Extreme localized exhumation at syntaxes initiated by subduction geometry', *Geophysical Research Letters,* 41(16), pp. 5861-5867.
Bierman, P. and Steig, E. J. (1996) 'Estimating rates of denudation using cosmogenic isotope abundances in sediment', *Earth Surface Processes and Landforms,* 21(2), pp. 125-139.
Binnie, S. A., Phillips, W. M., Summerfield, M. A. and Fifield, L. K. (2007) 'Tectonic uplift, threshold hillslopes, and denudation rates in a developing mountain range', *Geology,* 35(8), pp. 743-746.
Brandon, M. T. and Calderwood, A. R. (1990) 'High-pressure metamorphism and uplift of the Olympic subduction complex', *Geology,* 18(12), pp. 1252-1255.
Brandon, M. T., Roden-Tice, M. K. and Garver, J. I. (1998) 'Late Cenozoic exhumation of the Cascadia accretionary wedge in the Olympic Mountains, northwest Washington State', *Geological Society of America Bulletin,* 110(8), pp. 985-1009.
Brandon, M. T. and Vance, J. A. (1992) 'Tectonic evolution of the Cenozoic Olympic subduction complex, Washington State, as deduced from fission track ages for detrital zircons', *American Journal of Science,* 292(8), pp. 565-636.
Brardinoni, F. and Hassan, M. A. (2006) 'Glacial erosion, evolution of river long profiles, and the organization of process domains in mountain drainage basins of coastal British Columbia', *Journal of Geophysical Research: Earth Surface,* 111(F1).
Brardinoni, F. and Hassan, M. A. (2007) 'Glacially induced organization of channel-reach morphology in mountain streams', *Journal of Geophysical Research: Earth Surface,* 112(F3).
Brocklehurst, S. H. and Whipple, K. X. (2002) 'Glacial erosion and relief production in the Eastern Sierra Nevada, California', *Geomorphology,* 42(1-2), pp. 1-24.
Brocklehurst, S. H. and Whipple, K. X. (2004) 'Hypsometry of glaciated landscapes', *Earth Surface Processes and Landforms,* 29(7), pp. 907-926.
Brocklehurst, S. H. and Whipple, K. X. (2006) 'Assessing the relative efficiency of fluvial and glacial erosion through simulation of fluvial landscapes', *Geomorphology,* 75(3-4), pp. 283-299.
Brocklehurst, S. H. and Whipple, K. X. (2007) 'Response of glacial landscapes to spatial variations in rock uplift rate', *Journal of Geophysical Research: Earth Surface,* 112(F2), pp. F02035.
Brown, E. T., Stallard, R. F., Larsen, M. C., Raisbeck, G. M. and Yiou, F. (1995) 'Denudation rates determined from the accumulation of in situ-produced 10Be in the Luquillo Experimental Forest, Puerto Rico', *Earth and Planetary Science Letters,* 129(1-4), pp. 193-202.
Brozović, N., Burbank, D. W. and Meigs, A. J. (1997) 'Climatic limits on landscape development in the northwestern Himalaya', *Science,* 276(5312), pp. 571-574.
Burbank, D. W., Leland, J., Fielding, E., Anderson, R. S., Brozovic, N., Reid, M. R. and Duncan, C. (1996) 'Bedrock incision, rock uplift and threshold hillslopes in the northwestern Himalayas', *Nature,* 379(6565), pp. 505-510.
Carretier, S., Regard, V., Vassallo, R., Aguilar, G., Martinod, J., Riquelme, R., Pepin, E., Charrier, R., Herail, G., Farias, M., Guyot, J. L., Vargas, G. and Lagane, C. (2013) 'Slope and climate variability control of erosion in the Andes of central Chile', *Geology,* 41(2), pp. 195-198.
Christeleit, E. C., Brandon, M. T. and Shuster, D. L. (2017) 'Miocene development of alpine glacial relief in the Patagonian Andes, as revealed by low-temperature thermochronometry', *Earth and Planetary Science Letters,* 460, pp. 152-163.
Corbett, L. B., Bierman, P. R., Rood, D. H., Caffee, M. W., Lifton, N. A. and Woodruff, T. E. (2017) 'Cosmogenic 26Al/10Be surface production ratio in Greenland', *Geophysical Research Letters,* 44(3), pp. 1350-1359.
Crosson, R. and Owens, T. (1987) 'Slab geometry of the Cascadia subduction zone beneath Washington from earthquake hypocenters and teleseismic converted waves', *Geophysical Research Letters,* 14(8), pp. 824-827.

Daly, C., Neilson, R. P. and Phillips, D. L. (1994) 'A statistical topographic model for mapping climatological precipitation over mountainous terrain', *Journal of Applied Meteorology,* 33(2), pp. 140-158.
DeMets, C. and Dixon, T. H. (1999) 'New kinematic models for Pacific-North America motion from 3 Ma to present, I: Evidence for steady motion and biases in the NUVEL-1A model', *Geophysical Research Letters,* 26(13), pp. 1921-1924.
DiBiase, R. A., Whipple, K. X., Heimsath, A. M. and Ouimet, W. B. (2010) 'Landscape form and millennial erosion rates in the San Gabriel Mountains, CA', *Earth and Planetary Science Letters,* 289(1), pp. 134-144.
Dunne, J., Elmore, D. and Muzikar, P. (1999) 'Scaling factors for the rates of production of cosmogenic nuclides for geometric shielding and attenuation at depth on sloped surfaces', *Geomorphology,* 27(1), pp. 3-11.
Ehlers, T. A., Farley, K. A., Rusmore, M. E. and Woodsworth, G. J. (2006) 'Apatite (U-Th)/He signal of large-magnitude accelerated glacial erosion, southwest British Columbia', *Geology,* 34(9), pp. 765-768.
Flint, J. (1974) 'Stream gradient as a function of order, magnitude, and discharge', *Water Resources Research,* 10(5), pp. 969-973.
Glotzbach, C., Beek, P., Carcaillet, J. and Delunel, R. (2013) 'Deciphering the driving forces of erosion rates on millennial to million-year timescales in glacially impacted landscapes: An example from the Western Alps', *Journal of Geophysical Research: Earth Surface,* 118(3), pp. 1491-1515.
Godard, V., Bourlès, D. L., Spinabella, F., Burbank, D. W., Bookhagen, B., Fisher, G. B., Moulin, A. and Léanni, L. (2014) 'Dominance of tectonics over climate in Himalayan denudation', *Geology*, pp. G35342. 1.
Godard, V., Burbank, D., Bourlès, D., Bookhagen, B., Braucher, R. and Fisher, G. (2012) 'Impact of glacial erosion on ^{10}Be concentrations in fluvial sediments of the Marsyandi catchment, central Nepal', *Journal of Geophysical Research: Earth Surface,* 117(F3), pp. F03013.
Gosse, J. C. and Phillips, F. M. (2001) 'Terrestrial in situ cosmogenic nuclides: theory and application', *Quaternary Science Reviews,* 20(14), pp. 1475-1560.
Granger, D. E., Kirchner, J. W. and Finkel, R. (1996) 'Spatially averaged long-term erosion rates measured from in situ-produced cosmogenic nuclides in alluvial sediment', *Journal of Geology,* 104(3), pp. 249-257.
Hack, J. T. (1957) 'Studies of longitudinal stream profiles in Virginia and Maryland'.
Hallet, B., Hunter, L. and Bogen, J. (1996) 'Rates of erosion and sediment evacuation by glaciers: A review of field data and their implications', *Global and Planetary Change,* 12(1-4), pp. 213-235.
Herman, F., Seward, D., Valla, P. G., Carter, A., Kohn, B., Willett, S. D. and Ehlers, T. A. (2013) 'Worldwide acceleration of mountain erosion under a cooling climate', *Nature,* 504(7480), pp. 423-+.
Hobley, D. E., Sinclair, H. D. and Cowie, P. A. (2010) 'Processes, rates, and time scales of fluvial response in an ancient postglacial landscape of the northwest Indian Himalaya', *Geological Society of America Bulletin,* 122(9-10), pp. 1569-1584.
Koppes, M. N. and Montgomery, D. R. (2009) 'The relative efficacy of fluvial and glacial erosion over modern to orogenic timescales', *Nature Geoscience,* 2(9), pp. 644-647.
Lal, D. (1991) 'COSMIC-RAY LABELING OF EROSION SURFACES - INSITU NUCLIDE PRODUCTION-RATES AND EROSION MODELS', *Earth and Planetary Science Letters,* 104(2-4), pp. 424-439.
MacGregor, K. R., Anderson, R., Anderson, S. and Waddington, E. (2000) 'Numerical simulations of glacial-valley longitudinal profile evolution', *Geology,* 28(11), pp. 1031-1034.
Meigs, A. and Sauber, J. (2000) 'Southern Alaska as an example of the long-term consequences of mountain building under the influence of glaciers', *Quaternary Science Reviews,* 19(14), pp. 1543-1562.
Michel, L., Ehlers, T. A., Glotzbach, C., Adams, B. A. and Stübner, K. (2018) 'Tectonic and glacial contributions to focused exhumation in the Olympic Mountains, Washington, USA', *Geology*.
Montgomery, D. R. (2001) 'Slope distributions, threshold hillslopes, and steady-state topography', *American Journal of Science,* 301(4-5), pp. 432-454.
Montgomery, D. R. (2002) 'Valley formation by fluvial and glacial erosion', *Geology,* 30(11), pp. 1047-1050.
Montgomery, D. R. and Brandon, M. T. (2002) 'Topographic controls on erosion rates in tectonically active mountain ranges', *Earth and Planetary Science Letters,* 201(3-4), pp. 481-489.
Montgomery, D. R. and Greenberg, H. M. (2000) 'Local relief and the height of Mount Olympus', *Earth Surface Processes and Landforms,* 25(4), pp. 385-396.
Moon, S., Chamberlain, C. P., Blisniuk, K., Levine, N., Rood, D. H. and Hilley, G. E. (2011) 'Climatic control of denudation in the deglaciated landscape of the Washington Cascades', *Nature Geoscience,* 4(7), pp. 469-473.
Norton, K. P., Abbühl, L. M. and Schlunegger, F. (2010) 'Glacial conditioning as an erosional driving force in the Central Alps', *Geology,* 38(7), pp. 655-658.
Olen, S. M., Bookhagen, B. and Strecker, M. R. (2016) 'Role of climate and vegetation density in modulating denudation rates in the Himalaya', *Earth and Planetary Science Letters,* 445, pp. 57-67.
Ouimet, W. B., Whipple, K. X. and Granger, D. E. (2009) 'Beyond threshold hillslopes: Channel adjustment to base-level fall in tectonically active mountain ranges', *Geology,* 37(7), pp. 579-582.

Pazzaglia, F. J. and Brandon, M. T. (2001) 'A fluvial record of long-term steady-state uplift and erosion across the Cascadia forearc high, western Washington State', *American Journal of Science,* 301(4-5), pp. 385-431.
Portenga, E. W. and Bierman, P. R. (2011) 'Understanding Earth's eroding surface with 10 Be', *GSA Today,* 21(8), pp. 4-10.
Portenga, E. W., Bierman, P. R., Duncan, C., Corbett, L. B., Kehrwald, N. M. and Rood, D. H. (2014) 'Erosion rates of the Bhutanese Himalaya determined using in situ-produced 10 Be', *Geomorphology*.
Porter, S. C. (1964) 'Composite Pleistocene snow line of Olympic Mountains and Cascade Range, Washington', *Geological Society of America Bulletin,* 75(5), pp. 477-481.
Reiners, P. W., Ehlers, T. A., Mitchell, S. G. and Montgomery, D. R. (2003) 'Coupled spatial variations in precipitation and long-term erosion rates across the Washington Cascades', *Nature,* 426(6967), pp. 645-647.
Robl, J., Hergarten, S. and Stüwe, K. (2008) 'Morphological analysis of the drainage system in the Eastern Alps', *Tectonophysics,* 460(1), pp. 263-277.
Roering, J. J., Kirchner, J. W., Sklar, L. S. and Dietrich, W. E. (2001) 'Hillslope evolution by nonlinear creep and landsliding: An experimental study', *Geology,* 29(2), pp. 143-146.
Scherler, D., Bookhagen, B. and Strecker, M. R. (2013) 'Tectonic control on 10Be-derived erosion rates in the Garhwal Himalaya, India', *Journal of Geophysical Research: Earth Surface*.
Schmidt, K. M. and Montgomery, D. R. (1995) 'Limits to relief', *Science,* 270(5236), pp. 617.
Shuster, D. L., Ehlers, T. A., Rusmoren, M. E. and Farley, K. A. (2005) 'Rapid glacial erosion at 1.8 Ma revealed by 4He/3He thermochronometry', *Science,* 310(5754), pp. 1668-1670.
Stolar, D., Roe, G. and Willett, S. (2007) 'Controls on the patterns of topography and erosion rate in a critical orogen', *Journal of Geophysical Research: Earth Surface,* 112(F4).
Stone, J. O. (2000) 'Air pressure and cosmogenic isotope production', *Journal of Geophysical Research: Solid Earth (1978–2012),* 105(B10), pp. 23753-23759.
Tabor, R. W. and Cady, W. M. (1978) *The structure of the Olympic Mountains, Washington: Analysis of a subduction zone.* US Govt. Print. Off.
Thackray, G. D. (2001) 'Extensive early and middle Wisconsin glaciation on the western Olympic Peninsula, Washington, and the variability of Pacific moisture delivery to the northwestern United States', *Quaternary Research,* 55(3), pp. 257-270.
Thackray, G. D. (2008) 'Varied climatic and topographic influences on Late Pleistocene mountain glaciation in the western United States', *Journal of Quaternary Science,* 23(6-7), pp. 671-681.
Thomson, S. N., Brandon, M. T., Tomkin, J. H., Reiners, P. W., Vásquez, C. and Wilson, N. J. (2010) 'Glaciation as a destructive and constructive control on mountain building', *Nature,* 467(7313), pp. 313-317.
Valla, P. G., Shuster, D. L. and van der Beek, P. A. (2011) 'Significant increase in relief of the European Alps during mid-Pleistocene glaciations', *Nature Geoscience,* 4(10), pp. 688-692.
Vance, D., Bickle, M., Ivy-Ochs, S. and Kubik, P. W. (2003) 'Erosion and exhumation in the Himalaya from cosmogenic isotope inventories of river sediments', *Earth and Planetary Science Letters,* 206(3-4), pp. 273-288.
Von Blanckenburg, F., Belshaw, N. and O'Nions, R. (1996) 'Separation of 9Be and cosmogenic 10Be from environmental materials and SIMS isotope dilution analysis', *Chemical Geology,* 129(1-2), pp. 93-99.
Whipple, K. X., Kirby, E. and Brocklehurst, S. H. (1999) 'Geomorphic limits to climate-induced increases in topographic relief', *Nature,* 401(6748), pp. 39-43.
Willenbring, J. K. and von Blanckenburg, F. (2010) 'Long-term stability of global erosion rates and weathering during late-Cenozoic cooling', *Nature,* 465(7295), pp. 211-214.
Willett, S. D. (1999) 'Orogeny and orography: The effects of erosion on the structure of mountain belts', *Journal of Geophysical Research-Solid Earth,* 104(B12), pp. 28957-28981.
Wittmann, H., von Blanckenburg, F., Kruesmann, T., Norton, K. P. and Kubik, P. W. (2007) 'Relation between rock uplift and denudation from cosmogenic nuclides in river sediment in the Central Alps of Switzerland', *Journal of Geophysical Research: Earth Surface (2003–2012),* 112(F4).
Wobus, C., Whipple, K. X., Kirby, E., Snyder, N., Johnson, J., Spyropolou, K., Crosby, B. and Sheehan, D. (2006) 'Tectonics from topography: Procedures, promise, and pitfalls', *Geological Society of America Special Papers,* 398, pp. 55-74.
Yanites, B. J. and Ehlers, T. A. (2012) 'Global climate and tectonic controls on the denudation of glaciated mountains', *Earth and Planetary Science Letters,* 325, pp. 63-75.

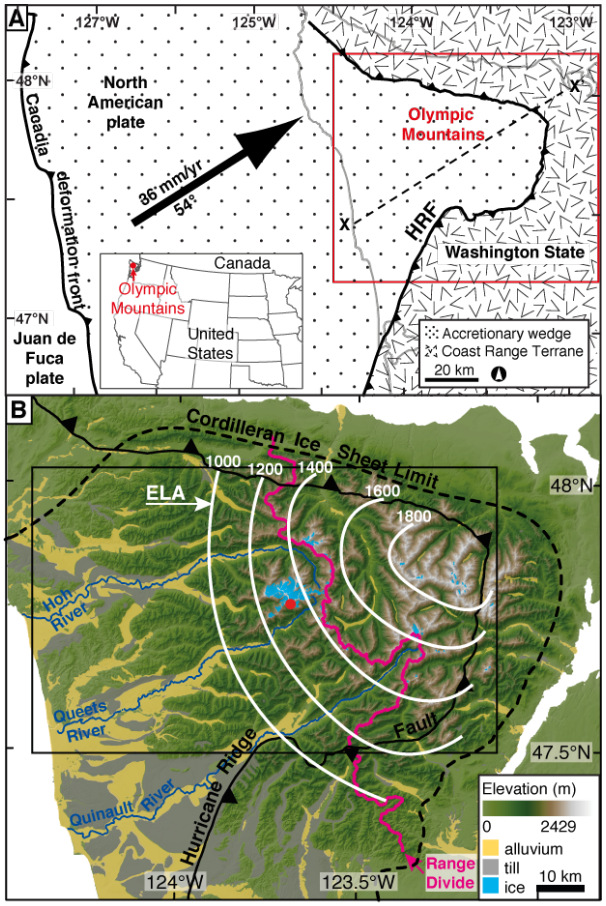

Figure 1. Topographic and geologic features of the Olympic Peninsula, Washington State, USA. A) Simplified geology based on Brandon et al. (1998). The relative velocity of the Juan de Fuca plate toward the North American plate is ~36 mm/yr with a bearing of ~54° (DeMets and Dixon, 1999). Red box denotes the extent of panel B. HRF – Hurricane Ridge Fault. Grey lines outline the coast of Washington State. Dashed black line is the cross-section line for Fig. 7. B) Elevation map of the Olympic Mountains. Ice, including extant alpine glaciers, is masked in blue. Undifferentiated Quaternary alpine glacial till and alluvial deposits are marked in grey and yellow, respectively. Contours of equilibrium line altitudes (ELA) from Porter (1964) are denoted by white lines (values shown in meters above sea level). Black box denotes the extent of Fig. 2 panels. A red dot marks Mount Olympus.

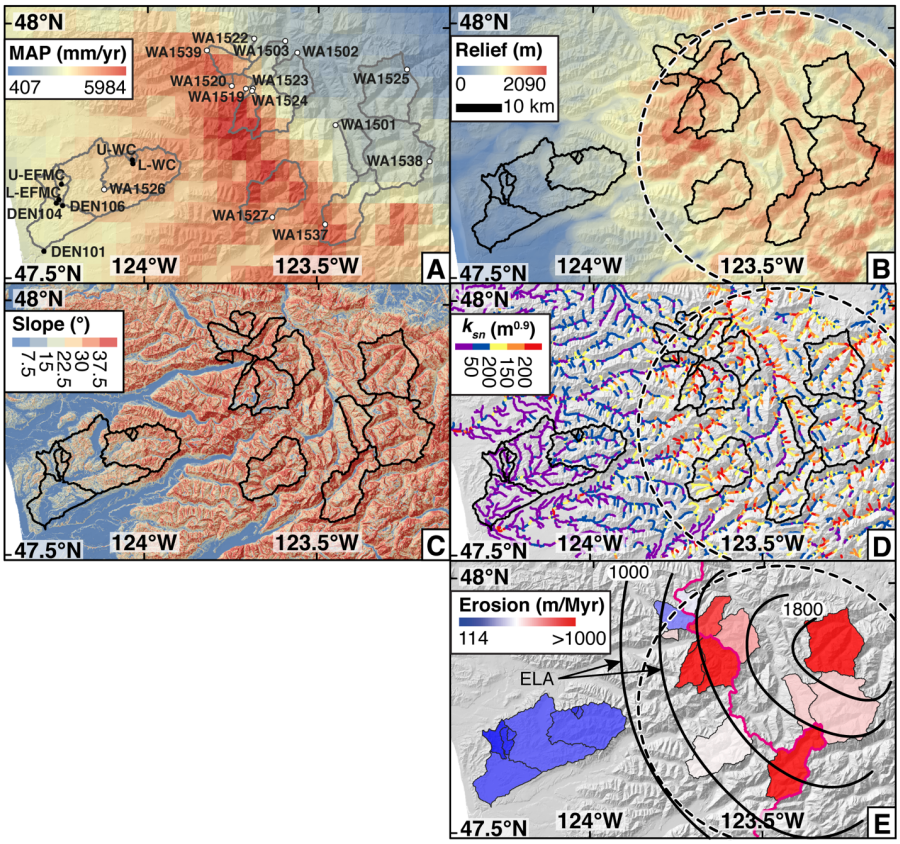

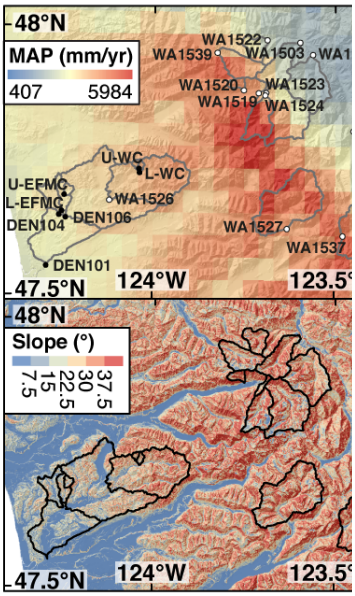

Figure 2. Attribute and erosion maps of the Olympic Mountains. Solid outlines denote the boundaries of sampled basins. High rugged core outlined in black/white dashed lines. A) Mean annual precipitation (MAP) map based on PRISM data (Daly et al., 1994). Open and closed circles mark new and previously published sample locations, respectively. B) Local relief (5-km relief) map. C) Hillslope angle map. D) Channel steepness (k_{sn}) map plotted for accumulation areas > 2 km^2. E) Basin-averaged erosion rate map. Range divide marked in magenta. Equilibrium line altitude (ELA) contours from Porter (Porter, 1964) are in black.

Deleted:

Formatted: Font:12 pt

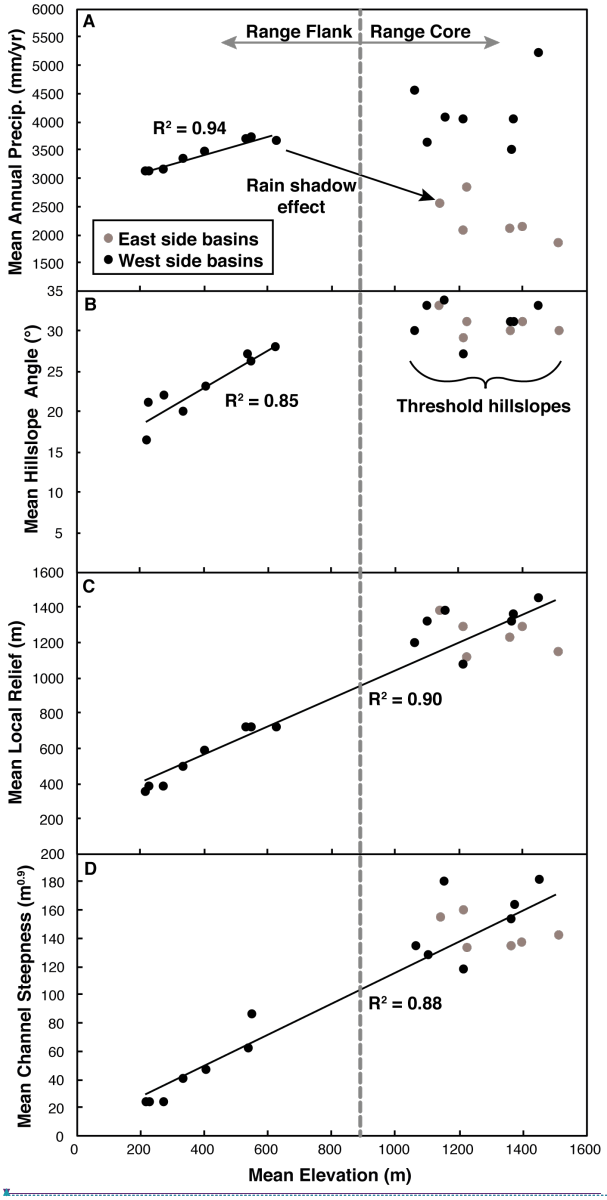

Deleted:

Formatted: Font:12 pt

Figure 3. Comparison of the mean basin elevation with other basin averaged metrics. A) Mean annual precipitation. B) Hillslope angle. C) Local relief (using a 5-km diameter circle. D) Channel steepness.

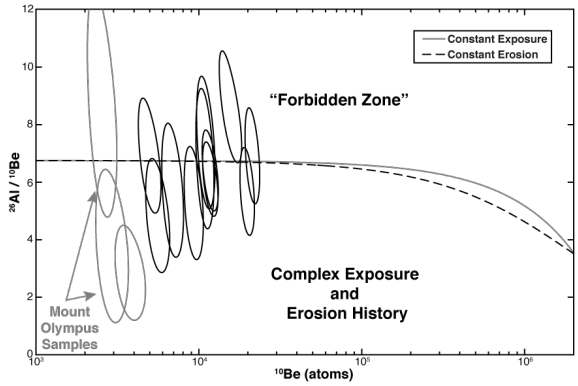

Figure 4. Erosion island plot for new Olympic Mountain samples. Each sample is represented by a 2σ error ellipse. Dashed, grey ellipses mark samples with poor ^{10}Be measurements, see text for discussion.

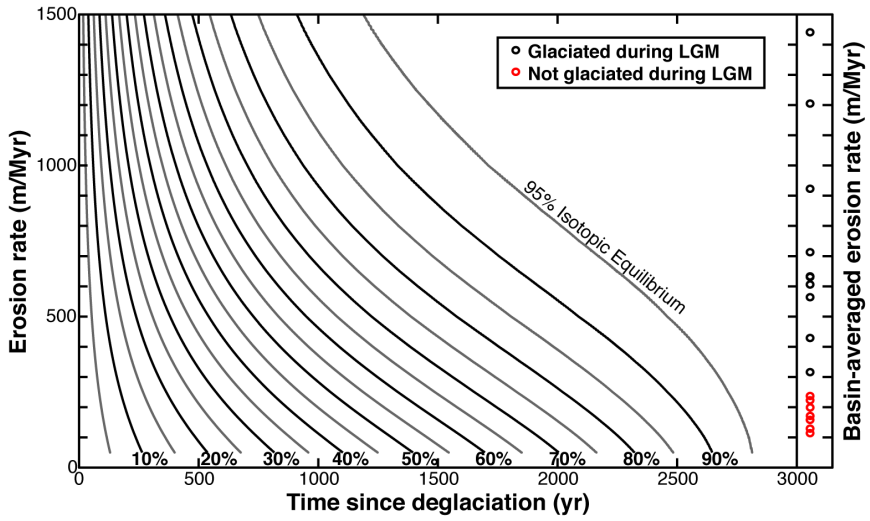

Figure 5. Predicted evolution of landscapes toward isotopic evolution after deglaciation. Black and grey lines denote 10% and 5% contour intervals, respectively. Basin-averaged erosion rates from the Olympic Mountains are shown on the right. Basins marked in red were not glaciated during the Last Glacial Maximum (LGM).

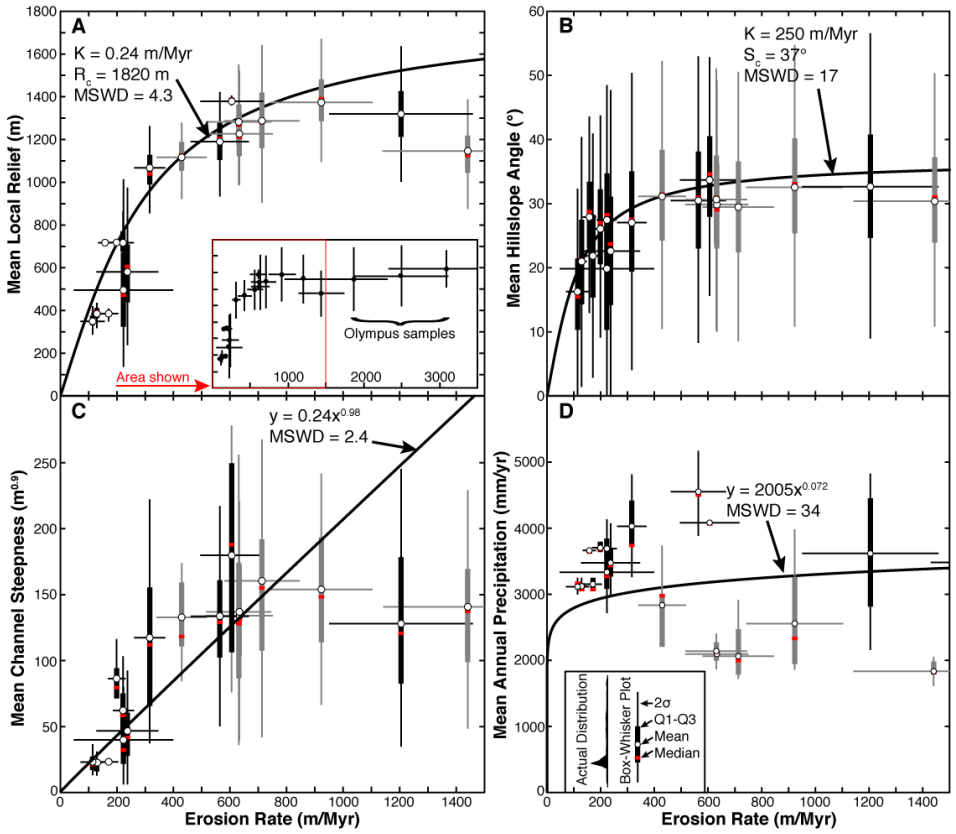

Figure 6. Plot of erosion rates with basin-averaged metrics. Due to the high degree of variation within a single basin, we have plotted basin metric data as box-and-whisker plots. Thin vertical bars denote 2 standard deviations. Thick vertical bars denote the central 50% of the data between the 1st and 3rd quartiles (Q1 and Q3). Red bars denote the medians and white circles denote means. Horizontal bars show 2σ confidence intervals on erosion rates. West and east side basins are shown in black and grey, respectively. A) Erosion rate versus mean local relief (5-km relief). Inset shows higher erosion rate samples not featured in other panels. B) Erosion rate versus mean hillslope angle. C) Erosion rate versus mean channel steepness. D) Erosion rate versus mean annual precipitation.

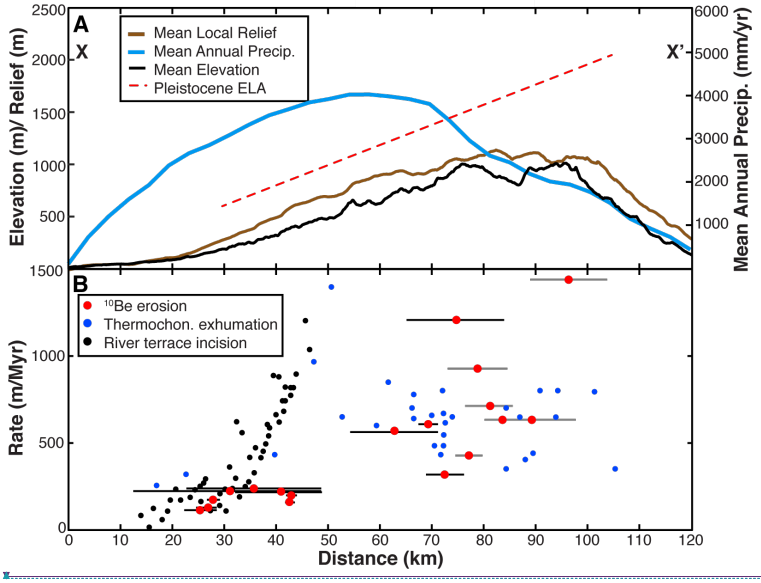

Figure 7. Comparison between estimated erosion and relief across the Olympic Mountains. A) Elevation and climate data across the Olympic Mountain range parallel to the direction of tectonic convergence (~54°). Maximum and mean elevations are shown in thin and thick black lines, respectively. Mean annual precipitation data (Daly et al., 1994) are shown in blue. Equilibrium line altitude (ELA) data (Porter, 1964) are represented by a red trend line. B) The blue circles show estimated rock uplift rates from apatite fission track data from Brandon et al. (1998). Black circles are rock uplift rate estimates from Pazzaglia and Brandon (2001) based on and river terrace incision. Basin-average erosion rates in this study are shown in red circles with bars denoting the width of the basins. See Fig. 1A for cross section location.

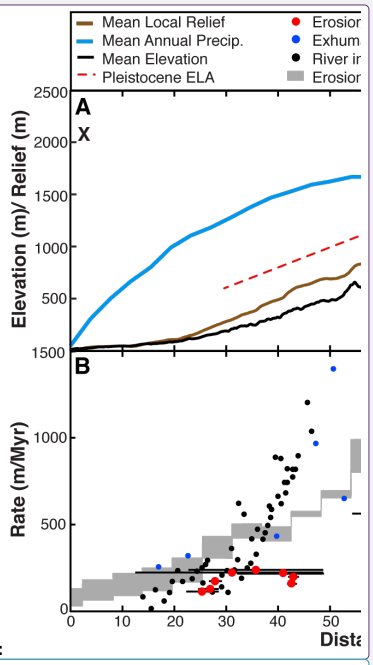

Deleted:

Formatted: Font:12 pt

Deleted: The grey envelope is the erosion pattern from Stolar et al. (2007) based on a coupled mechanical/landscape evolution model.

Table 1. Sample basin characteristics. Mean equilibrium line altitiude (ELA) based on estimates from Porter (1964). 2σ = 2 standard deviations on the mean. Curves represent simplified histograms with normalized counts . See labels below each column for minimum and maximum bin values. Basins in italics are from Belmont et al. (2007).

Sample Name	Latitude (°N)	Longitude (°W)	Area (km^2)	Range Side	ELA (m)	Elevation (m)			Mean Annual Prec. (mm/yr)		
						Mean	2σ	Histogram	Mean	2σ	Histogram
WA1501	47.810972	123.44503	48.0	East	1673	1364	646	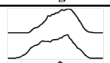	2093	220	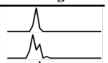
WA1502	47.948389	123.56092	66.8	East	1552	1215	786		2058	626	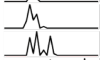
WA1503	47.969639	123.59908	40.9	East	1431	1143	800		2549	1139	
WA1519	47.878306	123.70736	114.8	West	1413	1375	762	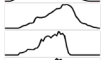	4013	2275	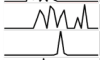
WA1520	47.885139	123.75147	6.5	West	1255	1158	570		4077	182	
WA1522	47.976972	123.68797	19.2	East	1339	1230	520	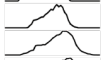	2831	911	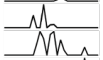
WA1523	47.876735	123.69469	74.9	West	1449	1367	692		3471	1710	
WA1524	47.876161	123.69537	35.6	West	1342	1454	810	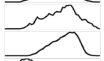	5200	1478	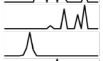
WA1525	47.916688	123.24247	133.1	East	1811	1515	636		1831	298	
WA1526	47.67787	124.11701	126.9	West	--	537	398		3686	414	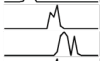
WA1527	47.62844	123.6316	115.4	West	1292	1064	652		4544	761	
WA1537	47.615017	123.47443	104.0	West	1438	1104	716	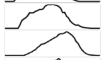	3608	1678	
WA1538	47.739067	123.17657	169.7	East	1734	1402	678		2137	440	
WA1539	*47.951718*	*123.81862*	35.6	West	1270	1215	526	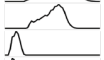	4022	949	
U-EFMC	*47.685616*	*124.23868*	3.5	West	--	275	162		3150	179	
L-EFMC	*47.653568*	*124.24006*	13.4	West	--	229	164		3118	143	
U-WC	*47.738694*	*124.04432*	1.6	West	--	629	234		3659	109	
L-WC	*47.728534*	*124.03657*	4.3	West	--	552	302		3699	176	
DEN104	*47.55637*	*124.28191*	33.8	West	--	220	158		3111	143	
DEN106	*47.644947*	*124.24263*	281.2	West	--	407	412	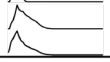	3471	529	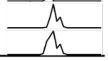
DEN101	*47.642348*	*124.23752*	391.1	West	--	335	422		3328	644	
								0 2450			0 6000

Table 2. Basin metrics for erosion processes. $2\sigma = 2$ standard deviations on the mean. Curves represent simplified histograms with normalized counts. See labels below each column for minimum and maximum bin values. Basins in italics are from Belmont et al. (2007). Values exclude data from ice coverd regions.

Sample Name	Hillslope Angle (°)			Channel Steepness ($m^{0.9}$)			Local Relief (m)		
	Mean	2σ	Histogram	Mean	2σ	Histogram	Mean	2σ	Histogram
WA1501	30	20	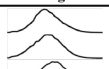	134	102	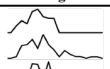	1227	246	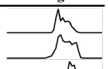
WA1502	29	20		160	152		1288	320	
WA1503	33	22		154	96		1374	332	
WA1519	31	24		163	154		1359	372	
WA1520	34	19		180	150		1379	58	
WA1522	31	20		133	72		1117	186	
WA1523	31	24		153	156		1317	386	
WA1524	33	26		181	144		1443	230	
WA1525	30	20		141	104		1147	278	
WA1526	27	20		62	48		717	174	
WA1527	30	22		134	96		1190	242	
WA1537	33	24		128	106		1320	292	
WA1538	31	22		137	124		1282	334	
WA1539	27	22		117	106		1067	224	
U-EFMC	22	18		23.3	3.0		386	28	
L-EFMC	21	18		23	20		385	72	
U-WC	28	16		N/A	N/A	N/A	718	20	
L-WC	26	17		86	28		718	20	
DEN104	16	17		23	17		350	72	
DEN106	23	24		47	50		581	324	
DEN101	20	24		40	48		496	384	
			0 70			0 450			0 2100

780

Table 3. Basin-averaged erosion rate sample data. Integration time was calculated by dividing the e-folding depth of the production of cosmic nuclides via spallation (0.6 m) by the erosion rate. Italicized samples are from Belmont et al. (2007). Underlined sampes had ^{10}Be measurements less that 10 times the blank measurement.

Sample Name	[^{10}Be] (atoms/g)	[^{10}Be] 2σ (atoms/g)	Be Erosion Rate (m/Myr)	Rate 2σ (m/Myr)	Integration Time (yr)	[^{26}Al] (atoms/g)	[^{26}Al] 2σ (atoms/g)	Al Erosion Rate (m/Myr)	Rate 2σ (m/Myr)	^{26}Al/^{10}Be	^{26}Al/^{10}Be 2σ
WA1501	11738	633	638	118	941	74391	6678	696	163	6.3	1.3
WA1502	9324	527	718	134	836	48421	7135	959	321	5.2	1.6
WA1503	6934	445	930	183	645	38878	6227	1152	414	5.6	1.9
WA1519	2980	288	2511	618	239	10783	3104	4814	3104	3.6	2.2
WA1520	10906	583	610	112	983	73333	10379	629	204	6.7	2.0
WA1522	15665	1129	432	90	1389	132290	9907	353	75	8.4	1.8
WA1523	3844	345	1881	442	319	10539	2435	4766	2429	2.7	1.4
WA1524	2573	255	3117	782	193	21763	4289	2551	1113	8.5	3.7
WA1525	5625	397	1451	301	414	26581	4208	2126	759	4.7	1.6
WA1526	19765	845	224	37	2673	111196	11661	278	71	5.6	1.3
WA1527	11048	596	564	104	1063	80390	9617	538	152	7.3	1.9
WA1537	5010	376	1213	256	495	33985	3912	1244	341	6.8	1.9
WA1538	11742	603	635	116	945	71021	6160	727	166	6.0	1.2
WA1539	21267	915	318	55	1889	145691	13348	320	76	6.9	1.4
U-EFMC	*21558*	*3018*	*171*	*34*	*3501*	--	--	--	--	--	--
L-EFMC	*27796*	*1668*	*129*	*20*	*4669*	--	--	--	--	--	--
U-WC	*29985*	*1799*	*158*	*25*	*3789*	--	--	--	--	--	--
L-WC	*22703*	*1362*	*199*	*31*	*3023*	--	--	--	--	--	--
DEN-101	*17407*	*11837*	*223*	*176*	*2685*	--	--	--	--	--	--
DEN-104	*31032*	*10551*	*114*	*43*	*5264*	--	--	--	--	--	--
DEN-106	*17150*	*7203*	*237*	*110*	*2528*	--	--	--	--	--	--

Page 5: [1] Deleted	Microsoft Office User	5/7/18 2:38:00 PM

Because our methods to calculate effective latitude and elevation do not incorporate temporal production fluctuations, w

Supplement of:
Tectonic controls of Holocene erosion in a glaciated orogen

Byron A. Adams[1,2], Todd A. Ehlers[1]

[1]Department of Geosciences, Univsität Tübingen, D-72074, Germany
[2]Now at the School of Earth Sciences, University of Bristol, Bristol, BS8 1RJ, UK

Correspondence to: Byron A. Adams (byron.adams@bristol.ac.uk)

This PDF file includes:

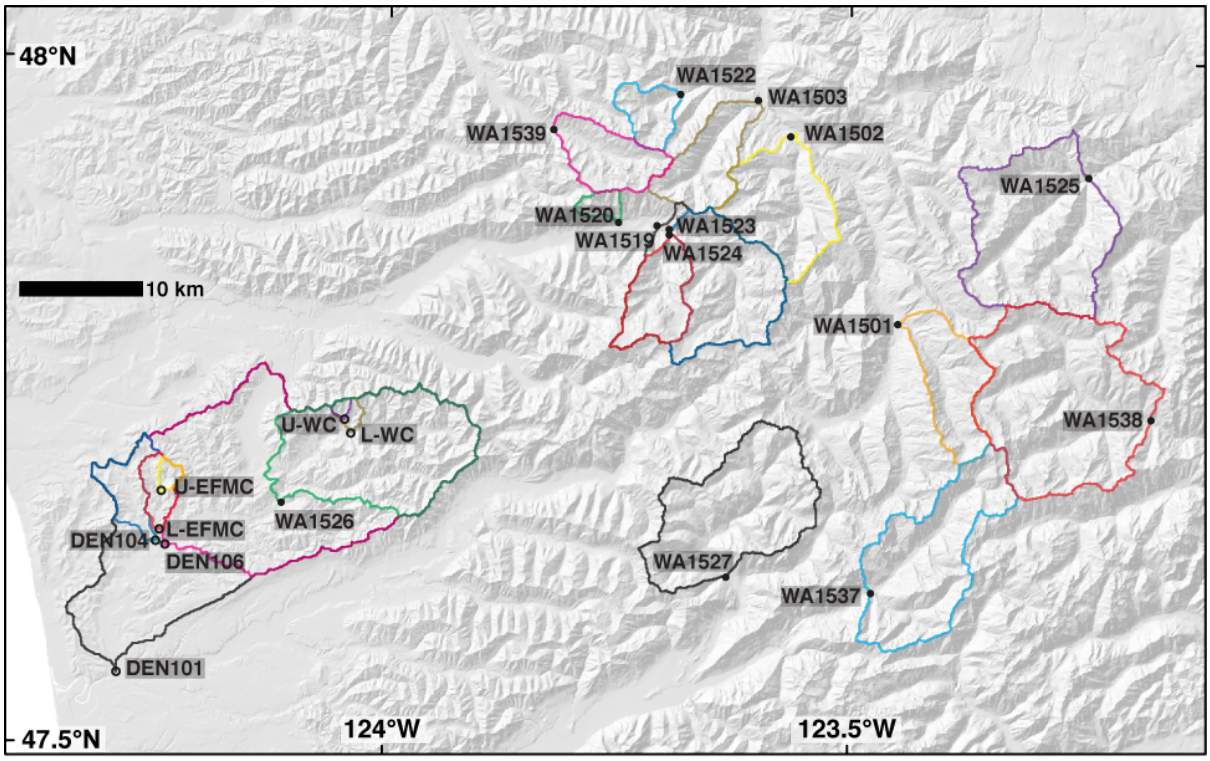

Figure S1. Basin sample location map. Samples marked with open circles are from Belmont et al. (2007).

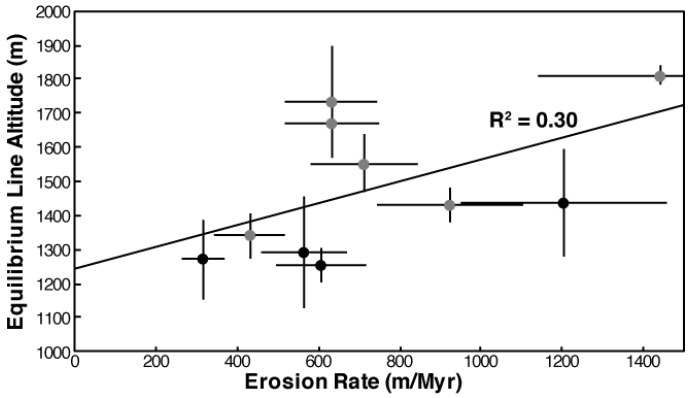

Figure S2. Comparison of basin-averaged erosion rates and equilibrium line altitudes (ELA). Black and grey data are from the west and east sides of the range, respectively.

Calculation of snow depth estimations

For this study, we utilized the MODIS/Terra Snow Cover Monthly L3 Global 0.05°, Version 6 dataset (Hall and Riggs, 2015), to estimate the distribution of snow for a given month. For any given pixel in the scene the value can vary between 0 and 100. While we consider these values to be spatially accurate they are only qualitative in that they do not have a magnitude equal to a physical dimension. To scale these data to represent snow depth values, we consider the snow cover values to be analogous to a percentage of the maximum snow depth in the Olympic Mountain range.

Our best estimate of maximum snow depth in the range comes from the Buckinghorse SNOTEL meteorological station (https://www.ncdc.noaa.gov/cdo-web/datasets/; Network ID: GHCND:USS0023B18S), located at 1484 m in the southern reaches of the Elwha Valley in the core of the range (Fig. S4 and S5). This station records the highest monthly snow depth measurements within the range. In the final step, we smoothed mean monthly snow cover data (2001-2015) using a bilinear algorithm and multiplied these percentages by the mean monthly snow depth station data (2009-2015). We do not assert that the resulting maps (Fig. S4) are completely accurate. However, we have calculated them to constrain the possible effect snow shielding may have on the calculation of erosion rates across the range. We assume a snow density of 0.25 g/cm^3 for shielding calculations.

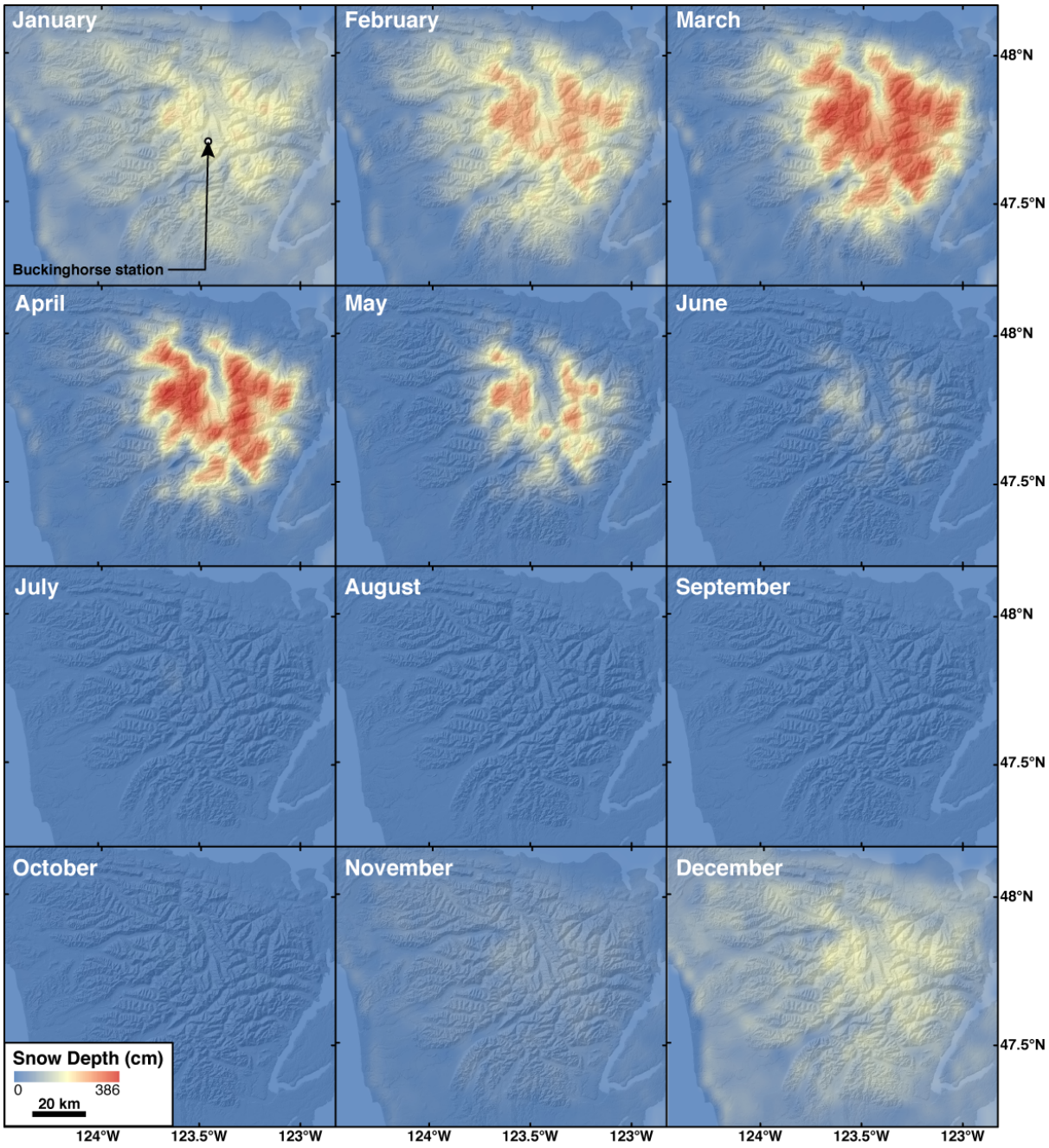

Figure S3. Monthly estimated snow depth map. The dot marks the position of the Buckinghorse SNOTEL meteorological

station.

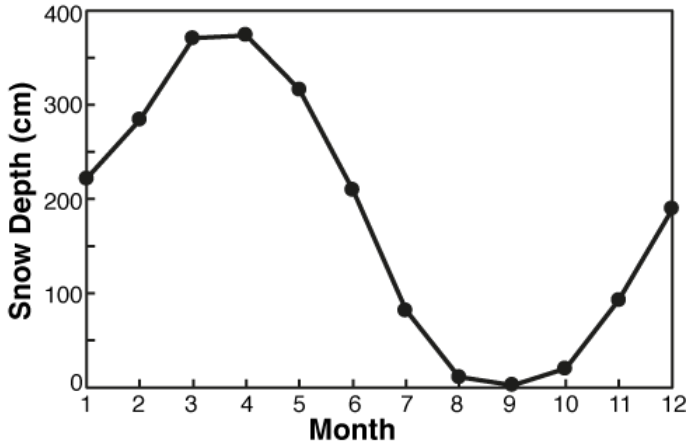

Figure S4. Mean monthly snow depth measurements from the Buckinghorse SNOTEL meteorological station. These means are calculated for the years 2009-2015.

Table S1. Laboratory and isotopic data for new Olympic Mountain samples.

Sample Name	Effective Latitude (°N)	Centroid Longitude (°E)	Effective Elevation (m)	Quartz (g)	Be from spike (g)	Total Al from ICP (g)	Laboratory Be Number	$^{10}Be/^{9}Be$ from AMS	$^{10}Be/^{9}Be$ 1σ	Be Blank Used	Laboratory Al Number	$^{26}Al/^{27}Al$ from AMS	$^{26}Al/^{27}Al$ 1σ	Al Blank Used
WA1501	47.761893	-123.38950	1397	90.382	3.29E-04	9.2640E-03	s09728	5.0260E-14	2.5300E-15	BA10	s09935	3.257E-14	2.850E-15	BA11
WA1502	47.856058	-123.57330	1266	88.882	3.29E-04	1.8151E-02	s09729	3.9650E-14	2.0600E-15	BA10	s09939	1.065E-14	1.500E-15	BA11
WA1503	47.96357	-123.65440	1195	88.350	3.28E-04	1.6448E-02	s09730	2.9910E-14	1.7300E-15	BA10	s09943	9.386E-15	1.400E-15	BA11
WA1519	47.86627	-123.65900	1421	90.386	3.28E-04	1.6600E-02	s09731	1.4260E-14	1.1200E-15	BA10	s09947	2.660E-15	7.420E-16	BA11
WA1520	47.902426	-123.77010	1184	81.778	3.27E-04	2.0658E-02	s09732	4.2830E-14	2.1100E-15	BA10	s09951	1.303E-14	1.670E-15	BA11
WA1522	47.977417	-123.71920	1252	51.239	3.26E-04	6.1441E-03	s09046	3.8700E-14	2.5800E-15	BA1	s10020	5.012E-14	3.490E-15	BA3
WA1523	47.89053	-123.63360	1404	73.762	3.28E-04	9.1110E-03	s09733	1.4880E-14	1.0900E-15	BA10	s09955	3.876E-15	8.750E-16	BA11
WA1524	47.832887	-123.70770	1505	99.716	3.47E-04	1.8004E-02	s09739	1.3250E-14	1.0000E-15	BA19	s09980	5.430E-15	1.010E-15	BA20
WA1525	47.862877	-123.29530	1547	84.053	3.27E-04	1.0421E-02	s09735	2.3580E-14	1.4600E-15	BA10	s09967	9.652E-15	1.450E-15	BA11
WA1526	47.674477	-124.01220	550	99.299	3.28E-04	2.1568E-02	s09734	9.1580E-14	3.7000E-15	BA10	s09959	2.296E-14	2.280E-15	BA11
WA1527	47.616827	-123.62340	1100	92.130	3.27E-04	1.9201E-02	s09735	4.8860E-14	2.4200E-15	BA19	s09976	1.731E-14	1.810E-15	BA20
WA1537	47.70025	-123.41140	1147	94.016	3.48E-04	8.3440E-03	s09740	2.2430E-14	1.4400E-15	BA19	s09984	1.722E-14	1.920E-15	BA20
WA1538	47.72078	-123.27090	1439	95.680	3.48E-04	1.0705E-02	s09741	5.0490E-14	2.3900E-15	BA19	s09988	2.849E-14	2.450E-15	BA20
WA1539	47.917853	-123.76290	1238	92.504	3.48E-04	1.4970E-02	s09742	8.6810E-14	3.5100E-15	BA19	s09992	4.037E-14	3.120E-15	BA20

Table S2. Blank data for new Olympic Mountain samples.

Blank Name	Laboratory Be Number	Be from spike (g)	$^{10}Be/^{9}Be$ from AMS	$^{10}Be/^{9}Be$ 1σ	Be Standard	Laboratory Al Number	Al from spike (g)	$^{26}Al/^{27}Al$ from AMS	$^{26}Al/^{27}Al$ 1σ	Al Standard
BA1	s09045	3.2750E-04	1.8410E-15	4.9500E-16	07KNSTD	--	--	--	--	--
BA10	s09737	3.2739E-04	1.9620E-15	3.6900E-16	07KNSTD	--	--	--	--	--
BA19	s09746	3.4758E-04	2.1870E-15	4.2600E-16	07KNSTD	--	--	--	--	--
BA3	--	--	--	--	--	s10024	2.5761E-03	1.647E-15	1.028E-15	KNSTD
BA11	--	--	--	--	--	s09967	2.5512E-03	1.905E-16	6.079E-16	KNSTD
BA20	--	--	--	--	--	s10008	2.5582E-03	2.077E-16	6.176E-16	KNSTD

Table S3. Shielding and erosion rate comparisons.

Sample Name	Topographic Shielding	Snow/Ice Shielding	Total Shielding	Topo+Snow Erosion Rate (m/Myr)	Erosion Rate 2σ (m/Myr)	Topo Only Erosion Rate (m/Myr)	Erosion Rate 2σ (m/Myr)	Percent Difference (%)
WA1501	0.95	0.87	0.82	638	118	726	136	12
WA1502	0.96	0.85	0.80	718	134	842	160	15
WA1503	0.95	0.86	0.81	930	183	1068	212	13
WA1519	0.95	0.85	0.80	2511	618	2922	725	14
WA1520	0.94	0.90	0.85	610	112	666	123	8
WA1522	0.95	0.87	0.82	432	90	492	103	12
WA1523	0.95	0.83	0.78	1881	442	2238	265	16
WA1524	0.94	0.87	0.81	3117	782	3558	898	12
WA1525	0.95	0.85	0.80	1451	301	1691	355	14
WA1526	0.97	0.96	0.92	224	37	235	39	4
WA1527	0.95	0.87	0.82	564	104	622	115	9
WA1537	0.93	0.86	0.79	1213	256	1396	297	13
WA1538	0.95	0.84	0.79	635	116	748	138	15
WA1539	0.96	0.87	0.83	318	55	361	63	12
U-EFMC	0.98	0.97	0.95	171	34	176	35	2
L-EFMC	0.98	0.97	0.96	129	20	131	20	2
U-WC	0.97	0.96	0.93	158	25	164	26	4
L-WC	0.98	0.96	0.93	199	31	207	32	4
DEN104	0.99	0.97	0.96	114	43	117	44	2
DEN106	0.97	0.96	0.93	237	110	246	114	3
DEN101	0.98	0.96	0.94	223	176	231	182	3

References

Belmont, P., Pazzaglia, F., and Gosse, J. C.: Cosmogenic 10 Be as a tracer for hillslope and channel sediment dynamics in the Clearwater River, western Washington State, Earth and Planetary Science Letters, 264, 123-135, 2007.

Hall, D., and Riggs, G.: MODIS/Terra snow cover Monthly L3 Global 0.05Deg CMG, Version 6. In: NASA National Snow and Ice Data Center, Distributed Active Center, Boulder, Colorado, USA, 2015.

Tectonic controls of Holocene erosion in a glaciated orogen

Byron A. Adams[1,2], Todd A. Ehlers[1]

[1]Department of Geosciences, Univsität Tübingen, D-72074, Germany
[2]Now at the School of Earth Sciences, University of Bristol, Bristol, BS8 1RJ, UK

Correspondence to: Byron A. Adams (byron.adams@bristol.ac.uk)

Abstract. Recent work has highlighted a strong, worldwide, alpine glacial impact on~~f~~ orogen erosion rates over the last 2 Ma. While it may be assumed that glaciers increased erosion rates when active, the degree to which past glaciations influence Holocene erosion rates through the adjustment of topography is not known. In this study, we investigate the influence of long-term tectonic and post-glacial topographic controls on erosion in a glaciated orogen, the Olympic Mountains, USA. We present 14 new ^{10}Be and ^{26}Al analyses which constrain Holocene erosion rates across the Olympic Mountains. Basin-averaged erosion rates scale with basin-averaged values of 5-km local relief, channel steepness, and hillslope angle throughout the range, similar to observations from non-glaciated orogens. These erosion rates are not related to mean annual precipitation or the marked change in Pleistocene alpine glacier size across the range, implying that glacier modification of topography and modern precipitation parameters do not exert strong controls on these rates. Rather, we find that despite ~~intense~~ spatial variations in glacial modification of topography, patterns of recent erosion are similar to those from estimates of long-term tectonic rock uplift. This is consistent with a tectonic model where erosion and rock uplift patterns are controlled by the deformation of the Cascadia subduction zone.

1 Introduction

Before the onset of Late Cenozoic cooling and glaciation, the topographic expression of mountain belts resulted from tectonic processes, and the fluvial and hillslope processes which acted as the primary agents of erosion. High rock uplift rates in many of these ranges led to the buildup of topography and in some cases high relief, steep river channels and hillslopes, and commensurate high erosion rates (Willett, 1999). Because of the covariation between climate, ~~these characteristics~~topography and rock uplift, erosion rates in fluvially dominated orogens have been shown to correlate with climatic and topographic metrics such as precipitation rate, relief, hillslope angle, and channel steepness via linear, non-linear and threshold relationships (Ahnert, 1970, Montgomery and Brandon, 2002, Ouimet et al., 2009, DiBiase et al., 2010). The development of rugged mountain belts led to an increase in cooler, higher elevation landscapes, which created the necessary conditions for alpine glaciers to form in~~In~~ the Late Cenozoic. ~~, alpine glaciers formed, and then advanced and receded many times due to climate oscillations.~~ These glaciers possessed variable capacity to erode at the same rate as the rivers that existed before them, and regional rock uplift rates. In many mountain ranges, glaciers appear to have accelerated erosion (Hallet et al., 1996, Shuster et al., 2005, Ehlers et al., 2006, Valla et al., 2011, Herman et al., 2013, Christeleit et al., 2017, Michel et al., 2018), while in other areas, glaciers may have done little to change erosion rates over the past few million years (Koppes and Montgomery, 2009, Thomson et al., 2010, Willenbring and von Blanckenburg, 2010).

As a result of Cenozoic climate change, the relationships between topographic metrics and observed Holocene (last ~12 kyr) erosion rates in glaciated mountain ranges are more complex than in purely fluvial settings (Moon et al., 2011, Godard et al., 2012, Glotzbach et al., 2013). These poorly understood relationships are likely caused for two reasons. (1)

Glaciers reorganized previously fluvial channel networks and relief to create a landscape with their preferred geometry, radically changing the orogen topography (Whipple et al., 1999, MacGregor et al., 2000, Brocklehurst and Whipple, 2002, Brocklehurst and Whipple, 2004, Brocklehurst and Whipple, 2006, Anderson et al., 2006, Adams and Ehlers, 2017). (2) Holocene erosion rates may be dominated by transient signals as surface process remove the topographic disequilibrium imposed by glacial erosion (Moon et al., 2011).

In light of the previous studies, what remains uncertain is how much (if any) signal of tectonic processes can be discerned from a heavily glaciated orogen, and the degree to which common relationships between erosion and topographic metrics hold in post-glacial landscapes. Here we address this uncertainty and test ~~the efficiency of~~whether Plio-Pleistocene glaciers ~~to mask~~have masked long-lived patterns of rock uplift as recorded by millennial-scale erosion rate estimates and modern topography. To do so, we have conducted a systematic study of basin-averaged erosion rates from ^{26}Al and ^{10}Be concentrations in modern river sediments from the Olympic Mountains, USA (Fig. 1). The Olympic Mountains are well suited for this study because the efficiency of Plio-Pleistocene glaciers was controlled by spatially variable glacial mass balance, and the orogen has been shown to contain a wide range of rock uplift rates. We use our new data, in addition to ^{10}Be concentrations from a previous study (Belmont et al., 2007), to investigate the spatial variations in erosion rates with respect to characteristics of the modern topography including local relief, hillslope angle, and channel steepness, as well as precipitation. Further, we utilize ^{26}Al/^{10}Be ratios, and new modelling efforts to investigate the degree to which cosmogenic nuclide inventories can accurately constrain erosion rates in glaciated mountain ranges.

2 Background

The Olympic Mountains are part of a chain of mountain ranges that define the forearc high of the Cascadia subduction zone (Fig. 1A). This forearc high marks the topographic and structural apex of an accretionary wedge which formed between the North American plate and the subducting Juan de Fuca plate (Tabor and Cady, 1978). The core of the range is comprised of an essentially unmetamorphosed, homogenous assemblage of medium- to fine-grained, greywacke interbedded with minor siltstone, mudstone, conglomerate, and basalt lenses. This group of rocks is referred to as the Olympic Subduction Complex, and is located in the footwall of the Hurricane Ridge Fault (Fig. 1). Pillow basalts, breccias, volcaniclastic rocks and diabase make up the hanging wall of the fault, referred to as the Coast Range Terrane. Sedimentological and bedrock cooling histories suggest accelerated rock uplift and unroofing of the range began around 17-12 Ma (Tabor and Cady, 1978, Brandon et al., 1998). Rock uplift rates have been interpreted across the range from Neogene thermochronometric exhumation rates (apatite fission track) and Quaternary river incision rates (Pazzaglia and Brandon, 2001). These rates vary from ~300 m/Myr at the fringes of the range to ~800 m/Myr in regions close to the geographic center of the range, forming a concentric pattern. Previous interpretations of these erosion rates suggest that they are governed by rock uplift rates (Brandon et al., 1998, Pazzaglia and Brandon, 2001, Batt et al., 2001). In most orogenic wedges, the rock velocity field is governed by the subducting plate geometry and convergence rate, as well as the pattern of accreted materials from the subducting plate (Willett, 1999). The Olympic Mountains are thought to be no different (Batt et al., 2001); however, the subduction zone dynamics are complicated by the significant arch in the subducting Juan de Fuca plate and the dome of accreted sedimentary units that make up the east-plunging Olympic Anticline (Brandon and Calderwood, 1990). Indeed, it is likely that these nuanced characteristics of the subduction zone may be responsible for the observed concentric pattern in erosion/rock uplift rates (Brandon et al., 1998, Pazzaglia and Brandon, 2001, Batt et al., 2001, Bendick and Ehlers, 2014).

The Olympic Mountains have a general dome shape where the major drainages exhibit a radial pattern. The dome is asymmetric where the locus of highest topography lies to the northeast of the range divide (Fig. 1B). Plio-Pleistocene alpine glaciers carved large valleys in the core of the range (Porter, 1964, Montgomery and Greenberg, 2000, Montgomery, 2002, Adams and Ehlers, 2017). The largest glaciers which occupied the Hoh, Queets and Quinault valleys all extended to the Pacific Ocean (Fig. 1B) (Thackray, 2001). Alpine glaciers were likely active in every valley of the Olympics (Porter, 1964); however, the size of the glaciers was highly variable, as the east flowing glaciers would have been limited to the rugged core of the range by the Cordilleran Ice Sheet (see glacial deposits Fig. 1B). This suggests that the west flowing glaciers may have been nearly twice as long as those flowing east. Due to the W-SW prevailing wind direction and the effects of topography on precipitation patterns, mean annual precipitation values decrease from ~6000 mm/yr in the southwest to less than 500 mm/yr in the northeast (Fig. 2A). This same precipitation gradient greatly influenced the Pleistocene equilibrium line altitude (ELA; the position where the ice flux in a glacier is at a maximum), and created an opposing pattern where the ELA increases at a rate of ~ 25 m/km toward the northeast (Porter, 1964) (Fig. 1B), thus controlling the size and efficiency of alpine glaciers (Adams and Ehlers, 2017). The range was bordered to the north and east by the Cordilleran Ice Sheet (Fig. 1B) (Porter, 1964), which also likely restricted the size of alpine glaciers. This dichotomy in glacier size and erosional capacity is likely to have influenced the pattern in erosion rates during glacial times. A recent study by Michel et al. (2018) shows that bedrock cooling histories record a near doubling of exhumation rates around the time of the onset of glaciation (2 Ma). This affect is most pronounced on the west side of the range, where valley glaciers were larger. While the impact of Plio-Pleistocene glaciation on more recent erosion has not been previously quantified, the suggestion of significant glacial erosion would imply that Holocene erosion rates may not simply be a function of rock velocities as suggested by older erosion histories discussed above.

3 Methods

3.1 Topographic analysis

Our topographic analysis is based on the 10 m National Elevation Dataset provided by the United States Geological Survey (www.ned.usgs.gov). Within this paper we calculate three topographic metrics which record relief at different spatial scales and controlled by different surface process – hillslope angle, local relief, and channel steepness. Each metric also has strengths and weaknesses in quickly eroding, glaciated ranges. There is good evidence that hillslope angle values can reach maximum values due to the limitations of the internal angle of friction of hillslope materials. In such high erosion areas, hillslope angle values become insensitive to changes in erosion rates (Schmidt and Montgomery, 1995). Local relief values may also be limited in glaciated ranges due to the buzzsaw effect, whereby efficiently eroding glaciers increase the area near their ELA and thus control mean elevations and restrict relief locally (Meigs and Sauber, 2000, Brozović et al., 1997).

Our local relief (*R*) map (Fig. 2B) was made by calculating the difference between the highest and lowest elevations within a 5 km-diameter circular window. The ~~This form of~~local relief metric is designed to encapsulate the relief of hillslopes and channels. The size of this window captures the elevation difference between peaks and valley floors of medium sized basins, but is small enough to detect changes in the relief structure of large drainage basins. The hillslope gradient (*S*) map (Fig. 2C) was calculated by finding the steepest angle of descent across a 3 x 3 pixel (30 x 30 m) square window.

The channel steepness map (Fig. 2C) was created by adjusting channel gradients (S) (m/m) by the non-linear change in downstream drainage area (A) (m^2) (Hack, 1957, Flint, 1974, Wobus et al., 2006):

$$S = k_s A^{-\theta} \quad (1)$$

where k_s is the channel steepness, and θ (dimensionless) is the channel concavity. ~~This calculation~~Eq. 1 normalizes slope values, for the concavity of the channel. For our calculations, we use $\theta = 0.45$. ~~This~~ A θ value of 0.45 has been shown to describe the concavity of fluvial systems in the Olympic Mountains (Adams and Ehlers, 2017). Since we utilize a single value of θ, we report normalized channel steepness values (k_{sn}) ($m^{0.9}$). We used the Profiler tool (Wobus et al., 2006) to extract and analyze our river channels, and calculated steepness values over 0.5 km reaches. To report a mean value for a basin we calculated the mean normalized channel steepness for all portions of a basin, which are governed by fluvial processes, which ~~. This~~ generally occurs at drainage areas > 1 km^2.

Normalized channel steepness index (k_{sn}) analysis, which quantifies channel relief, has been used successfully in a number of mixed fluvial and glacial landscapes as a fine scale measure of the erosion potential of glacial/fluvial processes in a landscape (Montgomery, 2001, Brardinoni and Hassan, 2006, Brardinoni and Hassan, 2007, Brocklehurst and Whipple, 2007, Robl et al., 2008, Hobley et al., 2010, Glotzbach et al., 2013, Adams and Ehlers, 2017). Many assumptions generally that are adopted in purely fluvial settings do not apply in mixed glacial-fluvial landscapes. For instance, in our study we do not require that the Olympic Mountains are in topographic steady-state (where erosion and rock uplift at a point are balanced and therefore elevations remain constant over time), nor do we imply that our slope-area analysis relates directly to the processes of glacial incision, or that rock uplift rates need to be spatially uniform. We emphasize that ~~this technique~~the normalized channel steepness index provides a robust, geometric construct for understanding the importance of spatial changes in channel relief without demanding an understanding of all parameters within a specific incision law (fluvial or glacial). Furthermore, channel relief is likely to control the relief and hypsometry of landscapes, even in glaciated ranges (e.g. Adams and Ehlers, 2017). Unlike hillslope angle calculations, channel steepness values may be able to record changes in erosion/rock uplift rates in regions where hillslopes have reached a threshold (Ouimet et al., 2009).

3.2 Processing sediment samples and calculating erosion rates

Basin-averaged erosion rates were calculated from concentrations of cosmogenic nuclides (^{10}Be and ^{26}Al) in quartz sand from modern river basins throughout the Olympic Mountains (see Fig. S1 for sample location detail). ~~This technique is~~Detrital cosmogenic techniques record~~s~~ the average erosion/denudation rate (we note that rates presented here incorporate both physical and chemical means of mass removal) integrated across the landscape upstream of the sample location (Brown et al., 1995, Granger et al., 1996, Bierman and Steig, 1996). Basins were selected to ensure a thorough sampling across precipitation, Pleistocene ELA, rock uplift, and topographic gradients. These basins are located within the Olympic Subduction Complex, where quartz is ubiquitous throughout the landscape.

Initial attempts to separate pure aliquots of quartz sand proved difficult due to the fine-grained nature of the lithologies found throughout the range. To reduce the need for aggressive hydrofluoric acid treatment, which would prematurely dissolve the quartz, we first disaggregated the 250-1000 µm sand fraction with a Selfrag, a high-voltage pulse disaggregater, at the University of Bern, Switzerland. From this stage on, samples were processed within the facilities at the University of Tübingen. After electronic disaggregation, sediments were re-sieved to 125-1000 µm and separated using a strong magnetic field and then cleaned in concentrated, room temperature aqua regia for 24 hours. Samples were further cleaned in boiling pyrophosphoric acid and then boiling sodium hydroxide at least 3 times. The quartz was then leached 1%

hydrofluoric acid while in an ultrasonic bath for 1 week. A final leach was performed on the samples with concentrated hydrofluoric acid before spiking with beryllium. Samples were not spiked with aluminum. Beryllium and aluminum were separated, oxidized and loaded into cathodes for mass spectrometer analysis using established protocols (Von Blanckenburg et al., 1996). Native Al concentrations within samples were measured with an inductively-coupled plasma optical emission spectrometer at the University of Tübingen. Beryllium and aluminum ratios were measured at the University of Cologne Centre for Accelerator Mass Spectrometry.

To calculate erosion rates, we followed the approach of Portenga and Bierman (2011), which simplifies each basin to a single point where the production rate is equal to the mean production rate of the entire basin, enabling the use of the CRONUS online calculator (Balco et al., 2008). Basin-averaged production rates were based on the elevation and latitude of each pixel in a basin using the scheme of Stone (2000). The effective elevation and latitude of each basin are the elevation and latitude values corresponding to this mean scaling factor (Table S1). We calculated topographic shielding due to obstacles according to the equations of Dunne et al. (Dunne et al., 1999), and snow shielding from the equations of Gosse and Phillips (Gosse and Phillips, 2001). Pixels under extant ice are assumed to be 100% shielded. Our snow depth maps are based on satellite snow cover data that were calibrated by snow depth observations in the Olympic Mountains (see Supplement for more details). For CRONUS calculations, the following inputs were used: Elevation Flag = std, Thickness = 1 cm, Density = 2.7 g/cm^3, Be Standard = 07KNSTD, Al Standard = KNSTD.

~~Because our methods to calculate effective latitude and elevation do not incorporate temporal production fluctuations, w~~We report erosion rates from the CRONUS calculator from the constant production rates determined by the constant production rate models of Lal (1991) and Stone (2000). To enable comparison between new and previous measurements, we recalculated erosion rates from 7 sand samples within the Olympic Mountains previously reported by Belmont et al. (2007).

3.3 Isotopic equilibrium modeling

The application of detrital cosmogenic nuclide techniques as an estimator of basin-averaged erosion rates in post-glacial landscapes is not yet a common practice as there is a high potential for violation of the assumptions inherit to the calculation of erosion rates from nuclide concentrations. The assumptions that can be most problematic for a glacial terrain are: the eroding materials are in isotopic equilibrium; and modern river sediment is spatially and temporally representative of all sediment in the basin. To explore the nature of isotopic equilibrium we describe new modeling efforts in ~~the~~ this section. The topic of sediment storage a mixing is discussed in Sections 4.2 and 5.1. Surface materials are in isotopic equilibrium when the production of cosmogenic nuclides is balanced by their removal through erosion and radioactive decay, in this state the concentration of nuclides in surface materials is steady over time. Since glacial ice intercepts, and thus shields underlying material from cosmic radiation, previously and currently glaciated basins may violate the isotopic equilibrium assumption if ice was present recently, and erosion has not been able to remove the older shielding signal (Moon et al., 2011, Portenga et al., 2014, Vance et al., 2003). Therefore, interpreting cosmogenic nuclide concentrations as direct measurements of erosion in some glaciated landscapes can lead to overestimated rates (Gosse and Phillips, 2001, Vance et al., 2003, Portenga et al., 2014).

To test the hypothesis that our samples are in isotopic equilibrium we conducted a suite of numerical models to constrain the evolution of the concentration of cosmogenically produced nuclides at depth, starting at a time just after a

period when ice completely shielded surface production. When the model starts, production occurs according to the equations of (Anderson et al., 1996):

$$N(z,t) = N_0 e^{-\lambda t} + \frac{P_0 e^{-\rho z/\Lambda}}{\lambda + \rho E/\Lambda}(1 - e^{-(\lambda+\rho E/\Lambda)t}) \quad (2)$$

where N is the cosmogenic nuclide concentration (atoms/g), t is time (yr), N_0 is the inherited concentration cosmogenic nuclides (atoms/g), E is the erosion rate (cm/yr), λ is the decay constant for ^{10}Be (1/yr), z is the depth below the surface (cm), P_0 is the ^{10}Be production rate at the surface (atoms/g/yr), Λ is the attenuation length for cosmogenic nuclide production (g/cm), and ρ is the material density (g/cm^3). In our models the following values were used: λ = 4.99e-7 1/yr, P_0 = 10 atoms/g/yr (though the results of this model are not sensitive to this value), Λ = 160 g/cm, and ρ = 2.7 g/cm^3.

Using a finite difference method, the model runs forward from the time of since unshielding, and surface concentrations increase over time as production occurs, and deeply shielded materials are eroded from the top of the model. The concentration at the surface is compared to the steady-state value to assess the approach toward isotopic equilibrium. A range of erosion rates which span the observed erosion rates in this study are tested.

3.4 Relationships between erosion rates and basin parameters

We performed non-linear, least-square regressions on our new and existing erosion rate data. To provide a better sense of the distribution of topographic metrics within a basin, we provide box-and-whisker plots within our bivariate plots, though our regressions discussed in the following sections are based on mean statistics. We included the uncertainties in both variables by using a Mote Carlo sampling protocol. ~~During our regression analysis, we chose to process all data together, as opposed to subsampling populations. This was decided to avoid the issue of small sample statistical bias, and because it was not obvious how to subsample our data *a priori*, without adding bias. These regressions included the influence of uncertainties on both variables.~~ Goodness of fit values were determined by the mean square weighted deviation (MSWD). For well-fit data, MSWD values tend toward 1 within an uncertainty based on the degrees of freedom (based primarily on the number of samples). Elevated MSWD values, are caused by the high degree of inter-sample variability, and suggest (1) the two variables shown in the plot are not highly correlated, (2) a more complex function exists between the two variables, or (3) that uncertainties are underestimated.

As a means to assess the relationship between erosion and hillslope processes we use a variation of the non-linear relationship proposed by Roering et al. (2001), which captures the effects of diffusive processes and landsliding:

$$E = \frac{KS}{1-(S/S_c)^2} \quad (3)$$

where E is the basin-averaged erosion rate (m/Myr), K is a rate constant related to the diffusivity of the eroding material (m/Myr), S is the basin-averaged hillslope gradient (m/m), and S_c is a critical slope at which soil flux approaches infinity (m/m).

We used a similar equation from Montgomery and Brandon (2002) to explore the relationship between erosion rates and 5-km local relief:

$$E = \frac{KR}{1-(R/\ R_c)^2} \quad (4)$$

where K is a different rate constant (m/Myr), R is the basin-averaged local relief normalized by the diameter of the moving window (m/m), and R_c is a limit to the possible values of local relief normalized by the diameter of the moving window (m/m).

Previous studies have suggested that that channel steepness values can vary spatially according to a relationship with basin-averaged erosion rates through a stochastic threshold model of fluvial channel incision (DiBiase et al., 2010). Such a model generally produces a non-linear relationship. However, using a model based solely on fluvial incision in the Olympic Mountains would be misleading as the modern river channel likely still reflect the preferred geometry of Plio-Pleistocene glaciers (Adams and Ehlers, 2017). Instead, we implemented a least-squares power function regression to explore possible connections between erosion and channel steepness, similar to other recent studies (Scherler et al., 2013):

$$E = Ck_{sn}{}^{p} \quad (5)$$

where C is the ~~pre-exponential~~ coefficient, ~~k_{sn} is the mean channel steepness value of the basin,~~ and p is the ~~power~~exponent. We used the same least-squares routine to analyze the relationship between erosion and precipitation (e.g. replace k_{sn} with the mean precipitation in Eq. 5).

4 Results

4.1 Topographic analysis

The topography of the Olympic Mountains is a mixture of high glacial cirque basins, wide and flat-floored valleys at low elevations, and very steep landscapes in between. This juxtaposition of varied landscapes creates skewed and multi-modal distributions of topographic metrics within drainage basins throughout the range (Table 1 and 2, Fig. 2B, 2C and 2D). While it is useful to report arithmetic means of basin statistics to simplify a landscape, it can often be difficult to constrain the significance of such means in the context of their relation to erosion rates. In complex landscapes not defined by uniform and steady surface processes, like the Olympic Mountains, normally distributed topographic metrics with good central tendency are unlikely, especially for metrics which capture fine spatial scale processes like those occurring at the scale of hillslopes and channel segments. To provide a better sense of these distributions, we have included simplified histograms next to our reported statistics in Table 1 and 2. Because of this size limitation we are not able to calculate an accurate channel steepness value for one of basins from a previous study, U-WC (Belmont et al., 2007).

Basin-averaged hillslope angles are generally high, in most cases above 28°, as is the standard deviation of hillslope angles within each basin (mean 2σ = 21°) (Table 2 and Fig. 2C). Basin-averaged channel steepness values range between 23 and 181 $m^{0.9}$, and also have proportionally large standard deviations (mean 2σ = 89 $m^{0.9}$) (Table 2 and Fig. 2D). Basin-averaged local relief values (calculated within a 5-km diameter window) range between 350 and 1443 m (Table 2 and Fig. 2B). Relative to hillslope angle and channel steepness values, local relief values exhibit smaller variance within sampled basins (mean 2σ = 219 m). The lower-elevation basins on the western flank of the range, which evaded Last Glacial Maximum (LGM) alpine glaciers (Thackray, 2001, Belmont et al., 2007), have the lowest topographic metric values of the sampled basins (8 basins: mean R = 544, mean S = 23, mean k_{sn} = 43). The mean values from the 8 glaciated, west side basins and the 6 glaciated, east side basins are effectively the same: mean R = 1296, mean S = 31, mean k_{sn} = 151; and mean R = 1239, mean S = 31, and mean k_{sn} = 143, respectively. Despite the rain shadow and the significant discrepancy in the size of alpine glaciers across the range divide, there is no difference in topographic metrics within the rugged core of the range across the divide.

There is a high degree of correlation between some basin-averaged precipitation values and basin-averaged

elevation (Fig. 3A.), as would be expected from the PRSIM precipitation dataset which includes an orographic precipitation model to do reanalysis simulations (Daly et al., 1994). This correlation is only strong on the western flank of the mountain where the topographic and precipitation gradients are smoothest. These same sub-group of basins also exhibit a strong correlation between basin-averaged hillslope angle and basin-averaged elevation (Fig. 3B). However, there is no correlation between elevation and precipitation or hillslope angle in the core of the range. There is good correlation between basin-averaged elevation and both basin-averaged local relief and channel steepness (Fig. 3C-D), across the range.

4.2 Cosmogenic basin-averaged erosion rates

While we present both ^{10}Be and ^{26}Al data (Table 3, see Tables S1 and S2 for complete nuclide analysis), we focus our analysis on erosion rates derived from ^{10}Be in this study (Fig. 2E) to provide a means of comparison to existing data from the Olympic Mountains (Belmont et al., 2007). To a first order, basins located at elevations < 1000 m have been eroding at slow rates, all less than 240 m/Myr, whereas basins in the higher, rugged core of the range have higher erosion rates reaching over 1400 m/Myr (Table 3 and Fig. 2E). We obtained the highest apparent erosion rates (> 1500 m/Myr) from the flanks of Mount Olympus, whose drainages contain the largest extant glaciers in the Olympic Mountains (basins WA1519, WA1523, WA1524). However, the very low ^{10}Be concentrations (i.e. high apparent erosion rates) from Mount Olympus may be a signature of isotopic disequilibrium. Samples WA1519, WA1523 and WA1524 come from basins which likely contained thick ice the longest, and still have small valley glaciers today. The ^{10}Be abundances for these three basins only range from 5-7 times the ^{10}Be blanks. These low abundances are likely caused by the shielding of rock and soil below glaciers. Such low measurements not only increase in the internal uncertainty of the concentration calculation, but also raises questions about the accuracy of the erosion rate calculation and interpretation. For this reason, we do not include these basins in our regression analysis.

Sample ^{26}Al/^{10}Be ratios from the Olympic Mountains mostly vary between 8.5 ± 3.5 (2σ) and 4.7 ± 1.6 (2σ) (Table 3 and Fig. 4). Nearly all samples have ^{26}Al/^{10}Be ratios that are statistically indistinguishable from the expected naturally occurring ratio (6.75; ~~)~~ Balco et al., 2008) (Table 3 and Fig. 4), suggesting that the sediments in our samples record a relatively simple erosion rate history over the integration time. As such, there is no significant influence of reworking older sediments in our measurements. Furthermore, because our erosion rate calculations assume a natural production rate ratio of 6.75, and our measured ratios are mostly indistinguishable from this value, ^{10}Be and ^{26}Al derived erosion rates are statistically indistinguishable, though the ^{26}Al derived rates are much less precise (Table 3). Two samples from Mount Olympus basins, WA1519 and WA1523, have much lower ratios.

Snow shielding can reduce production rates, and therefore, reduce calculated erosion rates by up to 16% in the core of the range, but only ~3% reduction is found in lower elevation basins on the western flank (Table S3). While it is difficult to assess our snow shielding estimates, we note the relative effect on erosion rates is similar to those based on snow-depth measurements within other snowy orogens (Wittmann et al., 2007, Norton et al., 2010, Scherler et al., 2013).

4.3 Isotopic equilibrium modeling

As seen in Eq. 2 the likelihood of being in isotopic equilibrium for any cosmogenic radionuclide is mostly controlled by the time since deglaciation and the local erosion rate (assuming an inheritance of zero). Figure 5 illustrates that quickly eroding terrains more quickly remove ice-shielded materials, and thus, these terrains can each a new equilibrium state faster after the ice recedes. In fact, our model output suggests that at relatively low erosion rates (~100

m/Myr), terrains can achieve isotopic equilibrium in a few thousand years. These results suggest that the cosmogenic nuclide inventories from many glaciated landscapes on Earth could record accurate erosion rates (barring other complicating factors).

4.4 Relationships between erosion rates and basin parameters

Our best-fit curve (MSWD = 17) suggests the observed relationship between hillslope gradient and erosion is controlled by a critical slope value of 37° and a rate constant of 250 m/Myr (Fig. 6B). These parameters fit our data considerably better than the previous boundary conditions suggested by Montgomery and Brandon (2002) for the Olympic Mountains (S_c = 40°, K = 500 m/Myr, MSWD = 54). Our regressions also record a limited local relief of 1820 m (K = 0.24 m/Myr, MSWD = 4.3) (Fig. 5A). These parameters are also different than those of Montgomery and Brandon (2002) based on rates from low-temperature thermochronometry (R_c = 1500, K = 0.25 m/Myr, MSWD = 13). Regressions from the least-squares technique shows a best-fit, nearly-linear model (i.e. the exponent is 0.98) for the relationship between erosion and channel steepness (Fig. 5C). The least-squares technique demonstrates that there is no strong linear or non-linear relationship between erosion and precipitation across the range (Fig. 5D).

5 Discussion

5.1 Reliability of cosmogenic erosion rates in the glaciated Olympic Mountains

While there are still a few minor extant valley/cirque glaciers, the Last Glacial Maximum occurred in the Olympics Mountains ~17 ka (Thackray, 2008). Therefore, most of our samples should largely reflect post ~~-recessional~~ glacial erosion rates. Our isotopic equilibrium model results show that even the slowest eroding landscapes in the Olympic Mountains could achieve isotopic equilibrium within ~3000 yrs (Fig. 5). Furthermore, the slowest eroding basins from the western flank of the range did not contain valley glaciers during the LGM (Thackray, 2001), and thus, these samples are even less likely to violate ~~this~~ the isotopic equilibrium assumption. The most recently deglaciated portions of the range are in the rugged core, where erosion rates are also higher, and where some landscapes can reach isotopic equilibrium in less than 1500 yrs (Fig. 5).

In landscapes where the cosmogenic nuclide inventories are a function of constant exposure or constant erosion, the ratio of ^{26}Al to ^{10}Be within sediments can be predicted based on the modeled (Lal, 1991, Balco et al., 2008) or measured (Corbett et al., 2017) ratios. ~~Most R~~recent~~ly~~ studies suggest that our samples should have natural ^{26}Al/^{10}Be ratios of ~6.75 (Balco et al., 2008)., ~~–~~ a value that is very close to most of our measured ratios ~~Based on our measured ^{26}Al/^{10}Be ratios~~ (Figure 4)., ~~,~~ Therefore, we find it unlikely that sediment storage and reworking (e.g. from terraces or moraines) has violated our assumptions that modern sediments record a representative sample of all sediment in the basin. If anomalously low concentration quartz was introduced into our samples via incision of older deposits (glacial or fluvial), ~~or through deep landslides,~~ we would expect to see depressed ^{26}Al/^{10}Be ratios. Similar to previous work (Belmont et al, 2007) we have assumed that there is no risk to calculated erosion rates due to quartz infertility or proportional quartz sourcing from all parts of our basins in the Olympic Mountains. While there are some quartz-free lithologies in the range, these rocks are a minor occurrence the in Olympic Subduction Complex, and we have avoided sampling the Coast Range Terrane completely. In locations where nested catchments are found, erosion rates are with error of each other, suggesting a proportional scouring of quartz from all parts of even the largest sampled basin (compare WA1526, DEN101, and DEN106).

5.2 Interpreting relationships between erosion and basin metrics

In landscapes with high fluvial and/or glacial erosion, soil production and hillslope transport may not be able to adjust to channel incision. In such a case, hillslope angles steepen and tend toward a threshold that is controlled by the strength of the material (Schmidt and Montgomery, 1995). Once hillslopes reach such a threshold, increases in erosion can only occur with a commensurate increase in hillslope failure (Burbank et al., 1996), and the form of these hillslopes are no longer sensitive to changes in erosion. However, the gradients of channels in these very steep landscapes are generally much lower than the internal angel of friction, and as such, still have the capacity to adjust to increases in erosion rate. Therefore, it has been suggested that the morphology of channels is a more robust metric to detect erosion rate variations (Ouimet et al., 2009, DiBiase et al., 2010).

Our data show that basin-averaged hillslope gradients cease to increase in basins eroding faster than ~300 m/Myr Fig. 6B). This limit has been observed in many other landscapes around the world (DiBiase et al., 2010, Ouimet et al., 2009, Montgomery and Brandon, 2002, Binnie et al., 2007). Basin-averaged hillslope angle values tend to reach a maximum around 34°, as also shown by Montgomery (2001) using 100 km^2 grids across the Olympic range. The extent to which these threshold hillslope angles are indicative of rock uplift rates or glacial modification is not completely clear. While it is possible that the weak lithologies and fast erosion rates of the Olympic Mountains may be setting these threshold hillslopes, it has also been documented that hillslope angles have likely been increased throughout the range via glaciers widening valleys (Montgomery, 2002, Adams and Ehlers, 2017), or eroding headward and migrating ridge tops (Adams and Ehlers, 2017).

Similarly, basin-averaged local relief values do not exceed ~1350 m despite increasing erosion rates (Fig. 6A). This apparent threshold relief may be due to the influence of the glacial buzzsaw effect, whereby efficiently eroding alpine glaciers have controlled the mean and range of elevations during the Plio-Pleistocene. If these local relief values are limited due to glacial incision, then this would be a transient topographic signal, and imply that local relief could have been higher in the past. As such, we do not suggest that the non-linear fit parameters for hillslope and local relief data presented here are related to topographic steady-state conditions; however, our fit parameters are not very different from those relating topography to long-term erosion rates (Montgomery and Brandon, 2002). Glaciers may have also reduced channel steepness values while active in the Plio-Pleistocene by incising into channel floors more deeply than rivers had previously (Adams and Ehlers, 2017). This effect may be seen in the apparent limit of channel steepness around 160 $m^{0.9}$ (Figure 6C).

What is clear from these regressions is that in as much as relationships between modern topography and erosion exist based on thermochronometric data in the Olympic Mountains (Montgomery and Brandon, 2002), so do relationships between modern topography and detrital cosmogenic erosion rates. One advantage to using detrital studies is the obvious choice for an erosion integration area (i.e. the average erosion rate is integrated across the area of the sampled basin), as opposed to selecting a given area around a specific point in the landscape for a bedrock sample. Indeed, subtle changes in the sampling area throughout the Olympic Mountains can have a large influence on the calculated topographic metric (i.e. changing the radius of a circle around a point can add topography across a drainage divide). However, there is a greater uncertainty regarding the integration timescale of cosmogenic rates in that it can often only be assumed that rates only integrate over hundreds to thousands of years. Our analyses provide good evidence for relationships between topographic metrics and basin-average erosion rates, which are likely the result of long-lived Miocene tectonics (Brandon et al., 1998), and Plio-Pleistocene climate change (e.g. hillslope gradient, local relief, channel steepness) (Porter, 1964, Montgomery and

Greenberg, 2000, Montgomery, 2002, Adams and Ehlers, 2017). The key question remaining for this study area, and similarly glaciated and tectonically active orogens elsewhere is - what are the controls on post-glacial erosion rates?

5.2 Orogenic processes governing erosion rates

With our new and previously published erosion rates, we have made several important observations in the previous sections that we elaborate on below. These observations are: 1) There is no relationship between precipitation and Holocene erosion rates across the range (Fig. 6D). 2) Basins with similar topographic characteristics have equivalent erosion rates, even across the range divide where glacial size changed drastically (compare black and grey samples in Fig. 6). 3) It is apparent from our regressions there are non-linear relationships with local relief, channel steepness and hillslope angle, and Holocene erosion rates (Fig. 6). In tectonically active and previously glaciated mountain ranges there are three common orogenic processes that are most often suggested to dominate Holocene erosion rate patterns: climate gradients (Carretier et al., 2013, Olen et al., 2016), glacial modification of the landscape (Moon et al., 2011, Glotzbach et al., 2013), and patterns of tectonic rock uplift (Adams et al., 2016, Scherler et al., 2013, Godard et al., 2014). In the following we explore the relevance and applicability of these explanations to our data set.

First, we find it highly unlikely that a precipitation gradient similar to the modern has a significant control on recent erosion rates. There is no clear relationship between modern precipitation and erosion rates (Fig. 6D). Even in the neighboring, glaciated Cascade Range (~70 km to the east of the Olympic Mountains) where the modern precipitation gradient is not as large, there is a strong linear relationship suggesting erosion scales with precipitation over diverse timescales, thus making it an important condition for setting Holocene and older erosion rates (Moon et al., 2011, Reiners et al., 2003).

Second, our data do not suggest that destabilization of the landscape via glacial incision has played a primary role in setting the Holocene erosion pattern. Despite the significant gradients in the Pleistocene ELA (Fig. 2E) and the change in glacier size, ~~across the range divide (Fig. 1B)~~and the estimated higher erosion Quaternary erosion rates (Michel et al., 2018) across the range divide (Fig. 1B), there is no statistical difference between the erosion rates across the range divide for basins of similar topographic characteristics (Fig. 2 and Fig. 5A, 5B, 5C), and there is a very weak correlation between ELA and erosion rates (Fig. S2). However, it has been observed that Plio-Pleistocene glaciers widened valleys in the Olympic Mountains (Montgomery, 2002, Adams and Ehlers, 2017), which led to the lengthening and steepening of hillslopes throughout the range. In the nearby Cascade Range, similar valley widening has led to hillslopes with higher likelihoods for failure (Moon et al., 2011). Unlike in the Olympic Mountains, findings from the Cascades suggest that the range was heavily influenced by glacial incision to an extent that the topographic form largely reflects relict glacial processes, and as a result, Holocene erosion rates are more likely to be correlated with precipitation in these landscapes further from equilibrium. Our analysis suggests that the changes in the landscape due to Plio-Pleistocene glaciation in the Olympic Mountains likely only steepened relatively small areas of hillslopes of landscapes relative to the already steep conditions imposed by high rock uplift and erosion rates. Similarly, glacial incision may have only influenced small relatively small portions of the channel network and range relief, which might appear as threshold values of channel steepness and local relief, or simply to make the distributions of these parameters within a basin more complex. Therefore, the landscapes examined the Olympics may have been only moderately perturbed by Plio-Pleistocene glacial incision, and they may still record a relatively close balance between recent erosion rates and rock uplift.

~~Taken together, we suggest that the Holocene erosion rates (Fig. 2E), mean elevation, local relief (Fig. 2B), and channel steepness (Fig. 2D) observed in the Olympic Mountains most closely record a rock uplift pattern that increases from the low relief flanks to the rugged core of the range (Fig. 7), similar to what has been shown in other datasets (Brandon et al., 1998;Batt et al., 2001;Pazzaglia and Brandon, 2001). Figure 7 illustrates the similarity of the trends in other rock uplift rate proxies, and the cosmogenic erosion rates presented here in a direction parallel to the convergence across the Olympic Mountain range. Adams and Ehlers (2017) proposed that a spatial pattern of rock uplift similar to the one described above was consistent with the observations of the bend in the subducting Juan de Fuca plate at the Cascadia subduction zone and the dome of accreted sediments in the core of the Olympic Mountains, which form the east plunging Olympic Anticline (Brandon and Calderwood, 1990). This pattern of focused rock uplift and erosion is also predicted for the geometry of the curved subducting Juan de Fuca plate (Crosson and Owens, 1987;Bendick and Ehlers, 2014). Our observations are in line with previous authors who have highlighted importance of subduction zone dynamics for setting the pace and pattern of erosion in the Olympic Mountains (Brandon and Vance, 1992;Pazzaglia and Brandon, 2001;Batt et al., 2001;Brandon et al., 1998;Stolar et al., 2007).~~

~~6 Conclusions~~

~~Whether~~ The balance between post-glacial erosion ~~rates balance~~ and longer-lived rock uplift ~~rates is strongly influenced by~~depends on whether post-glacial climate conditions ~~changes~~ (e.g. increase or decrease in precipitation), or topographic perturbations (e.g. hillslope steeping or channel shallowing) have changed the activity of extant surface processes~~ as compared to before the onset of glaciation~~. There are many examples of ranges where there have been significant changes to topography (Brardinoni and Hassan, 2006; 2007; ~~Simon H~~ Brocklehurst and Whipple, 2007; Glotzbach et al., 2013; Hobley et al., 2010; ~~D. R.~~ Montgomery, 2001; Robl et al., 2008) and erosion during and after glaciation (Moon et al., 2011, Reiners et al., 2003, Christeleit et al., 2017), and others where such changes are not clearly observed (Thomson et al., 2010). More generally, these changes were explored in a coupled ice dynamic/landscape evolution model testing the modification of topography and erosion rates due to alpine glaciation (Yanites and Ehlers, 2012). The results of ~~this study~~these numerical models suggest that the degree of erosion change before and after glaciation is a function of regional temperature and the rock uplift rate. These two parameters control the glaciers ability concentrate elevations at or near the ELA were ice erodes most efficiently. If too much or too little of the landscape lies above the ELA, then glacial erosion is not very efficient and little topographic perturbation occurs. In these landscapes, erosion rates may change during glacial periods, but interglacial erosion rates return to near rock uplift rates, as before. In the cases where glaciers were very effective agents of erosion, relief (on hillslopes or channels) is reduced during glaciation (Whipple et al., 1999; Adams and Ehlers, 2017), and post-glacial erosion rates can be lower than pre-glacial, and vice versa. As such, there is a sweet spot within mountain range conditions where glaciers are more efficient, and furthermore, even when glaciers are efficient it cannot be assumed how post-glacial rates might change. To put it another way, it should be assumed that landscapes will respond differently alpine glaciation depending on climate and topographic conditions before and after glaciation.

Figure 7 illustrates the similarity of the trends in other rock uplift rate proxies, and the cosmogenic erosion rates presented here in a direction parallel to the convergence across the Olympic Mountain range. When our new Holocene erosion rate pattern is compared with older patterns of estimated rock uplift rates (Fig. 7), there are a few apparent mismatches. In some locations, our rates are higher and lower than rock uplift rates (as might be expected in post-glacial

Formatted: Indent: First line: 1.27 cm

landscapes), but overall the pattern of increasing rates from the flanks to the core of the range is consistent between these datasets. ~~We suggest this long-lasting pattern is primarily controlled by tectonic forces, and while the Plio-Pleistocene alpine glaciers of the Olympic Mountains have created a wonderfully sculpted landscape, they have not radically altered the topography enough to drastically change the pattern of erosion.~~

Adams and Ehlers (2017) and Michel et al. (2018) proposed that a spatial pattern of rock uplift similar to the one described above was consistent with the observations of the bend in the subducting Juan de Fuca plate at the Cascadia subduction zone and the dome of accreted sediments in the core of the Olympic Mountains, which form the east-plunging Olympic Anticline (Brandon and Calderwood, 1990). This pattern of focused rock uplift and erosion is also predicted for the geometry of the curved subducting Juan de Fuca plate (Crosson and Owens, 1987, Bendick and Ehlers, 2014). We suggest this long-lasting pattern is primarily controlled by tectonic forces, and while the Plio-Pleistocene alpine glaciers of the Olympic Mountains have not radically altered the topography enough to drastically change the pattern of erosion.

Formatted: Indent: First line: 0 cm

~~When our new Holocene erosion rate pattern is compared with older patterns of estimated rock uplift rates (Fig. 7), there are a few apparent mismatches. In some locations, our rates are higher and lower than rock uplift rates (as might be expected in post-glacial landscapes), but overall the pattern of increasing rates from the flanks to the core of the range is consistent between these datasets. We suggest this long-lasting pattern is primarily controlled by tectonic forces, and while the Plio-Pleistocene alpine glaciers of the Olympic Mountains have created a wonderfully sculpted landscape, they have not radically altered the topography enough to drastically change the pattern of erosion.~~

6 Conclusions

Taken together, we suggest that the Holocene erosion rates (Fig. 2E), mean elevation, local relief (Fig. 2B), and channel steepness (Fig. 2D) observed in the Olympic Mountains most closely record a rock uplift pattern that increases from the low-relief flanks to the rugged core of the range (Fig. 7), similar to what has been shown in other datasets (Brandon et al., 1998, Batt et al., 2001, Pazzaglia and Brandon, 2001). Our ~~observations~~interpretations are in line with previous authors who have highlighted the importance of subduction zone dynamics for setting the pace and pattern of erosion in the Olympic Mountains (Brandon and Vance, 1992, Pazzaglia and Brandon, 2001, Batt et al., 2001, Brandon et al., 1998, Stolar et al., 2007). This result may be unexpected given the glacial impact that has been previously documented throughout the range (Porter, 1964; Montgomery and Greensburg, 2000; Montgomery, 2002; Adams and Ehlers, 2017), and further described in this manuscript. However, the Plio-Pleistocene glaciers impact on small- and range-scale may have been limited in the Olympic Mountains because large portions of the range may have already been at near-threshold conditions before glaciation (Montgomery, 2001), or a small proportion of the range was focused at the ELA during glacial periods. As such, post-glacial erosion rates exhibit the same spatial patterns and magnitudes as longer-term estimates. The alpine glaciers of the Olympic Mountains have left behind very scenic, sculpted landscapes, but these landscapes may have not been as significantly altered as once thought, at least not enough to drastically change post-glacial erosion.

Field Code Changed

Field Code Changed

Acknowledgments

We thank Lorenz Michel, Holger Sprengel, Roger Hoffman, Bill Baccus, Jerry Freilich and the Olympic National Park Rangers for assistance while in the field and logistics. We also acknowledge the help of Christine Lempe, Hella Whitmann, Mirjam Schaller, Dagmar Kost, and Jessica Starke with the processing of these stubborn samples. We are grateful to Karl

Lang, Matthew Jungers, and Mirjam Schaller for fruitful discussions. Frank Pazzaglia, George Hilley, Paul Bierman, and two anonymous reviewers are~~is~~ thanked for ~~his~~ their comments on an earlier version of this manuscript. This work was supported by a European Research Council (ERC) Consolidator Grant number 615703 to T. Ehlers. All data used in the manuscript are freely available in either the manuscript tables or online supplemental material. The authors declare that they have no conflict of interest.

References

Adams, B. and Ehlers, T. (2017) 'Deciphering topographic signals of glaciation and rock uplift in an active orogen: a case study from the Olympic Mountains, USA', *Earth Surface Processes and Landforms*.

Adams, B., Whipple, K., Hodges, K. and Heimsath, A. (2016) 'In situ development of high-elevation, low-relief landscapes via duplex deformation in the Eastern Himalayan hinterland, Bhutan', *Journal of Geophysical Research: Earth Surface*.

Ahnert, F. (1970) 'Functional relationships between denudation, relief, and uplift in large mid-latitude drainage basins', *American Journal of Science*, 268(3), pp. 243-&.

Anderson, R. S., Molnar, P. and Kessler, M. A. (2006) 'Features of glacial valley profiles simply explained', *Journal of Geophysical Research: Earth Surface*, 111(F1), pp. F01004.

Anderson, R. S., Repka, J. L. and Dick, G. S. (1996) 'Explicit treatment of inheritance in dating depositional surfaces using in situ 10Be and 26Al', *Geology*, 24(1), pp. 47-51.

Balco, G., Stone, J. O., Lifton, N. A. and Dunai, T. J. (2008) 'A complete and easily accessible means of calculating surface exposure ages or erosion rates from (10)Be and (26)Al measurements', *Quaternary Geochronology*, 3(3), pp. 174-195.

Batt, G. E., Brandon, M. T., Farley, K. A. and Roden-Tice, M. (2001) 'Tectonic synthesis of the Olympic Mountains segment of the Cascadia wedge, using two-dimensional thermal and kinematic modeling of thermochronological ages', *Journal of Geophysical Research: Solid Earth*, 106(B11), pp. 26731-26746.

Belmont, P., Pazzaglia, F. and Gosse, J. C. (2007) 'Cosmogenic 10 Be as a tracer for hillslope and channel sediment dynamics in the Clearwater River, western Washington State', *Earth and Planetary Science Letters*, 264(1), pp. 123-135.

Bendick, R. and Ehlers, T. A. (2014) 'Extreme localized exhumation at syntaxes initiated by subduction geometry', *Geophysical Research Letters*, 41(16), pp. 5861-5867.

Bierman, P. and Steig, E. J. (1996) 'Estimating rates of denudation using cosmogenic isotope abundances in sediment', *Earth Surface Processes and Landforms*, 21(2), pp. 125-139.

Binnie, S. A., Phillips, W. M., Summerfield, M. A. and Fifield, L. K. (2007) 'Tectonic uplift, threshold hillslopes, and denudation rates in a developing mountain range', *Geology*, 35(8), pp. 743-746.

Brandon, M. T. and Calderwood, A. R. (1990) 'High-pressure metamorphism and uplift of the Olympic subduction complex', *Geology*, 18(12), pp. 1252-1255.

Brandon, M. T., Roden-Tice, M. K. and Garver, J. I. (1998) 'Late Cenozoic exhumation of the Cascadia accretionary wedge in the Olympic Mountains, northwest Washington State', *Geological Society of America Bulletin*, 110(8), pp. 985-1009.

Brandon, M. T. and Vance, J. A. (1992) 'Tectonic evolution of the Cenozoic Olympic subduction complex, Washington State, as deduced from fission track ages for detrital zircons', *American Journal of Science*, 292(8), pp. 565-636.

Brardinoni, F. and Hassan, M. A. (2006) 'Glacial erosion, evolution of river long profiles, and the organization of process domains in mountain drainage basins of coastal British Columbia', *Journal of Geophysical Research: Earth Surface*, 111(F1).

Brardinoni, F. and Hassan, M. A. (2007) 'Glacially induced organization of channel-reach morphology in mountain streams', *Journal of Geophysical Research: Earth Surface*, 112(F3).

Brocklehurst, S. H. and Whipple, K. X. (2002) 'Glacial erosion and relief production in the Eastern Sierra Nevada, California', *Geomorphology*, 42(1-2), pp. 1-24.

Brocklehurst, S. H. and Whipple, K. X. (2004) 'Hypsometry of glaciated landscapes', *Earth Surface Processes and Landforms*, 29(7), pp. 907-926.

Brocklehurst, S. H. and Whipple, K. X. (2006) 'Assessing the relative efficiency of fluvial and glacial erosion through simulation of fluvial landscapes', *Geomorphology*, 75(3-4), pp. 283-299.

Brocklehurst, S. H. and Whipple, K. X. (2007) 'Response of glacial landscapes to spatial variations in rock uplift rate', *Journal of Geophysical Research: Earth Surface*, 112(F2), pp. F02035.

Brown, E. T., Stallard, R. F., Larsen, M. C., Raisbeck, G. M. and Yiou, F. (1995) 'Denudation rates determined from the accumulation of in situ-produced 10Be in the Luquillo Experimental Forest, Puerto Rico', *Earth and Planetary Science Letters*, 129(1-4), pp. 193-202.

Brozović, N., Burbank, D. W. and Meigs, A. J. (1997) 'Climatic limits on landscape development in the northwestern Himalaya', *Science*, 276(5312), pp. 571-574.
Burbank, D. W., Leland, J., Fielding, E., Anderson, R. S., Brozovic, N., Reid, M. R. and Duncan, C. (1996) 'Bedrock incision, rock uplift and threshold hillslopes in the northwestern Himalayas', *Nature*, 379(6565), pp. 505-510.
Carretier, S., Regard, V., Vassallo, R., Aguilar, G., Martinod, J., Riquelme, R., Pepin, E., Charrier, R., Herail, G., Farias, M., Guyot, J. L., Vargas, G. and Lagane, C. (2013) 'Slope and climate variability control of erosion in the Andes of central Chile', *Geology*, 41(2), pp. 195-198.
Christeleit, E. C., Brandon, M. T. and Shuster, D. L. (2017) 'Miocene development of alpine glacial relief in the Patagonian Andes, as revealed by low-temperature thermochronometry', *Earth and Planetary Science Letters*, 460, pp. 152-163.
Corbett, L. B., Bierman, P. R., Rood, D. H., Caffee, M. W., Lifton, N. A. and Woodruff, T. E. (2017) 'Cosmogenic 26Al/10Be surface production ratio in Greenland', *Geophysical Research Letters*, 44(3), pp. 1350-1359.
Crosson, R. and Owens, T. (1987) 'Slab geometry of the Cascadia subduction zone beneath Washington from earthquake hypocenters and teleseismic converted waves', *Geophysical Research Letters*, 14(8), pp. 824-827.
Daly, C., Neilson, R. P. and Phillips, D. L. (1994) 'A statistical topographic model for mapping climatological precipitation over mountainous terrain', *Journal of Applied Meteorology*, 33(2), pp. 140-158.
DeMets, C. and Dixon, T. H. (1999) 'New kinematic models for Pacific-North America motion from 3 Ma to present, I: Evidence for steady motion and biases in the NUVEL-1A model', *Geophysical Research Letters*, 26(13), pp. 1921-1924.
DiBiase, R. A., Whipple, K. X., Heimsath, A. M. and Ouimet, W. B. (2010) 'Landscape form and millennial erosion rates in the San Gabriel Mountains, CA', *Earth and Planetary Science Letters*, 289(1), pp. 134-144.
Dunne, J., Elmore, D. and Muzikar, P. (1999) 'Scaling factors for the rates of production of cosmogenic nuclides for geometric shielding and attenuation at depth on sloped surfaces', *Geomorphology*, 27(1), pp. 3-11.
Ehlers, T. A., Farley, K. A., Rusmore, M. E. and Woodsworth, G. J. (2006) 'Apatite (U-Th)/He signal of large-magnitude accelerated glacial erosion, southwest British Columbia', *Geology*, 34(9), pp. 765-768.
Flint, J. (1974) 'Stream gradient as a function of order, magnitude, and discharge', *Water Resources Research*, 10(5), pp. 969-973.
Glotzbach, C., Beek, P., Carcaillet, J. and Delunel, R. (2013) 'Deciphering the driving forces of erosion rates on millennial to million-year timescales in glacially impacted landscapes: An example from the Western Alps', *Journal of Geophysical Research: Earth Surface*, 118(3), pp. 1491-1515.
Godard, V., Bourlès, D. L., Spinabella, F., Burbank, D. W., Bookhagen, B., Fisher, G. B., Moulin, A. and Léanni, L. (2014) 'Dominance of tectonics over climate in Himalayan denudation', *Geology*, pp. G35342. 1.
Godard, V., Burbank, D., Bourlès, D., Bookhagen, B., Braucher, R. and Fisher, G. (2012) 'Impact of glacial erosion on ^{10}Be concentrations in fluvial sediments of the Marsyandi catchment, central Nepal', *Journal of Geophysical Research: Earth Surface*, 117(F3), pp. F03013.
Gosse, J. C. and Phillips, F. M. (2001) 'Terrestrial in situ cosmogenic nuclides: theory and application', *Quaternary Science Reviews*, 20(14), pp. 1475-1560.
Granger, D. E., Kirchner, J. W. and Finkel, R. (1996) 'Spatially averaged long-term erosion rates measured from in situ-produced cosmogenic nuclides in alluvial sediment', *Journal of Geology*, 104(3), pp. 249-257.
Hack, J. T. (1957) 'Studies of longitudinal stream profiles in Virginia and Maryland'.
Hallet, B., Hunter, L. and Bogen, J. (1996) 'Rates of erosion and sediment evacuation by glaciers: A review of field data and their implications', *Global and Planetary Change*, 12(1-4), pp. 213-235.
Herman, F., Seward, D., Valla, P. G., Carter, A., Kohn, B., Willett, S. D. and Ehlers, T. A. (2013) 'Worldwide acceleration of mountain erosion under a cooling climate', *Nature*, 504(7480), pp. 423-+.
Hobley, D. E., Sinclair, H. D. and Cowie, P. A. (2010) 'Processes, rates, and time scales of fluvial response in an ancient postglacial landscape of the northwest Indian Himalaya', *Geological Society of America Bulletin*, 122(9-10), pp. 1569-1584.
Koppes, M. N. and Montgomery, D. R. (2009) 'The relative efficacy of fluvial and glacial erosion over modern to orogenic timescales', *Nature Geoscience*, 2(9), pp. 644-647.
Lal, D. (1991) 'COSMIC-RAY LABELING OF EROSION SURFACES - INSITU NUCLIDE PRODUCTION-RATES AND EROSION MODELS', *Earth and Planetary Science Letters*, 104(2-4), pp. 424-439.
MacGregor, K. R., Anderson, R., Anderson, S. and Waddington, E. (2000) 'Numerical simulations of glacial-valley longitudinal profile evolution', *Geology*, 28(11), pp. 1031-1034.
Meigs, A. and Sauber, J. (2000) 'Southern Alaska as an example of the long-term consequences of mountain building under the influence of glaciers', *Quaternary Science Reviews*, 19(14), pp. 1543-1562.
Michel, L., Ehlers, T. A., Glotzbach, C., Adams, B. A. and Stübner, K. (2018) 'Tectonic and glacial contributions to focused exhumation in the Olympic Mountains, Washington, USA', *Geology*.

Montgomery, D. R. (2001) 'Slope distributions, threshold hillslopes, and steady-state topography', *American Journal of Science*, 301(4-5), pp. 432-454.
Montgomery, D. R. (2002) 'Valley formation by fluvial and glacial erosion', *Geology*, 30(11), pp. 1047-1050.
Montgomery, D. R. and Brandon, M. T. (2002) 'Topographic controls on erosion rates in tectonically active mountain ranges', *Earth and Planetary Science Letters*, 201(3-4), pp. 481-489.
Montgomery, D. R. and Greenberg, H. M. (2000) 'Local relief and the height of Mount Olympus', *Earth Surface Processes and Landforms*, 25(4), pp. 385-396.
Moon, S., Chamberlain, C. P., Blisniuk, K., Levine, N., Rood, D. H. and Hilley, G. E. (2011) 'Climatic control of denudation in the deglaciated landscape of the Washington Cascades', *Nature Geoscience*, 4(7), pp. 469-473.
Norton, K. P., Abbühl, L. M. and Schlunegger, F. (2010) 'Glacial conditioning as an erosional driving force in the Central Alps', *Geology*, 38(7), pp. 655-658.
Olen, S. M., Bookhagen, B. and Strecker, M. R. (2016) 'Role of climate and vegetation density in modulating denudation rates in the Himalaya', *Earth and Planetary Science Letters*, 445, pp. 57-67.
Ouimet, W. B., Whipple, K. X. and Granger, D. E. (2009) 'Beyond threshold hillslopes: Channel adjustment to base-level fall in tectonically active mountain ranges', *Geology*, 37(7), pp. 579-582.
Pazzaglia, F. J. and Brandon, M. T. (2001) 'A fluvial record of long-term steady-state uplift and erosion across the Cascadia forearc high, western Washington State', *American Journal of Science*, 301(4-5), pp. 385-431.
Portenga, E. W. and Bierman, P. R. (2011) 'Understanding Earth's eroding surface with 10 Be', *GSA Today*, 21(8), pp. 4-10.
Portenga, E. W., Bierman, P. R., Duncan, C., Corbett, L. B., Kehrwald, N. M. and Rood, D. H. (2014) 'Erosion rates of the Bhutanese Himalaya determined using in situ-produced 10 Be', *Geomorphology*.
Porter, S. C. (1964) 'Composite Pleistocene snow line of Olympic Mountains and Cascade Range, Washington', *Geological Society of America Bulletin*, 75(5), pp. 477-481.
Reiners, P. W., Ehlers, T. A., Mitchell, S. G. and Montgomery, D. R. (2003) 'Coupled spatial variations in precipitation and long-term erosion rates across the Washington Cascades', *Nature*, 426(6967), pp. 645-647.
Robl, J., Hergarten, S. and Stüwe, K. (2008) 'Morphological analysis of the drainage system in the Eastern Alps', *Tectonophysics*, 460(1), pp. 263-277.
Roering, J. J., Kirchner, J. W., Sklar, L. S. and Dietrich, W. E. (2001) 'Hillslope evolution by nonlinear creep and landsliding: An experimental study', *Geology*, 29(2), pp. 143-146.
Scherler, D., Bookhagen, B. and Strecker, M. R. (2013) 'Tectonic control on 10Be-derived erosion rates in the Garhwal Himalaya, India', *Journal of Geophysical Research: Earth Surface*.
Schmidt, K. M. and Montgomery, D. R. (1995) 'Limits to relief', *Science*, 270(5236), pp. 617.
Shuster, D. L., Ehlers, T. A., Rusmoren, M. E. and Farley, K. A. (2005) 'Rapid glacial erosion at 1.8 Ma revealed by 4He/3He thermochronometry', *Science*, 310(5754), pp. 1668-1670.
Stolar, D., Roe, G. and Willett, S. (2007) 'Controls on the patterns of topography and erosion rate in a critical orogen', *Journal of Geophysical Research: Earth Surface*, 112(F4).
Stone, J. O. (2000) 'Air pressure and cosmogenic isotope production', *Journal of Geophysical Research: Solid Earth (1978–2012)*, 105(B10), pp. 23753-23759.
Tabor, R. W. and Cady, W. M. (1978) *The structure of the Olympic Mountains, Washington: Analysis of a subduction zone.* US Govt. Print. Off.
Thackray, G. D. (2001) 'Extensive early and middle Wisconsin glaciation on the western Olympic Peninsula, Washington, and the variability of Pacific moisture delivery to the northwestern United States', *Quaternary Research*, 55(3), pp. 257-270.
Thackray, G. D. (2008) 'Varied climatic and topographic influences on Late Pleistocene mountain glaciation in the western United States', *Journal of Quaternary Science*, 23(6-7), pp. 671-681.
Thomson, S. N., Brandon, M. T., Tomkin, J. H., Reiners, P. W., Vásquez, C. and Wilson, N. J. (2010) 'Glaciation as a destructive and constructive control on mountain building', *Nature*, 467(7313), pp. 313-317.
Valla, P. G., Shuster, D. L. and van der Beek, P. A. (2011) 'Significant increase in relief of the European Alps during mid-Pleistocene glaciations', *Nature Geoscience*, 4(10), pp. 688-692.
Vance, D., Bickle, M., Ivy-Ochs, S. and Kubik, P. W. (2003) 'Erosion and exhumation in the Himalaya from cosmogenic isotope inventories of river sediments', *Earth and Planetary Science Letters*, 206(3-4), pp. 273-288.
Von Blanckenburg, F., Belshaw, N. and O'Nions, R. (1996) 'Separation of 9Be and cosmogenic 10Be from environmental materials and SIMS isotope dilution analysis', *Chemical Geology*, 129(1-2), pp. 93-99.
Whipple, K. X., Kirby, E. and Brocklehurst, S. H. (1999) 'Geomorphic limits to climate-induced increases in topographic relief', *Nature*, 401(6748), pp. 39-43.
Willenbring, J. K. and von Blanckenburg, F. (2010) 'Long-term stability of global erosion rates and weathering during late-Cenozoic cooling', *Nature*, 465(7295), pp. 211-214.
Willett, S. D. (1999) 'Orogeny and orography: The effects of erosion on the structure of mountain belts', *Journal of Geophysical Research-Solid Earth*, 104(B12), pp. 28957-28981.

Wittmann, H., von Blanckenburg, F., Kruesmann, T., Norton, K. P. and Kubik, P. W. (2007) 'Relation between rock uplift and denudation from cosmogenic nuclides in river sediment in the Central Alps of Switzerland', *Journal of Geophysical Research: Earth Surface (2003–2012)*, 112(F4).

Wobus, C., Whipple, K. X., Kirby, E., Snyder, N., Johnson, J., Spyropolou, K., Crosby, B. and Sheehan, D. (2006) 'Tectonics from topography: Procedures, promise, and pitfalls', *Geological Society of America Special Papers*, 398, pp. 55-74.

Yanites, B. J. and Ehlers, T. A. (2012) 'Global climate and tectonic controls on the denudation of glaciated mountains', *Earth and Planetary Science Letters*, 325, pp. 63-75.

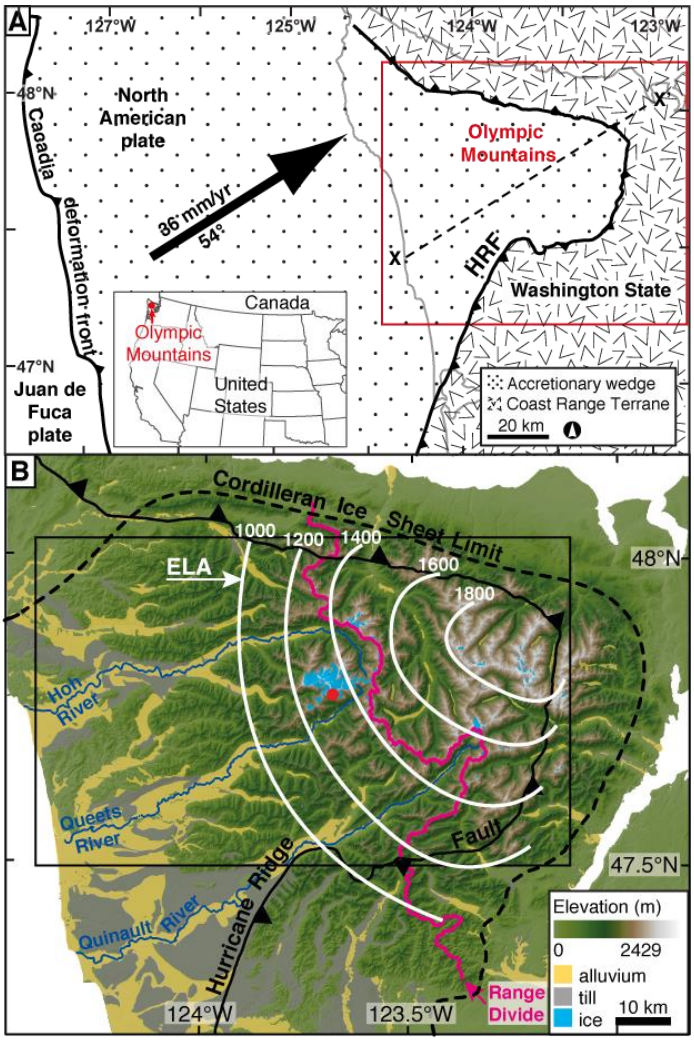

Figure 1. Topographic and geologic features of the Olympic Peninsula, Washington State, USA. A) Simplified geology based on Brandon et al. (1998). The relative velocity of the Juan de Fuca plate toward the North American plate is ~36 mm/yr with a bearing of ~54° (DeMets and Dixon, 1999). Red box denotes the extent of panel B. HRF – Hurricane Ridge Fault. Grey lines outline the coast of Washington State. Dashed black line is the cross-section line for Fig. 7. B)

Elevation map of the Olympic Mountains. Ice, including extant alpine glaciers, is masked in blue. Undifferentiated Quaternary alpine glacial till and alluvial deposits are marked in grey and yellow, respectively. Contours of equilibrium line altitudes (ELA) from Porter (1964) are denoted by white lines (values shown in meters above sea level). Black box denotes the extent of Fig. 2 panels. A red dot marks Mount Olympus.

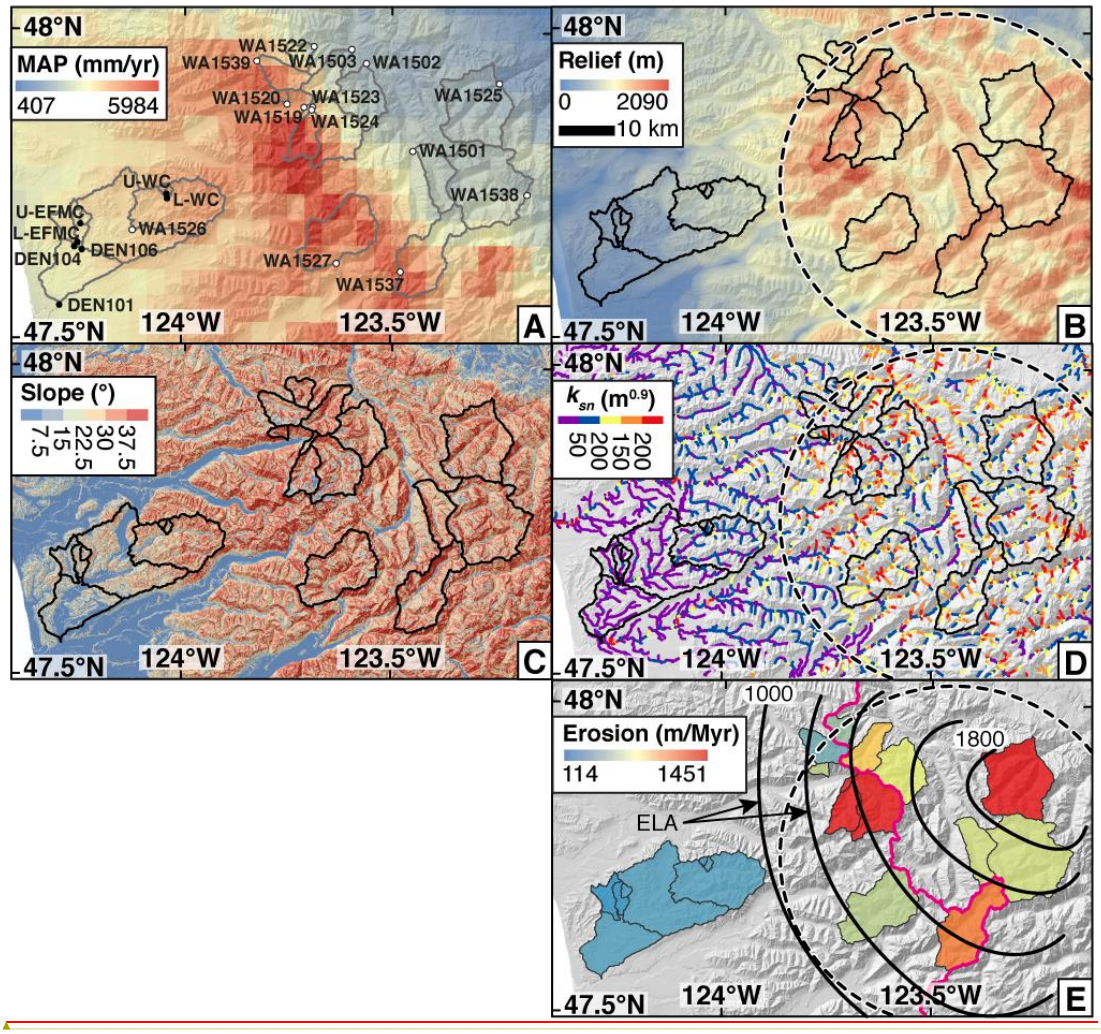

Formatted: Font: 12 pt

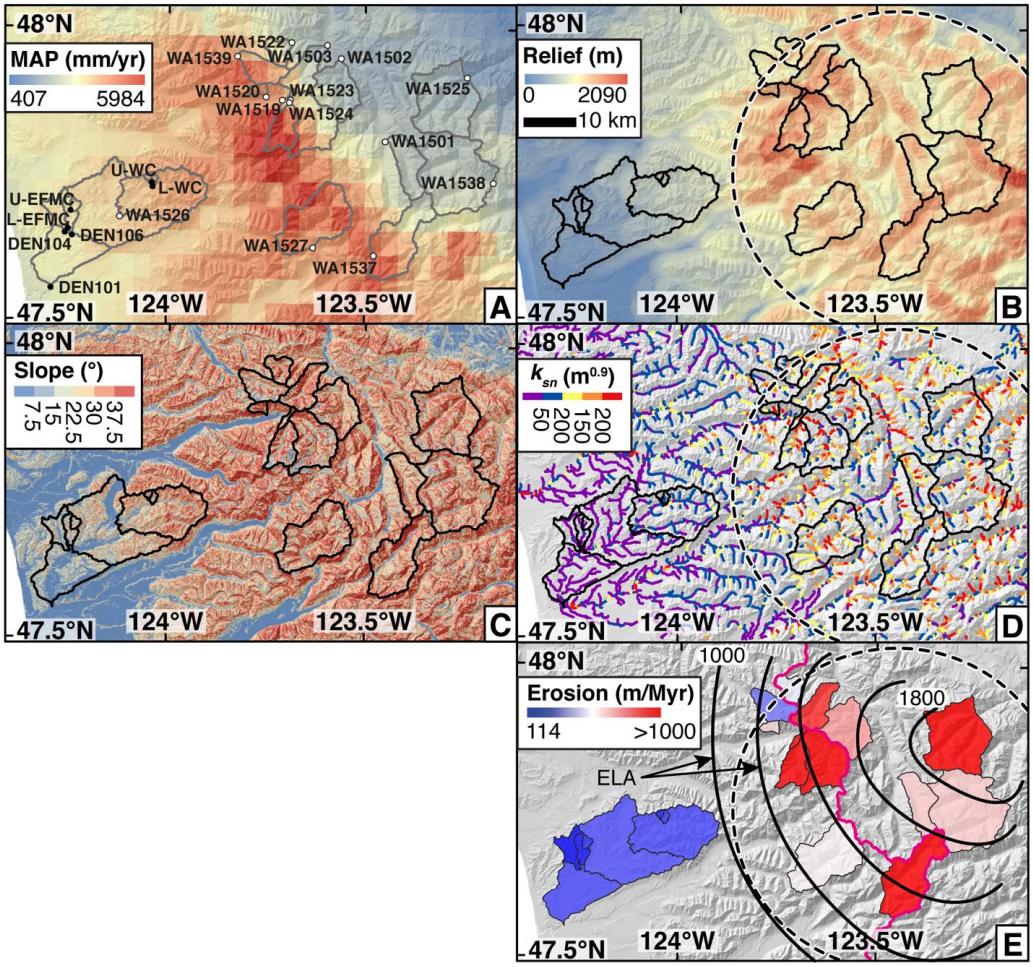

690 **Figure 2. Attribute and erosion maps of the Olympic Mountains.** Solid outlines denote the boundaries of sampled basins. High rugged core outlined in black/white dashed lines. A) Mean annual precipitation (MAP) map based on PRISM data (Daly et al., 1994). Open and closed circles mark new and previously published sample locations, respectively. B) Local relief (5-km relief) map. C) Hillslope angle map. D) Channel steepness (k_{sn}) map plotted for accumulation areas > 2 km^2. E) Basin-averaged erosion rate map. Range divide marked in magenta. Equilibrium line altitude (ELA) contours from 695 Porter (Porter, 1964) are in black.

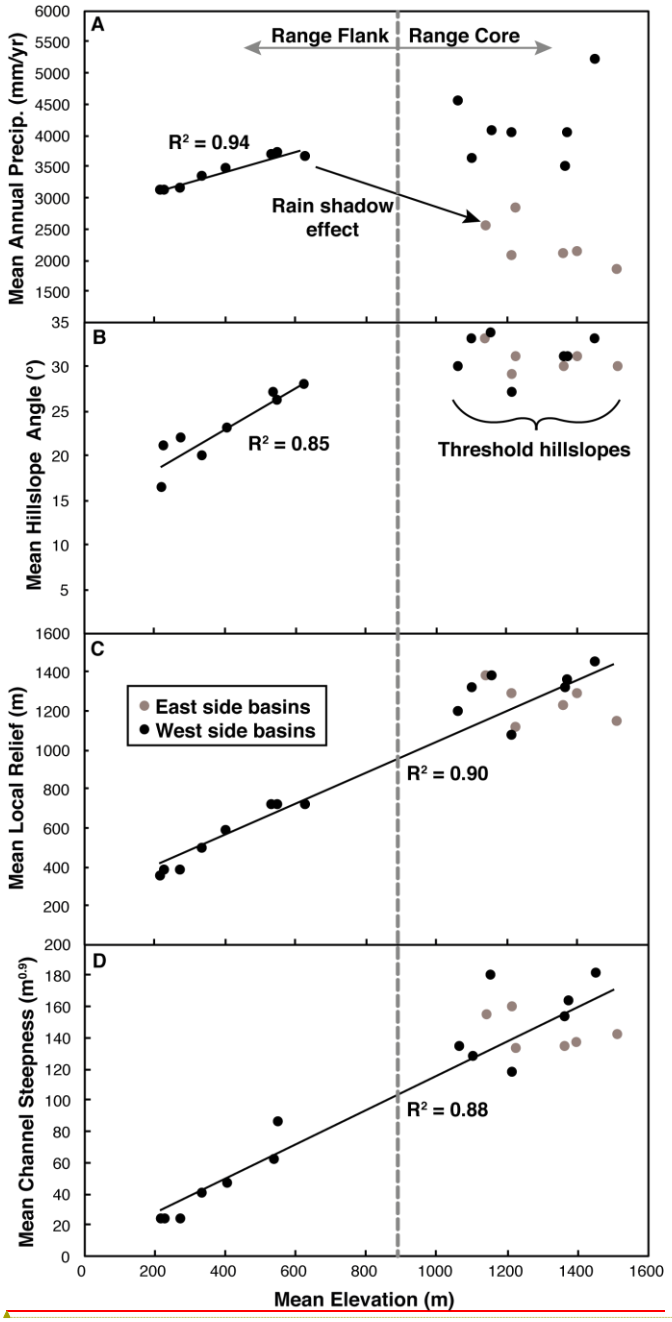

Formatted: Font: 12 pt

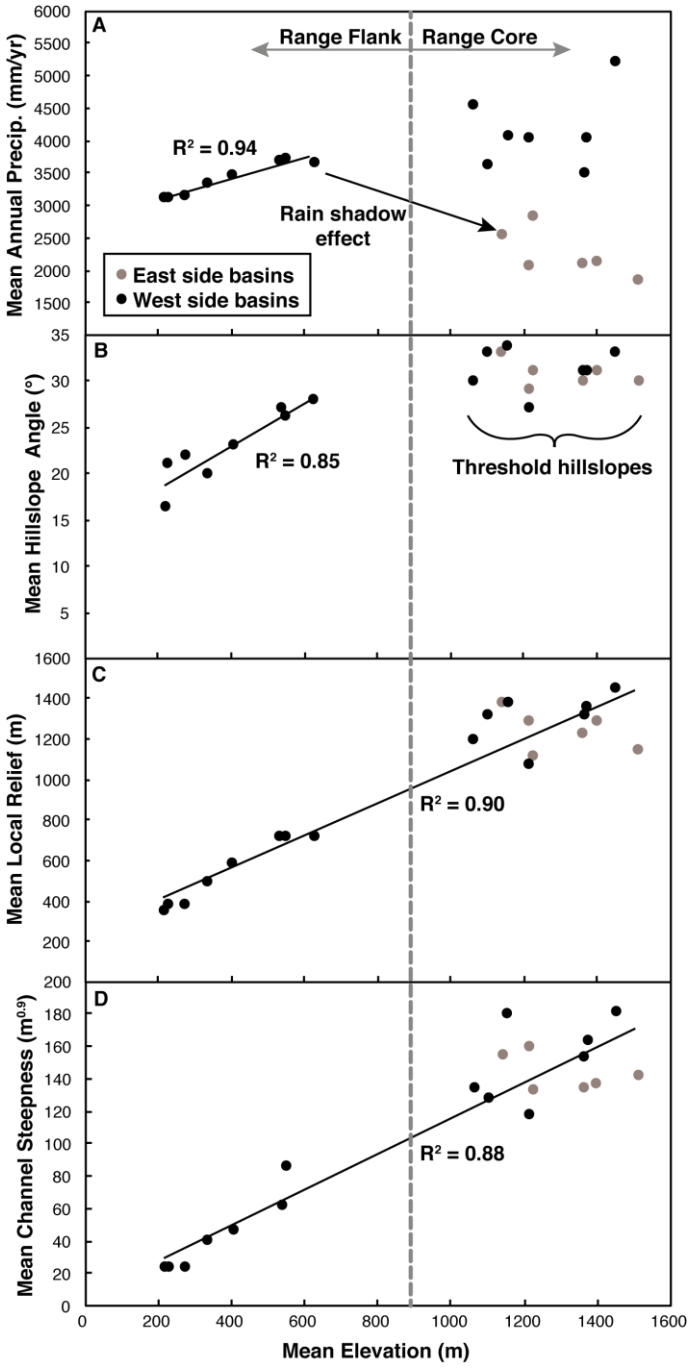

Figure 3. Comparison of the mean basin elevation with other basin averaged metrics. A) Mean annual precipitation. B) Hillslope angle. C) Local relief (using a 5-km diameter circle. D) Channel steepness.

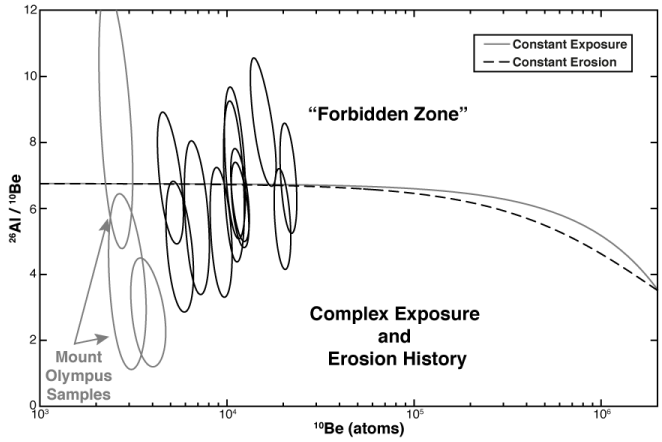

Figure 4. Erosion island plot for new Olympic Mountain samples. Each sample is represented by a 2σ error ellipse. Dashed, grey ellipses mark samples with poor ^{10}Be measurements, see text for discussion.

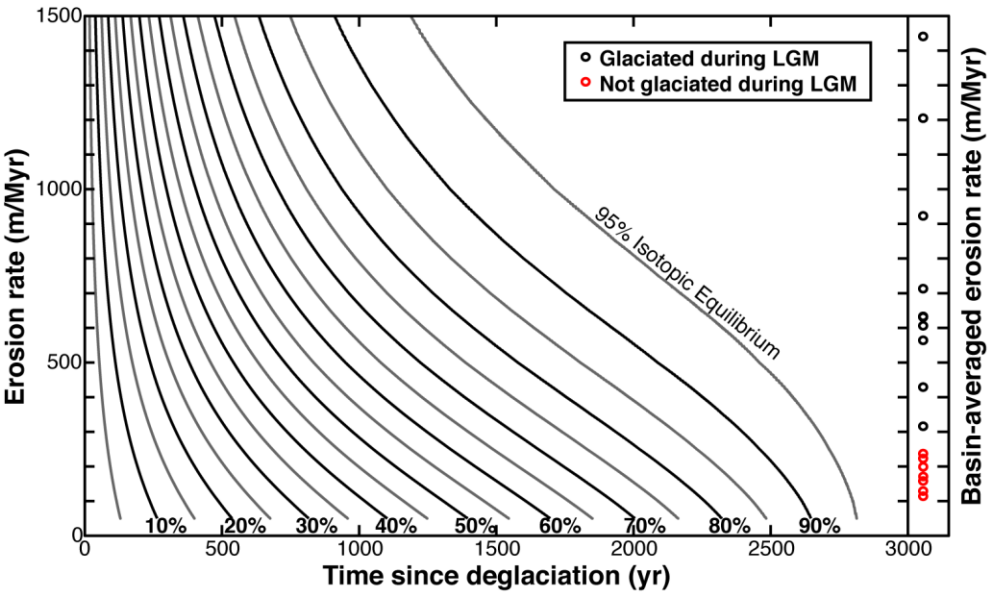

Figure 5. Predicted evolution of landscapes toward isotopic evolution after deglaciation. Black and grey lines denote 10% and 5% contour intervals, respectively. Basin-averaged erosion rates from the Olympic Mountains are shown on the right. Basins marked in red were not glaciated during the Last Glacial Maximum (LGM).

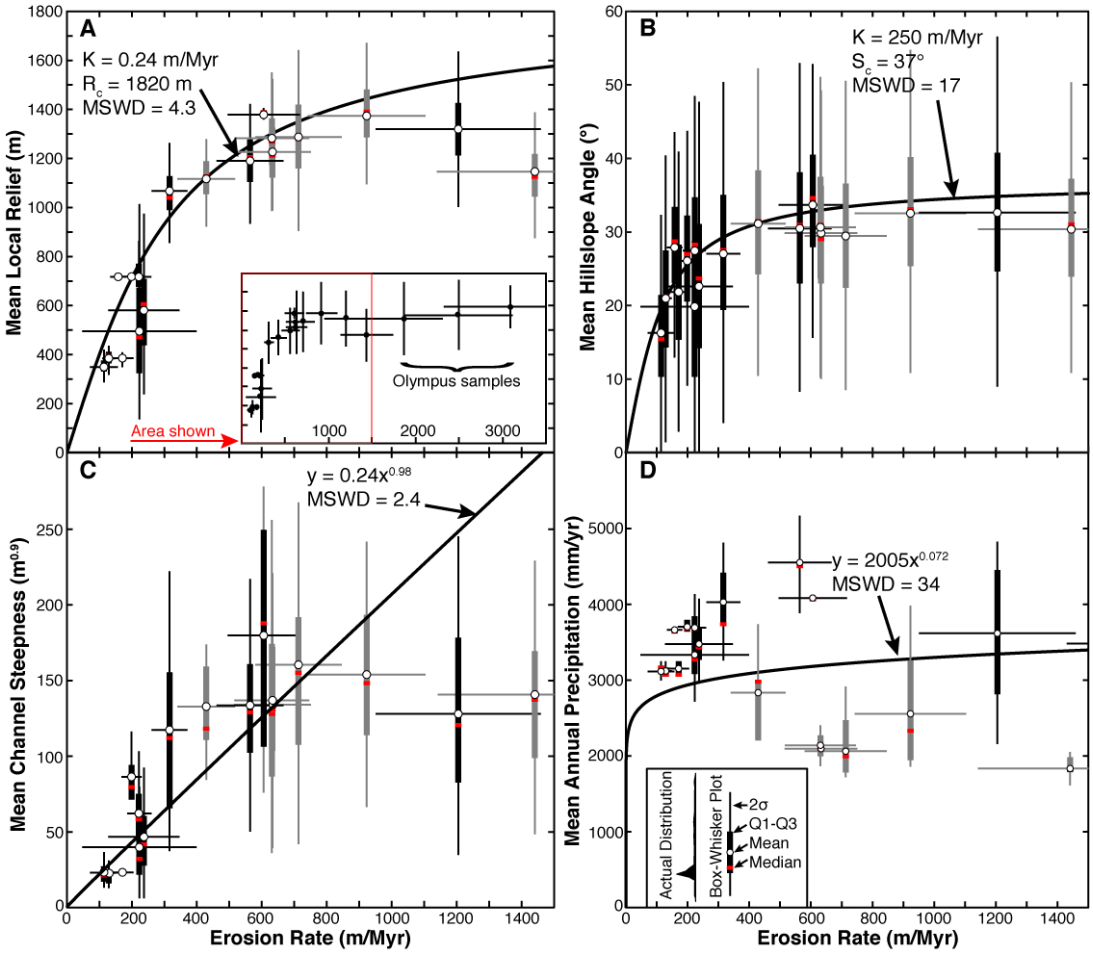

Figure 6. Plot of erosion rates with basin-averaged metrics. Due to the high degree of variation within a single basin, we have plotted basin metric data as box-and-whisker plots. Thin vertical bars denote 2 standard deviations. Thick vertical bars denote the central 50% of the data between the 1st and 3rd quartiles (Q1 and Q3). Red bars denote the medians and white circles denote means. Horizontal bars show 2σ confidence intervals on erosion rates. West and east side basins are shown in black and grey, respectively. A) Erosion rate versus mean local relief (5-km relief). Inset shows higher erosion rate samples not featured in other panels. B) Erosion rate versus mean hillslope angle. C) Erosion rate versus mean channel steepness. D) Erosion rate versus mean annual precipitation.

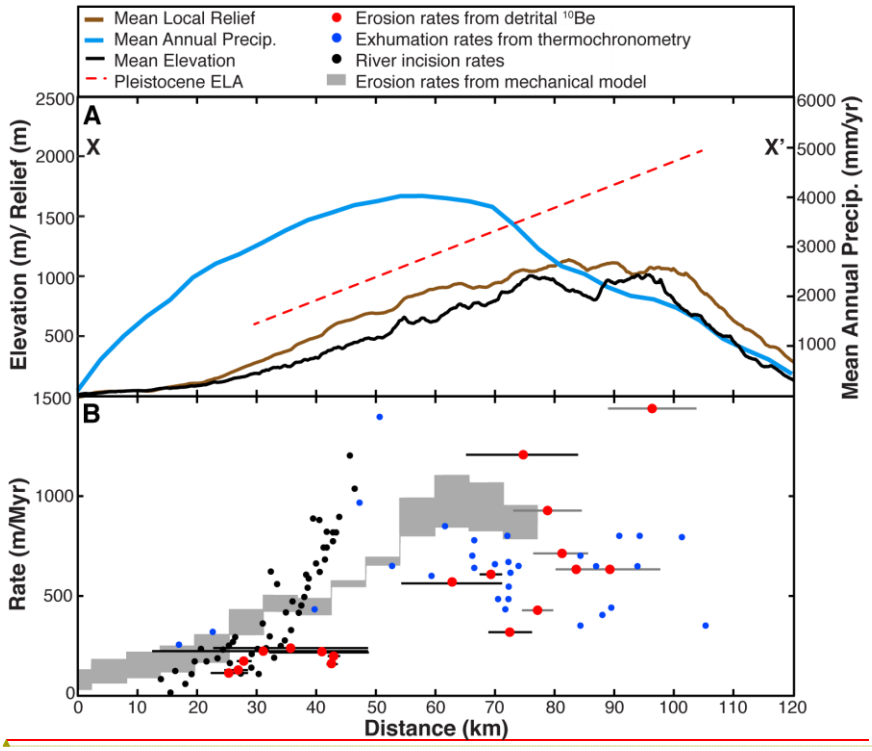

720

Formatted: Font: 12 pt

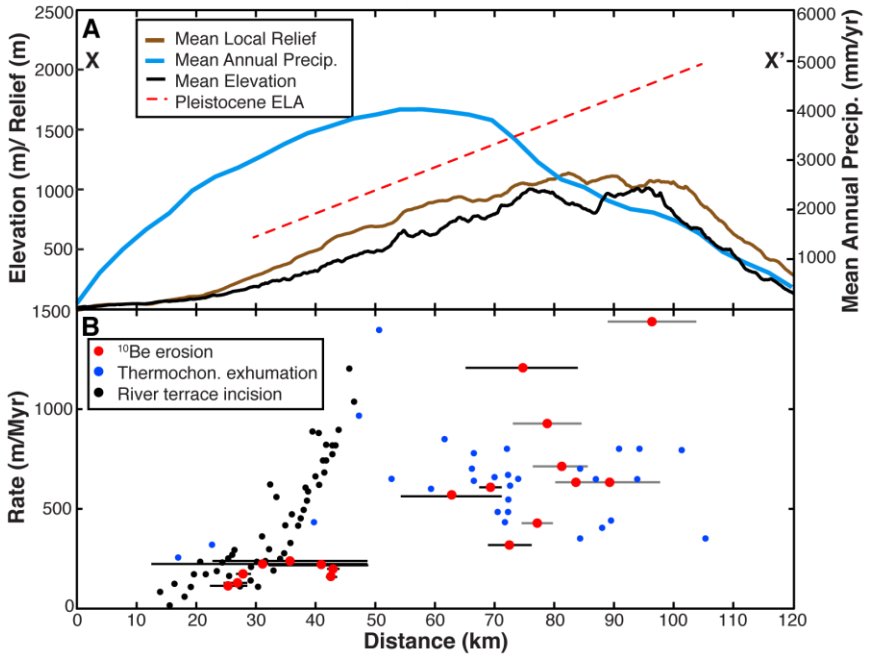

Figure 7. Comparison between estimated erosion and relief across the Olympic Mountains. A) Elevation and climate data across the Olympic Mountain range parallel to the direction of tectonic convergence (~54°). Maximum and mean elevations are shown in thin and thick black lines, respectively. Mean annual precipitation data (Daly et al., 1994) are shown in blue. Equilibrium line altitude (ELA) data (Porter, 1964) are represented by a red trend line. B) The blue circles show estimated rock uplift rates from apatite fission track data from Brandon et al. (1998). Black circles are rock uplift rate estimates from Pazzaglia and Brandon (2001) based on and river terrace incision. ~~The grey envelope is the erosion pattern from Stolar et al. (2007) based on a coupled mechanical/landscape evolution model.~~ Basin-average erosion rates in this study are shown in red circles with bars denoting the width of the basins. See Fig. 1A for cross section location.

Table 1. Sample basin characteristics. Mean equilibrium line altitiude (ELA) based on estimates from Porter (1964). 2σ = 2 standard deviations on the mean. Curves represent simplified histograms with normalized counts . See labels below each column for minimum and maximum bin values. Basins in italics are from Belmont et al. (2007).

Sample Name	Latitude (°N)	Longitude (°W)	Area (km^2)	Range Side	ELA (m)	Elevation (m)			Mean Annual Prec. (mm/yr)		
						Mean	2σ	Histogram	Mean	2σ	Histogram
WA1501	47.810972	123.44503	48.0	East	1673	1364	646		2093	220	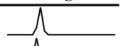
WA1502	47.948389	123.56092	66.8	East	1552	1215	786		2058	626	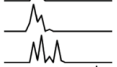
WA1503	47.969639	123.59908	40.9	East	1431	1143	800		2549	1139	
WA1519	47.878306	123.70736	114.8	West	1413	1375	762		4013	2275	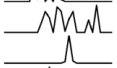
WA1520	47.885139	123.75147	6.5	West	1255	1158	570		4077	182	
WA1522	47.976972	123.68797	19.2	East	1339	1230	520		2831	911	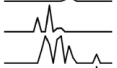
WA1523	47.876735	123.69469	74.9	West	1449	1367	692		3471	1710	
WA1524	47.876161	123.69537	35.6	West	1342	1454	810		5200	1478	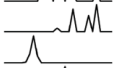
WA1525	47.916688	123.24247	133.1	East	1811	1515	636		1831	298	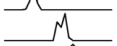
WA1526	47.67787	124.11701	126.9	West	--	537	398		3686	414	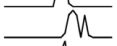
WA1527	47.62844	123.6316	115.4	West	1292	1064	652		4544	761	
WA1537	47.615017	123.47443	104.0	West	1438	1104	716		3608	1678	
WA1538	47.739067	123.17657	169.7	East	1734	1402	678	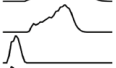	2137	440	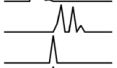
WA1539	*47.951718*	*123.81862*	35.6	West	1270	1215	526		4022	949	
U-EFMC	*47.685616*	*124.23868*	3.5	West	--	275	162		3150	179	
L-EFMC	*47.653568*	*124.24006*	13.4	West	--	229	164		3118	143	
U-WC	*47.738694*	*124.04432*	1.6	West	--	629	234		3659	109	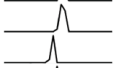
L-WC	*47.728534*	*124.03657*	4.3	West	--	552	302		3699	176	
DEN104	*47.55637*	*124.28191*	33.8	West	--	220	158		3111	143	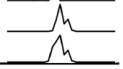
DEN106	*47.644947*	*124.24263*	281.2	West	--	407	412	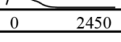	3471	529	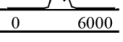
DEN101	*47.642348*	*124.23752*	391.1	West	--	335	422		3328	644	
								0 2450			0 6000

730

Table 2. Basin metrics for erosion processes. $2\sigma = 2$ standard deviations on the mean. Curves represent simplified histograms with normalized counts. See labels below each column for minimum and maximum bin values. Basins in italics are from Belmont et al. (2007). Values exclude data from ice coverd regions.

Sample Name	Hillslope Angle (°)			Channel Steepness ($m^{0.9}$)			Local Relief (m)		
	Mean	2σ	Histogram	Mean	2σ	Histogram	Mean	2σ	Histogram
WA1501	30	20		134	102		1227	246	
WA1502	29	20		160	152		1288	320	
WA1503	33	22		154	96		1374	332	
WA1519	31	24		163	154		1359	372	
WA1520	34	19		180	150		1379	58	
WA1522	31	20		133	72		1117	186	
WA1523	31	24		153	156		1317	386	
WA1524	33	26		181	144		1443	230	
WA1525	30	20		141	104		1147	278	
WA1526	27	20		62	48		717	174	
WA1527	30	22		134	96		1190	242	
WA1537	33	24		128	106		1320	292	
WA1538	31	22		137	124		1282	334	
WA1539	27	22		117	106		1067	224	
U-EFMC	22	18		23.3	3.0		386	28	
L-EFMC	21	18		23	20		385	72	
U-WC	28	16		N/A	N/A	N/A	718	20	
L-WC	26	17		86	28		718	20	
DEN104	16	17		23	17		350	72	
DEN106	23	24		47	50		581	324	
DEN101	20	24		40	48		496	384	
			0 70			0 450			0 2100

735

Table 3. Basin-averaged erosion rate sample data. Integration time was calculated by dividing the e-folding depth of the production of cosmic nuclides via spallation (0.6 m) by the erosion rate. Italicized samples are from Belmont et al. (2007). Underlined sampes had ^{10}Be measurements less that 10 times the blank measurement.

Sample Name	[^{10}Be] (atoms/g)	[^{10}Be] 2σ (atoms/g)	Be Erosion Rate (m/Myr)	Rate 2σ (m/Myr)	Integration Time (yr)	[^{26}Al] (atoms/g)	[^{26}Al] 2σ (atoms/g)	Al Erosion Rate (m/Myr)	Rate 2σ (m/Myr)	^{26}Al/^{10}Be	^{26}Al/^{10}Be 2σ
WA1501	11738	633	638	118	941	74391	6678	696	163	6.3	1.3
WA1502	9324	527	718	134	836	48421	7135	959	321	5.2	1.6
WA1503	6934	445	930	183	645	38878	6227	1152	414	5.6	1.9
WA1519	2980	288	2511	618	239	10783	3104	4814	3104	3.6	2.2
WA1520	10906	583	610	112	983	73333	10379	629	204	6.7	2.0
WA1522	15665	1129	432	90	1389	132290	9907	353	75	8.4	1.8
WA1523	3844	345	1881	442	319	10539	2435	4766	2429	2.7	1.4
WA1524	2573	255	3117	782	193	21763	4289	2551	1113	8.5	3.7
WA1525	5625	397	1451	301	414	26581	4208	2126	759	4.7	1.6
WA1526	19765	845	224	37	2673	111196	11661	278	71	5.6	1.3
WA1527	11048	596	564	104	1063	80390	9617	538	152	7.3	1.9
WA1537	5010	376	1213	256	495	33985	3912	1244	341	6.8	1.9
WA1538	11742	603	635	116	945	71021	6160	727	166	6.0	1.2
WA1539	21267	915	318	55	1889	145691	13348	320	76	6.9	1.4
U-EFMC	*21558*	*3018*	*171*	*34*	*3501*	--	--	--	--	--	--
L-EFMC	*27796*	*1668*	*129*	*20*	*4669*	--	--	--	--	--	--
U-WC	*29985*	*1799*	*158*	*25*	*3789*	--	--	--	--	--	--
L-WC	*22703*	*1362*	*199*	*31*	*3023*	--	--	--	--	--	--
DEN-101	*17407*	*11837*	*223*	*176*	*2685*	--	--	--	--	--	--
DEN-104	*31032*	*10551*	*114*	*43*	*5264*	--	--	--	--	--	--
DEN-106	*17150*	*7203*	*237*	*110*	*2528*	--	--	--	--	--	--